SEMI-ANNUAL PROGRESS REPORT

Grant DE-FC26-03NT41828

Refinery Integration of By-Products from Coal-Derived Jet Fuels

Leslie R. Rudnick, Andre Boehman, Chunshan Song, Bruce Miller, John Andresen

March 18, 2004 – September 17, 2004

Date Issued: October 18, 2004

The Pennsylvania State University
The Energy Institute
C205 Coal Utilization Laboratory
University Park, PA 16802

Disclaimer

This report was prepared as an account of work sponsored by an agency of the United States Government. Neither the United States Government nor any agency thereof, nor any of their employees, makes any warranty, express or implied, or assumes any legal liability or responsibility for the accuracy, completeness, or usefulness oof any information, apparatus, product, or process disclosed, or represents that its use would not infringe privately owned rights. Reference herein to any specific commercial product, process, or service by trade name, trademark, manufacturer, or otherwise does not necessarily constitute or imply its endorsement, recommendation, or favoring by the United States Government or any agency thereof. The views andd opinions of authors expressed herein do not necessarily state or reflect those of the United States Government or any agency thereof.

Abstract
This report summarizes the accomplishments toward project goals during the first twelve months of the project to assess the properties and performance of coal based products. These products are in the gasoline, diesel and fuel oil range and result from coal based jet fuel production from an Air Force funded program. Specific areas of progress include generation of coal based material that has been fractionated into the desired refinery cuts, acquisition and installation of a research gasoline engine, and modification of diesel engines for use in evaluating diesel produced in the project. The desulfurization of sulfur containing components of coal and petroleum is being studied so that effective conversion of blended coal and petroleum streams can be efficiently converted to useful refinery products. Equipment is now in place to begin fuel oil evaluations to assess the quality of coal based fuel oil. Coal samples have procured and are being assessed for cleaning prior to use in coking studies.

TABLE OF CONTENTS

Disclaimer ii

Abstract iii

LIST OF TABLES vi

LIST OF FIGURES viii

Introduction xii

Executive Summary xiii

Experimental xv

Results and Discussion xv

Conclusions xv

Technical Discussion 1

Objectives 3

Scope of Work for Year 1 6

Tasks to be Performed 7

Task 1. Pilot-Scale Fuel Production at PARC 8
- Subtask 1.1 LCO Procurement 8
- Subtask 1.2 Catalyst Preparation 9
- Subtask 1.3 Hydrotreatment of Blended Product 10
- Subtask 1.4 Fractionation into Refinery Product Slate 10
  - Parametric Study for Coal-Tar Processing Approach 11
  - Decant Oil Hydrotreating for Co-coking Approach 13

Task 2. Evaluation of Coal-Based Gasoline and Diesel Products in IC Engines and Related Studies 19
- Subtask 2.1 Impact on Gasoline Quality and Performance 20
  - 2.1.1 Preparation of Laboratory Instrumentation 20
  - 2.1.2 Impact on Chemical and Physical Properties 23
  - 2.1.3 Impact on SI Engine Emissions and Performance 23
- Subtask 2.2 Impact on Diesel Fuel Quality and Performance 24
  - 2.2.1 Acquisition, Installation and Instrumentation of Ignition Test Equipment 24
  - 2.2.2 Developmennt of Analytical Methods and Test Procedures 27
  - 2.2.3 Evaluation of Capabilities and Needs for Supplemmental Measurements and Analyses 27
  - 2.2.4 Impact on Chemical and Physical Properties 28
  - 2.2.5 Impact on CI Engine Emissions and Performance 34

Task 3. Desulfurization, Denitrogenation, Saturation of Aromatics, Chemicals from Coal 35
- Subtask 3.1 Desulfurization and Denitrogenation 36
  - 3.1.1 Experimental 39
  - 3.1.1.1. Hydrodesulfurization of 4,6-DMDBT 39
  - 3.1.1.2. Adsorptive Denitrogenation 41
  - 3.1.2 Results and Discussion 44

3.1.2.1 The Effect of Nitrogen Compound on 4,6-DMDBT HDS 44
3.1.2.2 NiMo Supported on Mesoporous Support MCM-41 48
3.1.2.3. Adsorptive Denitrogenation in Batch System 51
3.1.2.4. Adsorptive Denitrogenation in Flow System 54
3.1.3 Summary 60
3.1.3.1 Hydrosulfurization of 4,6-DMDBT 60
3.1.3.2 Adsorptive Denitrogenation for Deep Hydrodesulfurization 61
3.1.4 Future Work 61
3.1.4.1 Development of Deep Hydrodesulfurization Catalysts 61
3.1.4.2 Adsorptive Denitrogenation of Model Feed for Deep Hydrodesulfurization 63
Subtask 3.2 Saturation of Two-Ring Aromatics 64
3.2.1 Experimental 64
3.2.1.1 Catalyst Preparation 63
3.2.1.2 Experimental 64
3.2.2 Results and Discussion 65
3.2.3 Summary 71
3.2.4 Future work 72
Subtask 3.3 Value-Added Chemicals from Naphthalene and Biphenyl 73
3.3.1 Experimental 74
3.3.1.1 Catalysts 74
3.3.1.2 Catalyst Evaluation 75
3.3.2 Results and Discussion 77
3.3.2.1 Types of Zeolites on the Methylation of 2-MN 77
3.3.2.2 SiO_2/Al_2O_3 Ratio of HZSM-5 on the Methylation of 2-MN 78
3.3.2.3 Iron modification of HZSM-5 on the Methylation of 2-MN 81
3.3.2.3.1 Effect of Iron modification 81
3.3.2.3.2 Effect of preparation method 81
3.3.2.3.3 Effect of Iron Source 84
3.3.2.2.4 Effect of Fluorine Source 86
3.3.3 Summary 88
3.3.4 Future Work 88

Task 4. Evaluation of Coal-Based Fuel Oil Products 90
Subtask 4.1 Fuel Analysis 90
4.1.1. Major, Minor, and Trace Elemental Analysis 91
Subtask 4.2 Fuel Atomization 94
Subtask 4.3 Watertube Boiler Combustion Tests 100
4.3.1 Description of the Research Boiler and Anciallary Equipment 100
4.3.2 Fuel Oil Combustion Test Results 103
4.3.3. Determination of Metals Emissions and Form of Mercury from Stationary Sources 105
4.3.3.1 Experimental Procedure 107
4.3.3.2 Emissions Results 109

Task 5. Pitch and Coal Material 125
Subtask 5.1 Sample Procurement and Preparation 126
Subtask 5.2 Examine Resid from Fractionation of Deeply HDT RCO/LCO as a Pitch Material 137
Subtask 5.3 Co-coking Coal and Heavy Petroleum Stream 137
Subtask 5.4 Analysis of Co-coking Coke 140
Subtask 5.5 Distillation and Analysis of Co-coking Binder Pitch 157
Subtask 5.6 Manufacture and Testing of Carbon Artifacts 160

References 162

List of Acronyms and Abbreviations 173

List of Tables

Table 1. United LCO and Koppers RCO Simulated Distillations 9

Table 2. Summary of Composition of HDT Blends of 1:1, 2:1 and 3:1 RCO/LCO 12

Table 3. Hydrotreating Operating Conditions Summary 17

Table 4. Product Drum Analyses 18

Table 5. Product Gravities and Weights 19

Table 6. Thresholds Limits for Impact on Sooting Tendency 34

Table 7. Composition and properties of CoMo and NiMo sulfide and Ni phosphide catalysts 40

Table 8. The concentration of each compounds in model fuel 42

Table 9. Kinetic Results for the Effect of Nitrogen Compounds on Hydrodesulfurization of 4,6-DMDBT … 47

Table 10. Rate constants of 4,6-DMDBT HDS over sulfided NiMo catalysts supported MCM-41 or Al_2O_3 49

Table 11. The capacity of nitrogen compounds over several adsorbents in batch system 54

Table 12. The adsorption capacity on several adsorbents in flow system 55

Table 13. Properties of Selected Catalyst Supports 64

Table 14. Reduction and Reaction Conditions 66

Table 15. Physical properties of the catalysts 76

Table 16. Iron modified ZSM-5 catalysts and their corresponding preparation conditions. 76

Table 17. Analysis of the No. 6 Fuel Oil used in the Combustion/Emission Tests 91

Table 18. Chemical Analysis of the No. 6 Fuel Oil 93

Table 19. Droplet Size Distribution for No. 6 Fuel Oil Spray using the Faber Oil Gun 99

Table 20. Summary of the Average Boiler Operation and Combustion Data 104

Table 21. Metal Partitioning in Oil-Fired Combustors 107

Table 22. Total Emissions Measured during Combustion Tests and Calculated Emissions Based on AP-42 Emission Factors 110

Table 23. Emission Factors for Metals from Oil-fired Combustors 111

Table 24. Average Weight % of Each Element in Solid and Gas Phase in Flue Gas Measured During

Combustion Tests 117

Table 25. Properties of Froth Effluent Samples 133

Table 26. Mass balances of sieving the froth streams collected. 135

Table 27. Elemental analysis of the sieved fraction of Sample#10 135

Table 28. Conditions and Yields from the Experimental Delayed Coker 141

Table 29. Distribution of Textural Composition of Coke From Run #13 Using 100% Decant Oil, Vol. % 147

Table 30. Petrographic Analysis of Carbon Textures in Coker Sample #14 by Size and Origin, Vol. % 153

Table 31. Proportion of Textures Derived from Coal and Decant Oil Compared with the Normalized Concentration of Decant Oil Textures in Coke from Run #14, Vol. % 154

Table 32. Petrographic Analysis of Carbon Textures in Coker Sample #35 by Size and Origin, Vol. % 155

Table 33. Proportion of Textures Derived from Pittsburgh Seam Coal and Decant Oil Compared with the Normalized Concentration of Decant Oil Textures in Coke from Run #35, Vol. % 156

List of Figures

Figure 1. Possible Integration of Coal into Existing Refineries 3

Figure 2. Ricardo "Hydra" Single-Cylinder Research Engine and Bedplate in the Diesel Combustion and Emissions Laboratory 21

Figure 3. Fuel Delivery Apparatus to Provide Premixed Prevaporized Fuel Samples to the CFR Octane Rating Engine for Ignition Studies 22

Figure 4. Ignition Process for n-Heptane at ϕ=0.05 and Increasing Compression Ratio 26

Figure 5. Tetralin Smoke Point vs. Weight % 29

Figure 6. Decalin Smoke Point vs. Weight % 30

Figure 7. Phenanthrene Smoke Point vs. Weight % 31

Figure 8. Fluorene Smoke Point vs. Weight % 32

Figure 9. Comparison of Smoke Point vs. Weight %, tetralin (circle), decalin (square), phenanthrene (diamond), and Fluorene (plus sign) 33

Figure 10. Scheme of 4,6-DMDBT HDS via ring hydrogenation (k_1) and direct C-S bond hydrogenolysis (k_2) pathways 37

Figure 11. Schematic diagram of adsorptive denitrogenation apparatus 43

Figure 12. The effect of quinoline on hydrodesulfurization of 4,6-DMDBT over NiMo 46

Figure 13. The comparison of the HDS rate constants over NiMo catalysts 49

Figure 14. The adsorption amounts of nitrogen compounds over zeolite-based adsorbents and sulfide adsorbents at 80ºC in batch system. 51

Figure 15. The adsorption amounts of nitrogen compounds over zeolite-based adsorbents and sulfide adsorbents at room temperature in batch system …..... 52

Figure 16. The selectivity between quinoline and indole over several adsorbents after denitrogenation…. 53

Figure 17. Breakthrough of nitrogen concentration on several adsorbents in flow system 55

Figure 18. Breakthrough of sulfur concentration on several adsorbents in flow system …..... 57

Figure 19. Conversion vs. TOS for the hydrogenation of tetralin over Pd catalysts on various supports at 225°C and 600 psig hydrogen pressure in the presence of 100 ppm benzothiophene 66

Figure 20. t-DHN to c-DHN ratio as a function of TOS for the hydrogenation of tetralin over Pd catalysts on various supports at 225°C and 600 psig hydrogen pressure in the presence of 100 ppm benzothiophene …. 67

Figure 21. Conversion vs. TOS for the hydrogenation of tetralin over Pd catalysts on various supports at 225°C and 600 psig hydrogen pressure in the presence of 100 ppm benzothiophene…..... 68

Figure 22. t-DHN to c-DHN ratio as a function of TOS for the hydrogenation of tetralin over Pd catalysts on various supports at 225°C and 600 psig hydrogen pressure in the presence of 100 ppm benzothiophene…..... 69

Figure 23. Conversion and t-DHN/c-DHN ratio vs. TOS for the hydrogenation of tetralin over Pd catalysts on CBV90A and MCM-41(50) supports at 225°C and 600 psig hydrogen pressure in the presence of 100 ppm benzothiophene…. 69

Figure 24. Hydrogenation of tetralin over Pd catalysts on various supports at 225°C and 600 psig hydrogen pressure in the presence of 37 ppm benzothiophene. 70

Figure 25. t-DHN to c-DHN ratio as a function of TOS for the hydrogenation of tetralin over Pd catalysts on various supports at 225°C and 600 psig hydrogen pressure in the presence of 37 ppm benzothiophene..... 71

Figure 26. Picture of the flow reaction system 77

Figure 27. Effect of catalyst type in methylation of 2-MN with methanol. Reaction condition: temperature: 300 ^{o}C; Feed (2-MN:methanol: mesitylene=1:5:5 mol ratio): 1.98 ml/hr; Catalyst: 0.3 gram; Gas flow: 20 ml/min 79

Figure 28. Methylation of 2-MN with methanol over HZSM-5 zeolite with different SiO_2/Al_2O_3 ratio. Reaction conditions: temperature: 300 ^{o}C; Feed (2-MN:methanol: mesitylene=1:5:5 mol ratio):1.98 ml/hr; Catalyst: 0.3 gram; Gas flow: 20 ml/min 80

Figure 29 Methylation of 2-MN with methanol over HZSM-5 zeolite and Iron-substitute ZSM-5 molecular sieve catalyst (M-Fe-01). Reaction conditions: temperature: 300 ^{o}C; Feed (2-MN:methanol: mesitylene=1:5:5 mol ratio): 1.98 ml/hr; Catalyst: 0.3 gram; Gas flow: 20 ml/min 83

Figure 30 Effect of preparation method on the methylation of 2-MN with methanol over Iron-substitute ZSM-5 molecular sieve catalysts. Reaction conditions: temperature: 300 ^{o}C; Feed (2-MN: methanol: mesitylene=1:5:5 mol ratio): 1.98 ml/hr; Catalyst: 0.3 gram; Gas flow: 20 ml/min 84

Figure 31 Effect of iron source on the methylation of 2-MN with methanol over Iron-substitute ZSM-5 molecular sieve catalysts. Reaction conditions: temperature: 300 ^{o}C; Feed (2-MN:methanol: mesitylene=1:5:5 mol ratio): 1.98 ml/hr; Catalyst: 0.3 gram; Gas flow: 20 ml/min 85

Figure 32. Effect of fluoride source on the methylation of 2-MN with methanol over Iron-substitute ZSM-5 molecular sieve catalysts. Reaction conditions: temperature: 300 ^{o}C; Feed (2-MN: methanol: mesitylene=1:5:5 mol ratio): 1.98 ml/hr; Catalyst: 0.3 gram; Gas flow: 20 ml/min 87

Figure 33. Schematic diagram of the Faber oil gun. 95

Figure 34. Sketch of the atomization test facility 96

Figure 35. Flow diagram of the atomization test facility. 97

Figure 36. Schematic diagram of the research boiler system. 101

Figure 37. Classification of trace elements by their behavior during combustion and gasification. Taken from Clarke and Sloss 106

Figure 38. Modified Ontario-Hydro sample train..... 108

Figure 39. Analytical procedure for the PSU method 109

Figure 40. Measured and calculated emissions for selected elements. 115

Figure 41. Measured and calculated emissions for selected elements. 116

Figure 42. Average partitioning of elements between solid and gas phase by weight percent for tests 1A, 2A and 2B. 118

Figure 43. Partitioning of elements between solid and gas phase by weight % for test RI-PSU-1A..... 119

Figure 44. Partitioning of elements between solid and gas phase by weight % for test RI-PSU-2A..... 120

Figure 45. Partitioning of elements between solid and gas phase by weight % for test RI-PSU-2A..... 121

Figure 46. Froth flotation setup of the plant and the corresponding ten samples taken..... 129

Figures 47. Particle size distribution of Sample 1. 130

Figures 48. Particle size distribution of Sample 2. 130

Figures 49. Particle size distribution of Sample 3. 130

Figures 50. Particle size distribution of Sample 4. 130

Figures 51. Particle size distribution of Sample 5. 131

Figures 52. Particle size distribution of Sample 6. 131

Figures 53. Particle size distribution of Sample 7. 131

Figures 54. Particle size distribution of Sample 8. 131

Figures 55. Particle size distribution of Sample 9 132

Figures 56. Particle size distribution of Sample 10 132

Figure 57: Froth sample #9 where the larger particles are very pure and highly reactive vitrinite particles while the smaller white particles are inertinite and very small particles are mostly clay 134

Figure 58. Schematics of removing clay, commonly referred to as “slime” and inertinites from the froth. 134

Figure 59. Changes in the organic composition of sample#10 by the elimination of -45 micron particles. 136

Figure 60: Schematic of the delayed coking process and subsequent distillation. 139

Figure 61. Different distillation cuts obtained from the liquid product from the co-coking run#35 and their respective yields. 157

Figure 62. GC-MS traces of the different distillation cuts. 158

Figure 63. Comparison of typical coal tar pitch compounds with that found for the co-coking pitch. 159

Figure 64. Comparion of the viscosity profile of the co-coking pitch and a standard coal tar pitch. 160

Figure 65. Carbon artifact preparation route..... 161

Figure 66. Schematic of the 7 day baking process. 161

Introduction

This program is investigating the fate of each major product from a refinery complex, except jet fuel, resulting from the refinery integration of coal-derived jet fuel production via a combined RCO/LCO strategy by studying the physical and chemical nature of all products that are perturbed by introduction of coal components into the refinery.

The impact of the proposed research is to provide the scientific and fundamental engineering basis to integrate the production of coal-based jet fuel into existing refinery operations in a time frame consistent with availability and economic forecasts related to petroleum-derived as opposed to coal-based feedstocks. The results of these studies lead to the integration of all non-jet-fuel streams into current refinery operations in concert with desired production of coal-based jet fuel engine testing toward the end of the first decade of the new century. For successful utilization of coal-based jet fuels all non-jet-fuel components must fit existing and future product stream specifications.

Executive Summary

Penn State has been working for more than a decade on the development of an advanced, thermally stable, coal-based jet fuel, JP-900. Two process routes to JP-900 have been identified, one involving the hydrotreating of blends of refined chemical oil (a by-product of the coal tar industry) with light cycle oil, and the other involving the addition of coal to delayed cokers. However, no refinery is operated for the primary purpose of making jet fuel. The conversion of the jet fuel section of a refinery to production of coal-based JP-900 would necessarily impact the quantity and quality of the other refinery products, such as gasoline, diesel fuel, fuel oil, and coke. The overall objective of this project is to examine the characteristics and quality of the streams *other than the jet fuel*, and to determine the effect those materials would have on other unit operations in the refinery.

The present report documents the activities of the first twelve months of what is envisioned to be a four-year program. Our collateral work on jet fuel, funded by the Air Force Office of Scientific Research, is focused exclusively on that product. Thus as we branch out into the study of the other refinery streams, under this present contract, much of the initial effort has necessarily been devoted to equipment acquisition and installation, and to the first experiments.

The overall project involves pilot-scale production of materials at PARC Technical Services (Harmarville, PA). The coal-based gasoline and diesel fuel will be evaluated in appropriate internal combustion engines. Desulfurization, denitrogenation, and saturation of aromatics will be tested. The coal-based fuel oil will be tested in a research boiler. The pitch and coke produced will also be characterized. These interrelated activities are designed to evaluate the full range of products from coal-based thermally stable jet fuel production and to lead toward process integration in existing refineries.

The hydrotreatment of blends of refined chemical oil and light cycle oil, followed by fractionation of the total product, has been performed at PARC. The various distillation cuts have been provided to the researchers at Penn State for analytical characterization and for use in the appropriate evaluation tests. In addition, decant oil was hydrotreated at several levels of severity for use in the co-coking work.

For evaluation of gasoline quality and performance, we have acquired and installed a Ricardo Hydra single-cylinder research engine. The engine can now operate under load and on fuels of interest. Work is continuing on instrumentation and facilities hook-up to the engine test stand.

To assess the impact on diesel fuel quality and performance, two existing engine test stands, using Navistar and DCC turbodiesel engines were enhanced. In addition, new instrumentation for testing ignition quality was purchased and is being installed. The ignition quality test has recently become an ASTM method; we will participate in a

round-robin evaluation of this test, which will provide a useful external comparison of data on the coal-based fuels at no additional cost to the project.

The desulfurization of 4,6-dimethyldibenzothiophene and of dibenzothiophene in decalin was studied over commercial cobalt-molybdenum and nickel-molybdenum catalysts. Quinoline was used as a model compound to investigate the effect of the presence of nitrogen compounds of the desulfurization process. The desulfurization can be explained by pseudo-first-order kinetics, and is strongly inhibited by the presence of quinoline. A flow reactor was designed and constructed for saturation of aromatics. The first series of experiments involved palladium on various supports as the catalysts for saturation. Selective methylation of 2-methylnaphthalene with methanol has been studied for the production of 2.6-dimethylnaphthalene, which would be a value-added coal-based by-product for the petrochemical industry.

For fuel-oil evaluation, a high-temperature in-furnace camera was procured and installed in a water-tube research boiler. Shakedown tests of the camera are underway.

Samples of as-mined coal and of froth flotation products from a Consol mine in Washington County. Pennsylvania were obtained. These materials will be used in co-coking experiments. Some of the froth flotation products still have significant ash yield, suggesting that secondary cleaning processes may be necessary to have a low-ash feed to the coker. A pitch product has been isolated by distillation of the heavy distillate from a co-coking experiment. Characterization of these materials is in progress.

Experimental

The respective experimental details for each of the tasks of this project are described within the individual Tasks I – V detailed later in this report.

Results and Discussion

The results of each task of this project are documented and discussed within the appropriate Task I – V detailed later in this report.

Conclusions

Each of the individual tasks of this project has progressed as proposed or to a greater extent than originally proposed. Each task individually contributes to the ultimate goal of refinery integration. This first semiannual report describes the procurement of equipment into the appropriate laboratories, the establishment of experimental procedures and the generation of early results that indicate the relevance and feasibility of the proposed work. Progress has been made to produce hydrotreated products, differing from conventional refinery products but also compatible with conventional materials. A new approach has generated similar materials not having the added cost of hydrotreating. These materials will be evaluated in the next reporting period and be compared with extensively hydrotreated gasoline, diesel and fuel oil fractions. Engines have been installed which will provide detailed performance measurements on both the gasoline and diesel components in this process. Equipment to provide detailed understanding of the quality of fuel oil has been procured as has equipment needed to study the heavy components available through the process of generating the desired jet fuels within a conventional petroleum refinery complex.

Technical Discussion

Background

Penn State has been involved in a multi-phase fifteen-year program to develop an advanced thermally stable jet fuel for the Air Force [1-4]. This fuel would resist breaking down at high temperatures (900°F), so it could be used for cooling sensitive parts on high-performance aircraft, as well as providing the propulsion. It is provisionally called JP-900.

At its inception, the JP-900 program presumed that this new fuel would be made entirely or substantially from coal. There are three reasons for this.

Scientific validity. Penn State's researchers have shown clearly that the kinds of chemicals in the fuel that make it stable at 900°F (hydroaromatics and naphthenes) can be derived in abundant amounts from coal. This has been demonstrated in numerous peer-reviewed publications [5-10].

Long-term security. Unlike petroleum, coal is a secure, domestic energy resource for which centuries' worth of reserves remain in the U.S.

Stable procurement. Both petroleum and natural gas are vulnerable to significant price spikes. In contrast, coal companies are willing to write twenty-year delivery contracts at a guaranteed stable price. In turn, this would help stabilize the price of military fuel for decades to come.

To ultimately produce an advanced thermally stable coal-based jet fuel a practical and economically viable process, compatible with current refinery practice, is necessary. The evaluation of this scenario is the subject of this proposal. No refinery is operated for the specific purpose of making jet fuel. Furthermore, refineries are highly integrated, in that many of the individual operations are dependent on, or use streams from, other operations. Therefore, in order to insure that the production of coal-based JP-900 in the jet fuel section of a refinery is acceptable to refinery operators, it is crucial to have data showing the effect of the by-products from coal-based JP-900 production (i.e., the $<180^{o}C$ and the $>270^{o}C$ fractions) on the quantity and quality of the other refinery products: gasoline, diesel, fuel oil, pitch, and coke.

Options for integrating coal, or a coal liquid product that is currently available commercially (a by-product coal tar distillate from the metallurgical coke industry) into existing refineries are illustrated in **Figure 1**. With respect to the first two options, coal can either be added to the coker directly or be co-processed with the resid. Of these, addition of the coal to coker has been selected – in consultation with our refinery partner – as the better option to produce sufficient quantities of coal-based fuel for thermal stability and combustion testing. Each of these approaches has a unique set of technical challenges in terms of specifying the proper feedstocks (for both petroleum- and coal-based components), process conditions (temperature and pressure) and processing approaches.

Previous work at Penn State has resulted in significant progress in identifying the remaining critical barriers to realization of coal-based fuels [11-20].

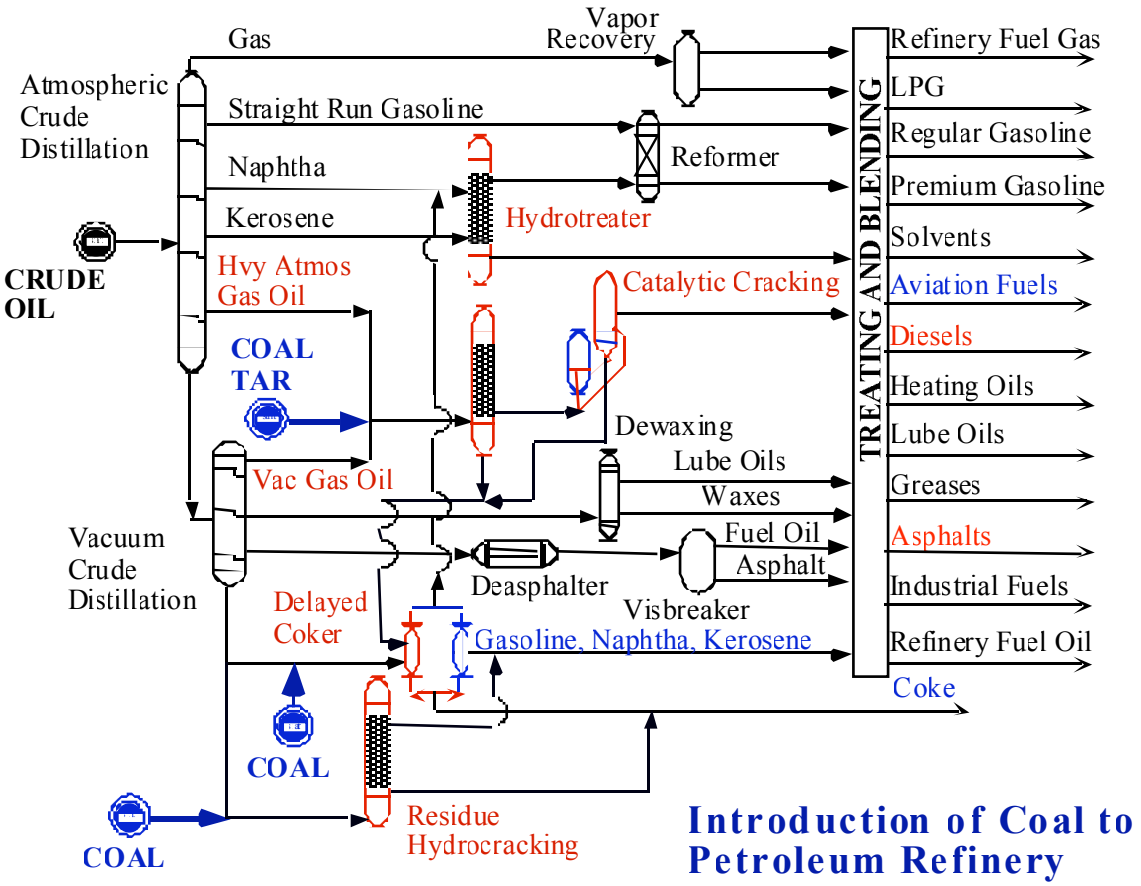

Figure 1. Possible integration of coal into existing refineries.

Objectives

A number of potential JP-900-type jet fuels have been produced by Pennsylvania Applied Research Corporation (PARC) from the hydrotreatment of a coal-derived refined chemical oil (RCO) and its mixture with a petroleum-derived light cycle oil (LCO).

The overall objective of this project is to examine the characteristics and quality of the streams other than the jet fuel, and what effect those materials would have on the

other unit operations in the refinery, the quality and value of the other products. Broadly, these additional by-products are the liquids lighter and heavier than jet fuel itself, i.e., the <180^{o}C and the >270^{o}C fractions produced after hydrotreating the RCO/LCO blend and fractionating to recover the jet fuel and other refinery streams.

Prior to the beginning of this project, virtually all work was focused on the jet fuel. However, as we have noted above, no refinery is run for the specific purpose of making jet fuel. Therefore, to make these processes acceptable for adoption in refineries, it is vital to assess their impact on the other major operations and products in a refinery. The acquisition of that knowledge is the basis of this project.

These studies will impact all of the major product streams in a conventional petroleum-based refinery. Therefore, replacing petroleum feedstock with domestic coal, gasoline, diesel, fuel oil and pitch components will favorably impact reducing dependence on, and security of supply of, foreign petroleum resources.

The objectives of the project are to:

- Investigate and develop an understanding of the most promising refinery integration of all process streams resulting from the production of coal-based jet fuel.

- Demonstrate the quality of each of the process streams in terms of refinery requirements to maintain a stable, profitable refinery operation.

- Demonstrate the performance of key process streams in practical testing used for application of these streams.

This fundamental research was proposed as a four-year program. In this document we report activities and accomplishments for the first contract year. The approach chosen draws on previous work that has now successfully produced a coal-based JP-900 fuel at pilot-plant scale for initial investigations in the fuel stabilization and combustion studies [21-23]. In that work, it has been shown that hydrotreated blends of light cycle oil and refined chemical oil (a coal-derived liquid) resulted in the most thermally stable product to date.

This program is investigating the fate of each major product from a refinery complex, except jet fuel, resulting from the refinery integration of coal-derived jet fuel production via a combined RCO/LCO strategy by studying the physical and chemical nature of all products that are perturbed by introduction of coal components into the refinery.

The impact of the proposed research is to provide the scientific and fundamental engineering basis to integrate the production of coal-based jet fuel into existing refinery operations in a time frame consistent with availability and economic forecasts related to petroleum-derived as opposed to coal-based feedstocks. The results of these studies lead to the integration of all non-jet-fuel streams into current refinery operations in concert

with desired production of coal-based jet fuel engine testing toward the end of the first decade of the new century. For successful utilization of coal-based jet fuels all non-jet-fuel components must fit existing and future product stream specifications.

Coal tar fractions have been successfully demonstrated to be suitable feedstocks for the production of jet fuels for high-speed aircraft [22-23]. The jet fuel, as prepared and evaluated in our Air Force project, is a 180-270^{o}C product cut from a mixture of RCO/LCO total liquid product. Of this product the <180^{o}C cut represents ~4% of the total product and the >270^{o}C fraction represents just over 40% of the total liquid product [24]. These streams must either be blended as is, chemically converted and then blended, converted to chemicals, or used as feed to the coker.

Scope of Work for Year 1

The technical approach consists of five carefully planned goals whose successful completion will lead to the achievement of the project objectives. These goals include:

- pilot-scale fuel production at PARC,

- evaluation of coal-based gasoline and diesel products in internal combustion engines,

- desulfurization, and denitrogenation of coal-based fuels, the saturation of aromatics to improve stability and the development of chemicals from coal,

- evaluation of coal-based fuel oil, and

- evaluation of pitch and coke materials from coal-based fuel production.

These interrelated goals are designed to evaluate the full utilization of products from coal-based thermally stable jet fuel production and lead toward process integration into existing refineries.

Tasks to be Performed

We are critically analyzing the performance and value of the streams produced from combination of coal-derived components and normal refinery process streams.

The critical analyses include:

- evaluation of gasoline range material in spark-ignited gasoline engines

- evaluation of diesel-range product for use in compression-ignited diesel engines

- evaluation of heavier range materials as heating oils and boiler fuels

- evaluation of products from co-coking strategies as precursors to higher value cokes and carbons.

The following summarizes the technical achievements for the first six months of the first project year.

Task 1. Pilot-Scale Fuel Production at PARC
(G. Wilson (PARC), L. Rudnick)

Subtask 1.1 LCO and RCO procurement

Light cycle oil (LCO) was procured from United Refining Company in Warren, PA. Refined chemical oil (RCO) was procured from Koppers, Inc., Harmarville, PA. These materials were blended to provide a feedstock RCO/LCO blend that was upgraded by deep hydrotreatment and fractionated in subsequent tasks. Simulated distillation (D2887) of LCO and RCO samples is shown in **Table 1**.

Table 1 United LCO and Koppers RCO Simulated Distilllations

SAMPLE	LCO PR 1244	RCO PR 1238	1:1 RCO:LCO PR 1251
Instrument	5880	5880	5880
IBP	350	335	341
5%	451	390	396
10%	485	429	431
20%	516	433	436
30%	533	435	440
40%	553	437	486
50%	570	438	534
60%	593	451	551
70%	618	500	577
80%	651	545	625
90%	684	598	667
95%	705	650	704
FBP	771	894	813
% at 356F (180C)	0.15	1.91	1.36
% at 518F (270C)	31.2	74.0	45.5
% at 572F (300C)	50.9	85.1	68.1

Subtask 1.2 Catalyst Preparation

Catalyst, necessary for the deep hydrotreating of total liquid product (TLP), was obtained in this task. In previous work [1, 24], PARC has identified a Criterion Syncat-3 cobalt-molybdenum or Syncat 37, nickel-molybdenum catalysts as effective in converting the coal-based blend to a deeply hydrotreated total liquid product. This product has been found to be rich in hydroaromatic components and as a result the jet fuel is thermally very stable. These catalysts must be activated by presulfiding after drying in a flow of

hydrogen. The SYNCAT catalyst is received by PARC pre-impregnated with a sulfur compound, however, PARC employs a treatment with kerosene containing 0.25 wt% dimethyldisulfide to ensure proper sulfiding prior to use.

Subtask 1.3 Hydrotreatment of Blended Product

Production of deeply hydrotreated total liquid product (TLP) to provide material for other tasks in this project by large-scale production of TLP is necessary. In this subtask, the blended RCO/LCO was catalytically hydrotreated at a rate necessary to produce a target LHSV of 0.85 at 710°F using high purity hydrogen. The non-jet-fuel components co-produced with the jet fuel was isolated by fractional distillation for further characterization and testing at Penn State University.

Since the best conditions for hydrotreatment and the optimum ratio of RCO/LCO is still being assessed, this subtask is being studied on a smaller scale than will eventually be used to produce production quantities. Subtask 1.4 describes work at smaller scale to isolate gasoline, diesel and fuel oil range products for evaluation.

Subtask 1.4 Fractionation into Refinery Product Slate

The total liquid product produced in Task 1.3 was distilled to provide fractions corresponding to gasoline, diesel, and fuel oil range refinery product streams. These materials will be used in many of the remaining tasks of the proposal. Distillation of the composite total liquid product is directed at evaluation of all non-jet fuel range material. The total liquid product was distilled in PARC's 150-gallon still using "narrow cut" techniques. This is the same still used in PARC's distillation of jet fuel range product as

a part of our AFOSR contract. Standard D2887 simulated distillation analysis were performed on lower boiling fractions to insure that the boiling range of the fractions correspond to conventional refinery stream specifications. These materials were transferred to Penn State University for further evaluation.

Parametric Study for Coal-Tar Processing Approach

This work is focusing on a parametric study to define optimum hydrotreating conditions, and how varying operating conditions can affect the performance features of each of the fractions that will need to be integrated into an existing refinery.

PARC Technical Services studies involved the procurement of starting materials and the hydrotreating and distillation of refinery products from the hydrotreated total liquid products. RCO and LCO were blended in ratios of 1:1, 2:1 and 3:1 by weight. These materials were then hydrotreated under a variety of hydrotreating conditions aimed at providing a range of low, intermediate and high levels of naphthalene conversion. The extent of hydrotreating severity was followed by measuring the degree of naphthalene conversion and the extent of desulfurization.

These materials were shipped to Penn State for evaluation as part of the various tasks depending on the boiling range of the product. A summary of the yield structure for fractional distillation cuts from the hydrotreated blends is shown in **Table 2.**

Table 2 - Summary of Composition of HDT Blends of 1:1, 2:1 and 3:1 RCO/LCO

1:1 FEED

	X864 (P67-64-1)			X865 (P67-64-2)			X866 (P67-64-3)			X867 (P67-64-5)			X868 (P67-65-1)		
	Charge Sulfur (ppm): 1750 Nitrogen (ppm): 1200			Charge Sulfur (ppm): 2000 Nitrogen (ppm): 1800			Charge Sulfur (ppm): 929 Nitrogen (ppm): 403			Charge Sulfur (ppm): 780 Nitrogen (ppm): 130			Charge Sulfur (ppm): 41 Nitrogen (ppm): 11.6		
	cut1	cut2	btms	cut1	cut2	btms	cut1	cut2	btms	cut1	cut2	btms	cut1	cut2	btms
	OP-180C	180-270C	270C+	OP-180C	180-270C	270C+	OP-180C	180-270C	270C+	OP-180C	180-270C	270C+	OP-180C	180-270C	270C+
wt %	6.9	56.5	31.8	4.7	57.6	36.7	5.5	58.9	35.3	4.6	63.2	31.9	5.6	64.7	29.2
vol %	7.8	56.9	30.6	5.4	58.3	35.3	6.3	65.9	33.8	5.2	63.8	30.6	6.2	65.7	28
Nitrogen (ppm)	227	967	915	277	1500	937	22	205	984	3	16	428	1	1	55
Sulfur(ppm)	28	160	3700	78	68	3400	4	23	2800	12	61	1400	4	1	155
Sim.Dist (D2287)	OP-356F	356-518F	518-572F	OP-356F	356-518F	518-572F	OP-356F	356-518F	518-572F	OP-356F	356-518F	518-572F	OP-356F	356-518F	518-572F
IBP (%off)	180	357	503	176	335	485	176	308	484	176	277	467	178	288	468
5	213	410	532	185	374	517	184	355	519	184	346	521	185	365	516
10	228	419	544	216	417	534	215	389	538	215	371	540	216	375	531
20	266	423	562	240	423	552	235	391	558	234	390	561	250	383	551
30	375	426	573	274	427	569	273	393	577	269	392	578	274	415	570
40	295	431	588	278	434	581	277	394	589	276	393	591	286	426	582
50	313	438	601	288	440	598	290	395	606	287	395	607	312	430	598
60	327	461	618	311	460	615	312	401	622	310	406	620	330	435	610
70	341	483	636	323	481	633	328	433	640	328	438	637	345	459	626
80	343	501	659	342	502	658	344	458	663	344	459	658	357	489	649
90	354	520	687	374	521	685	347	476	690	356	478	687	360	517	681
95	382	536	711	353	536	708	357	491	713	360	494	711	368	530	711
EP	390	566	896	392	565	837	391	521	833	474	525	846	460	562	863
Key GC Comps															
cyclohexane	3.00	0.05	0.00	4.06	0.29	0.00	4.67	0.03	0.00	5.73	0.04	0.00	6.47	0.00	0.00
ETBenzene	6.56	0.12	0.00	6.00	0.02	0.00	5.90	0.00	0.00	5.84	0.04	0.00	3.67	0.04	0.00
xylenes	14.54	0.03	0.00	20.80	0.17	0.00	18.12	0.62	0.00	17.03	0.45	0.00	11.80	0.67	0.00
tetralin	4.89	36.86	0.00	1.62	31.25	0.00	1.33	40.85	0.00	1.48	39.16	0.00	1.77	34.68	0.00
naphthalene	0.25	11.63	0.00	0.14	16.75	0.00	0.00	5.73	0.00	0.00	1.76	0.00	0.00	2.41	0.00
subst. naph.	0.00	9.66	66.92	0.00	11.11	66.66	0.00	9.24	67.30	0.00	10.72	67.02	0.00	6.03	61.74
Unidentified	70.76	41.65	33.08	67.38	40.41	33.34	69.98	43.53	32.70	69.92	47.83	32.98	76.29	56.17	38.26

2:1 FEED

	X871 (P67-66-1)			X872 (P67-66-3)			X873 (P67-66-4)			X874 (P67-66-5)		
	Charge Sulfur (ppm): 144 Nitrogen (ppm): 119			Charge Sulfur (ppm): 1400 Nitrogen (ppm): 1300			Charge Sulfur (ppm): 225 Nitrogen (ppm): 163			Charge Sulfur (ppm): 79 Nitrogen (ppm): 10.5		
	cut1	cut2	btms	cut1	cut2	btms	cut1	cut2	btms	cut1	cut2	btms
	OP-180C	180-270C	270C+	OP-180C	180-270C	270C+	OP-180C	180-270C	270C+	OP-180C	180-270C	270C+
wt %	7.2	64.8	27.1	5.7	60.5	31.7	6.7	63.8	27.3	9.9	59.7	21.6
vol %	8.1	65.2	25.8	6.5	61.1	30.2	7.7	64.3	25.8	11.1	59.7	20.7
Nitrogen (ppm)	1	3.6	295	319	1000	2000?	8.5	18.6	518	68	9	94.7
Sulfur(ppm)	1	3.4	423	4.7	38.6	935?	1	101	444	5.5	3.4	94.1
Sim.Dist (D2287)	OP-356F	356-518F	518-572F	OP-356F	356-518F	518-572F	OP-356F	356-518F	518-572F	OP-356F	356-518F	518-572F
IBP (%off)	177	312	490	177	352	480	177	282	491	167	338	493
5	186	355	523	215	400	525	184	346	528	183	356	525
10	217	373	540	232	440	540	201	359	542	187	362	539
20	259	390	560	273	445	558	228	289	563	219	390	558
30	375	393	578	277	449	571	257	392	578	268	392	571
40	279	394	591	288	457	588	274	393	592	277	383	584
50	305	395	607	312	464	602	278	394	609	307	395	599
60	317	397	623	327	468	623	303	397	627	320	397	611
70	338	418	639	343	493	636	317	403	643	340	424	627
80	345	444	662	345	527	662	342	439	668	347	449	650
90	356	470	695	347	547	693	355	466	706	358	472	685
95	359	486	723	356	567	720	358	482	748	362	487	713
EP	392	518	910	459	697	862	397	515	959	427	518	860
Key GC Comps												
cyclohexane	4.71	0.00	0.00	1.90	0.00	0.00	7.65	0.06	0.00	9.60	0.00	0.00
ETBenzene	4.88	0.00	0.00	5.54	0.00	0.00	6.84	0.03	0.00	4.12	0.00	0.00
xylenes	17.62	0.10	0.00	20.62	0.00	0.00	17.63	0.36	0.00	11.96	0.00	0.00
tetralin	0.93	45.10	0.00	1.58	33.66	0.09	1.07	40.94	0.00	2.35	40.81	0.00
naphthalene	0.00	5.13	0.00	0.12	29.06	0.09	0.07	10.28	0.00	0.14	4.91	0.00
subst. naph.	0.00	7.74	66.68	0.00	9.99	67.92	0.00	8.43	67.70	0.00	3.46	65.29
Unidentified	71.86	41.73	33.32	70.24	27.29	31.90	66.74	39.90	32.30	71.83	50.82	34.71

3:1 FEED

	X875 (P67-67-1)			X876 (P67-67-2)			X877 (P67-67-4)		
	Charge Sulfur (ppm): 206 Nitrogen (ppm): 50			Charge Sulfur (ppm): 196 Nitrogen (ppm): 474			Charge Sulfur (ppm): 629 Nitrogen (ppm):m1400		
	cut1	cut2	btms	cut1	cut2	btms	cut1	cut2	btms
	OP-180C	180-270C	270C+	OP-180C	180-270C	270C+	OP-180C	180-270C	270C+
wt %	10.2	68.2	19.8	8.6	61.5	25.9	6.1	64.4	29.2
vol %	11.6	67.7	18.8	9.8	61.8	24.5	7	65	27.9
Nitrogen (ppm)	6.4	18.2	276	54.5	162	1500	0	64	2000
Sulfur(ppm)	15.4	18.5	81.4	112.1	9	631	906	1100	2100
Sim.Dist (D2287)	OP-356F	356-518F	518-572F						
IBP (%off)	167	320	477	172	334	487	176	320	491
5	183	357	528	183	367	529	183	361	530
10	187	386	542	196	389	542	215	389	543
20	219	390	560	234	391	562	235	391	562
30	267	392	573	374	393	579	274	394	580
40	276	393	582	278	394	591	277	396	590
50	293	394	599	306	395	609	285	400	608
60	315	396	610	318	399	629	311	401	628
70	335	408	627	341	402	644	327	402	644
80	345	440	648	346	433	668	344	432	665
90	356	464	683	358	463	706	346	462	698
95	359	480	716	389	480	732	349	479	722
EP	390	517	880	459	516	936	399	516	854
Key GC Comps									
cyclohexane	9.60	0.00	0.00	6.01	0.00	0.00	3.96	0.03	0.00
ETBenzene	4.31	0.00	0.00	0.04	0.00	0.00	7.54	0.00	0.00
xylenes	14.35	0.00	0.00	16..63	0.33	0.00	22.18	0.06	0.00
tetralin	1.05	46.38	0.00	6.52	46.17	0.06	1.40	31.53	0.00
naphthalene	0.00	6.08	0.00	0.62	16.01	0.04	0.17	31.95	0.00
subst. naph.	0.00	5.23	65.75	0.00	8.10	66.72	0.00	9.57	66.47
Unidentified	45.60	36.37	34.01	47.30	24.13	32.95	41.25	22.17	33.14

Table 2. Summary of Composition of HDT Blends of 1:1, 2:1 and 3:1 RCO/LCO

Based on evaluation of the above materials and studies from our AFOSR jet fuel program an optimized HDT 1:1 RCO/LCO JP-900 prototype coal-based fuel is being prepared in sufficient quantity to supply non-jet-fuel subtasks of this refinery integration project. Progress to date includes procurement of the RCO and LCO, blending and initiation of first-stage hydrotreatment of the blend. Evaluations are in progress and will be discussed in the next project report.

Further evaluation of the jet fuels, as part of our AFOSR program, will provide guidance for selecting scale-up conditions in future years of the refinery integration program and evaluating the most relevant non-jet fuel fractions as a part of this program.

Decant Oil Hydrotreating for Co-Coking Approach

Decant oil (Heavy FCC Cycle Oil) was hydrotreated at several different levels of severity to produce feeds for Penn State's co-coking component of the Refinery Integration Study. The Decant Oil was provided by United Refining, Warren Pennsylvania and contained a high level of sulfur (3.5 wt%) and is a heavy oil with a high gravity (1.1203 gm/ml, API –5.2)

PARC's adiabatic hydrotreatment pilot unit, P67 was used for the hydrotreating. The catalysts charges were:

Reactor 1 2148 ml, 2474 gm, Criterion NiMo Syncat-37

Reactor 2 2656 ml, 3060 gm, Criterion NiMo Syncat-37

Total 4804 ml, 5534 gm

Seven hydrotreated products were produced with a range of sulfur removal from 37.9 to 99.0 wt%.

Pilot Unit Description

In the configuration used for this study, P67 consists of two reactors operated in series. Three standard quench zones were included in the set up of Reactor 1 which contained catalytically inert quartz glass beads. Reactor 2 is not equipped with quench but heat loss does occur in the transfer line between the two reactors.

Hydrogen was recycled after amine scrubbing to remove H_2S and the purity was maintained at 95 to 98%. Minimum bleed off was used within the constraint of maintaining recycle H_2 purity. Make-up hydrogen is thereby minimized to supplying the hydrogen consumed in the operation plus losses due to the on-line gas chromatograph demand.

The total liquid product was taken as fractionator bottoms after partial stripping of H_2S and ammonia in the fractionation tower. In some cases this operation resulted in small amounts of fractionation tower overhead. In such cases the furnace oil tower overhead was combined with the fractionation tower bottoms. The tower system was operated at atmospheric pressure.

Hydrotreating Operation

A sulfiding procedure was provided by the catalyst vendor and was modified to fit PARC's unit. The SYNCAT-37 catalyst was received pre-impregnated with a sulfur compound. A commercial diesel containing 0.25wt% sulfur as dimethyl disulfide in addition too the naturally occurring sulfur in the base diesel (about 300 ppm) was used as the catalyst activation feedstock. The sulfur in the feedstock would ensure that the catalyst had an adequate supply of sulfur during the sulfiding procedure. Catalyst bed temperatures were brought up to Rx1 530°F and Rx 2 545°F prior to switching to run feed.

Operation on Run Feed -Run P67-69-1 Through 7

The run feed was set at 5500gm/hr. (about 1 LHSV) and the inlet hydrogen rate at 75 scf/hr. (2,400 scf/bbl). Inlet gas purity was initially targeted at 98 % hydrogen minimum. Unit pressure was maintained at 600 psig for runs 1 through 5 and was increased to 1200 psig for runs 6 and 7.

The decant oil was processed for 10 days (Feb 3 through 13, 2004). Feed was processed at nominally seven different conditions representing seven levels of severity. To achieve this reactor temperature and feed rate were varied in the first four runs. The results for the first four runs confirmed our expectation that the decant oil difficult to desulfurize. Since the first drum of product (Run 1) had not achieved the target level of desulfurization it was decided to re-pass it at a reduced feed rate. The desulfurization level achieved was still only 82%. It was therefore decided, in the interest of time, to

increase the reactor pressure to 1200 psig rather than reduce the feed rate further to achieve a target of about 95% desulfurization. Runs 5 and 6 achieved desulfurization levels of 88 and 99%, respectively. A decrease in reactor temperature was made in Run 7 to attempt to produce a product with a lower Desulfurization level than the 88% of Run 5. However, the product maintained 99 % Desulfurization in the limited time remaining.

The summary of the daily operating conditions for each run is given in **Table 3** together with the sulfur and nitrogen levels in the feed and the product. This information is further condensed in **Table 4** with the addition of the net weights and volumes of the seven samples shipped to Penn State. The API and specific gravities of the seven products are given in **Table 5.**

CATALYST **CRITERION SYNCAT-37 (PC-723)**

CHARGE	*ml*	*gm*
Rx1	2148	2474
Rx2	2656	3060
Total	4804	5534

Heats On 1100 2/3
Start Diesel in 1100 2/4
Start Run Feed: 2400 2/4 PR1542

Pressure Test 1500 psig

Runs 1-5 NOMINAL RUN PRESSURE 600 PSIG
Runs 6-7 NOMINAL RUN PRESSURE 1200 PSIG

Run No	Time	Date	FEED	REACTOR 1				REACTOR 2				WABT	LHSV	Inlet gas	Quench	Makeup	%H2	HYDROGEN	WT. BAL	PRODUCT ANALYSES				
			gm/hr	IN	OUT	MAX	WABT	IN	OUT	MAX	WABT	COMB		SCFB	SCFB	SCFB	INLET	CONSUMP	% (8 HR)	S, wt%	N, PPM	Spec Grav	%DES	%DEN
		2004	8hrAv				8HR AVG				8HR AVG	8HR AVG	8HR AVG					SCFB		(1)	(1)	gm/ml		
	0000	2/5	*Started Run Feed*																*Feed Drum 1*	*3.54*	*1300*	*1.1203*	*-5.2 API*	
																			Feed Drum 3	3.44	1374			
																			Feed Drum 4					
P67-69-1	1430 grab	2/5	5490	529	594	594	556	545	615	615	581	568	1.02	2440	0	2611	98.2	975	100.9		1300	1.0760	100.0	0.0
	0800 grab	2/6	5490	530	596	596	557	545	614	614	582	570	1.02	2511	0	1786	98.2	685	99.0		1200	1.0760	100.0	7.7
P67-69-1	*08-20*	*2/5-6*	*Product Drum No 1*																	*2.20*	*1300*		*37.9*	*0.0*
P67-69-2	1600	2/6	Increasing temp																					
	04 grab	2/7	5274	560	666	666	603	577	637	637	610	606	0.98	2598	0	2148	97.7	908	99.0	1.67	1100	1.0679	52.8	
P67-69-2	*20-08*	*2/6-7*	*Product Drum No 2*																	*1.75*	*1200*		*50.6*	*7.7*
P67-69-3	0400	2/8	3875	567	687	687	622	590	651	651	629	626	0.72	3517	0	3428	97.9	1159	99.7	nr	nr	1.0575		
	04 grab	2/9	4144	568	685	685	621	590	647	647	626	624	0.77	3388	0	4879	98.7	1081	99.2	1.16	968	1.0568	67.2	
P67-69-3	*08-04*	*2/7-9*	*Product Drum No 3*																	*1.22*	*1000*		*65.5*	*23.1*
P67-69-4	**0400**	2/9	**STARTED RAISING TEMPERATURES**																				100.0	100.0
	15 grab	2/9	4090	607	716	716	668	632	678	678	663	666	0.76	3500	0	5577	97.5	1185	99.3	0.58	917	1.0568	83.6	29.5
	08 grab	2/10	3821	608	712	712	669	662	692	692	680	675	0.71	3283	0	2626	95.7	1080	100	0.56	935	1.0583	84.2	28.1
P67-69-4	*04-16*	*2/9-10*	*Product Drum No 4*																	**0.64**	**944**		**81.9**	**27.4**
P67-69-5	**1600**	**2/10**	**STARTED 2ND PASS OF Drum No 1**																					
	08 grab	2/11	2691	607	652	652	634	660	675	675	667	650	0.50	4602	0	1455	95.6	657	99.7	0.49	625	1.0451	**86.2**	**51.9**
	900	**2/11**	**STARTED RAISING TEMPERATURES**																					
P67-69-5	*16-12*	*2/10-11*	*Product Drum No 5*																	*0.42*	*678*		*88.1*	*47.8*
P67-69-6	**1345**	**2/11**	**STARTED RAISING PRESSURE TO 1200 PSIG**																					
	08 grab	2/12	2745	686	786	786	753	716	757	757	744	749	0.51	4020	0	4775	95.2	1268	97.5	0.0087	78	1.0246	99.8	94.0
	08 grab	2/13	2745	688	794	794	754	722	759	759	746	750	0.51	2858	0	4333	95.2	1288	97.1	0.0130	132	1.0239	99.6	89.8
	12-08	**2/11-13**	*Product Drum No 6*																	**0.0411**	**179**	**1.0254**	**98.8**	**86.2**
																				0.0591	**185**			
	09	**2/13**	**STARTED TO REDUCE TEMPARTURE**																					
	1600	**2/13**	2745	**655**	**771**	**771**	**735**	**694**	**740**	**740**	**733**	**734**	**0.51**	**3095**	**0**	**4587**	**97.2**	**1300**	**96.5**					
	08-12	**2/13**																		**0.0141**	**137**		**99.6**	**89.5**
	12-16	**2/13**																		**0.0254**	**141**		**99.3**	**89.2**
	16-18	**2/13**																		**0.0368**	**108**		**99.0**	**91.7**
	08-1800	**2/13**	*Product Cans for Drum No 7*																	**0.0348**	**147**	**1.0224**	**99.0**	**88.7**

Start Saving Product 0300, 2/5

(1) 2nd sample after re-mixing drum

Table 3. Hydrotreating Operating Conditions Summary

Catalyst **CRITERION SYNCAT-37 (PC-723)**

Run Feed: **UNITED REFINING DECANT OIL**

NOMINAL RUN PRESSURE 600 PSIG
NOMINAL RUN PRESSURE 1200 PSIG

Drum No	Run No	Time	Date	Rx1 WABT 8HR AVG	Rx2 WABT	Rx1+2 WABT 8HR AV	LHSV 8HR AV	Inlet gas Nominal SCFB	H2 Consup Nominal SCFB	PRODUCT ANALYSES S, wt% (1)	N, PPM (1)	Spec Grav gm/ml	%HDS	%HDN	Net Wt. in drum lbs	gallons
		0000	2/5	*Started Run Feed*						*3.54*	*1300*	*1.1203*	*-5.2 API*			
										3.44	1374					
1	*P67-69-1*	*08-20*	*2/5-6*	*556*	*582*	*568*	*1.02*	*2500*	*750*	*2.20*	*1300*	*1.0810*	*37.9*	*0.0*	*26.4*	*2.9*
2	*P67-69-2*	*20-08*	*2/6-7*	*603*	*610*	*606*	*0.98*	*2600*	*908*	*1.75*	*1200*	*1.0730*	*50.6*	*7.7*	*133.8*	*15.0*
3	*P67-69-3*	*08-04*	*2/7-9*	*622*	*626*	*624*	*0.75*	*3450*	*1100*	*1.22*	*1000*	*1.0591*	*65.5*	*23.1*	*377.2*	*42.7*
4	*P67-69-4*	*04-16*	*2/9-10*	*669*	*680*	*675*	*0.74*	*3400*	*1150*	*0.64*	*944*	*1.0575*	*81.9*	*27.4*	*304.2*	*34.5*
	P67-69-5	**1600**	**2/10**	**STARTED 2ND PASS OF Drum No 1**												
5	*P67-69-5*	*16-12*	*2/10-11*	*634*	*667*	*650*	*0.50*	*4600*	*657*	*0.42*	*678*	*1.0489*	*88.1*	*47.8*	*91.6*	*10.5*
	P67-69-6	1345	2/11	STARTED RAISING PRESSURE TO 1200 PSIG												
6	*P67-69-6*	*12-08*	*2/11-13*	*754*	*745*	*750*	*0.51*	*3000*	*1268*	*0.0411*	*179*	*1.0254*	*98.8*	*86.2*	*260.8*	*30.5*
										0.0591	*185*	*(1)*				*0.0*
7	*P67-69-7*	*08-1800*	*2/13*	*735*	*733*	*734*	*0.51*	*3100*	*1300*	*0.0348*	*147*	*1.0224*	*99.0*	*88.7*	*49.9*	*5.9*

(1) 2nd sample after re-mixing drum

Table 4. Product Drum Analyses

Table 5 Product Gravities and Weights

			weight, lbs		
	API	SpGr	Gross	Tare	Net
P67-69-1 (TLP Drum 1)	-0.6	1.0810	29.8	3.4	26.4
P67-69-2 (TLP Drum 2)	0.7	1.0703	149.6	15.8	133.8
P67-69-3 (TLP Drum 3)	2.1	1.0591	418.0	40.8	377.2
P67-69-4 (TLP Drum 4)	2.3	1.0575	345.0	40.8	304.2
P67-69-5 (TLP Drum 5)	3.4	1.0489	107.4	15.8	91.6
P67-69-6 (TLP Drum 6)	6.5	1.0254	301.6	40.8	260.8
P67-69-7 (TLP Drum 7)	6.9	1.0224	65.7	15.8	49.9

GC analyses were attempted on two of the early hydrotreated products on PARC's HP-6890 GC using a 150 meter Petrocal column and an FID detector. The elution times on this column have been characterized for tetralin, decalin, naphthalene, methylnaphthalene and all eight isomers of dimethylnaphthalene using pure compounds. For the same column the elution times of higher substitute methyl naphthalenes are known approximately and are consolidated into groups as tri, tetra, penta and hexa-methylnaphthalenes. It was found that the hydrotreated decant oil is primarily composed of multi-substituted naphthalenes and higher boiling, more complex components which our system cannot identify. Further hydrotreated products were therefore not analyzed.

Task 2. Evaluation of Coal-based Gasoline and Diesel Products in IC Engines and Related Studies

(Andre Boehman)

By introducing coal-derived streams into the refinery, several perturbations to the quality and quantity of refinery streams may result and directly impact vehicular fuels production. The coal contribution to the refinery streams will affect the quality, composition and performance of the resulting vehicular fuels. The fraction of the hydrotreated streams that boils below 180°C will be directed to the gasoline pool. Having components from coal is expected to boost octane number and aromatic content, and therefore, boost value. The >270°C cut of the hydrotreated stream would be low in sulfur due to the severe hydrotreatment. The effect on flash point will need to be determined if this stream is sent to the fuel oil pool and/or diesel pool. If this stream is combined with diesel fuel, it will add cycloparaffins, which will increase energy density [25] and boost value. However, the impact on cetane number and sooting tendency is unclear. The following task structure will permit assessment of the impact of refinery integration of JP-900 production on gasoline and diesel fuel.

Subtask 2.1. Impact on Gasoline Quality and Performance

Under this subtask, our efforts have focused on preparation of facilities for the SI engine testing activity. So, the majority of the progress to report is on Subtask 2.1.1.

Subtask 2.1.1. Preparation of Laboratory and Instrumentation

Under this subtask, we have acquired and installed the Ricardo Hydra single-cylinder research engine for use under Task 2.1.2. At present, we have completed the process of setup for the Hydra and can operate the engine under load and on fuels of interest. We continue work on instrumenting the engine for combustion analysis and

building a data acquisition and computerized operator interface. We are configuring a National Instruments "PXI" data acquisition system and Labview software to operate the engine and perform real-time combustion analyses.

Figure 2 shows the Ricardo Hydra single-cylinder research engine in the laboratory at the Energy Institute. **Figure 3** shows the modified fuel delivery system for the ignition quality tests.

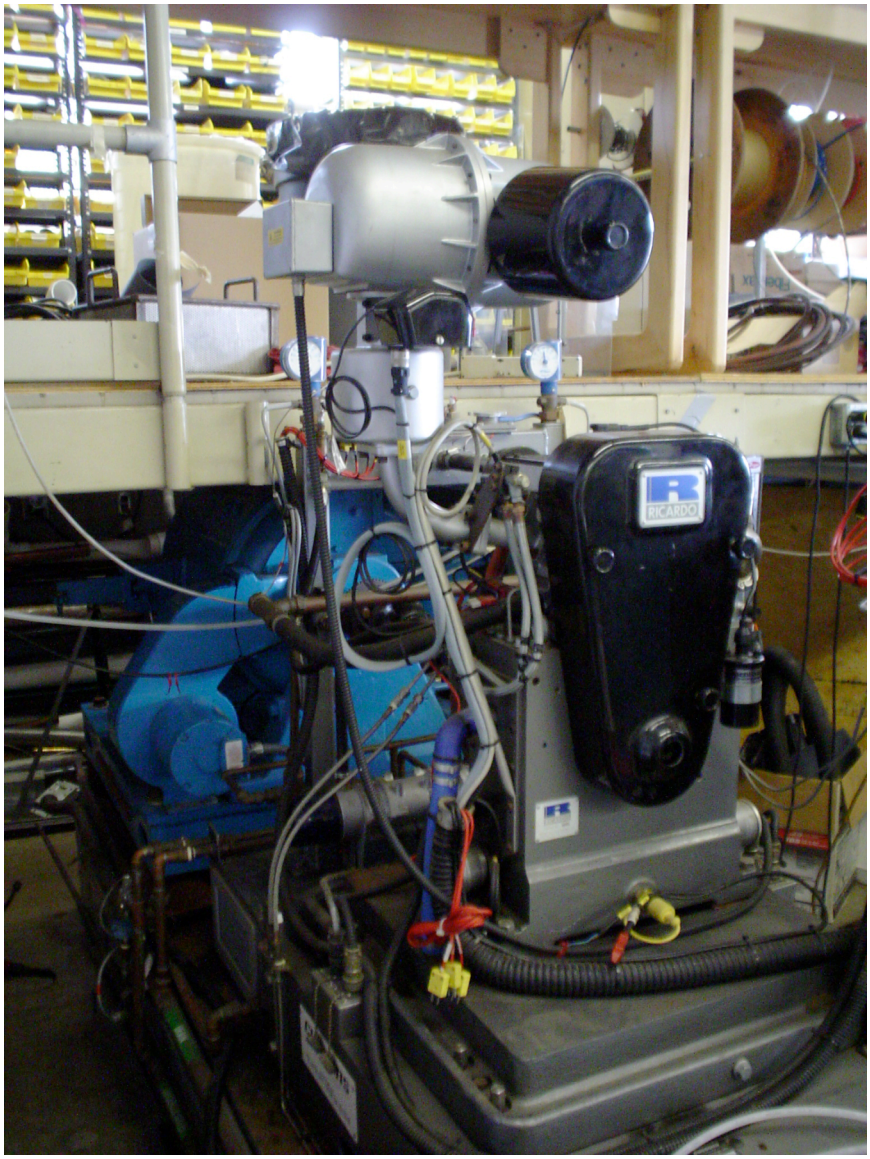

Figure 2 Ricardo "Hydra" Single-Cylinder Research Engine and Bedplate in the Diesel Combustion and Emissions Laboratory

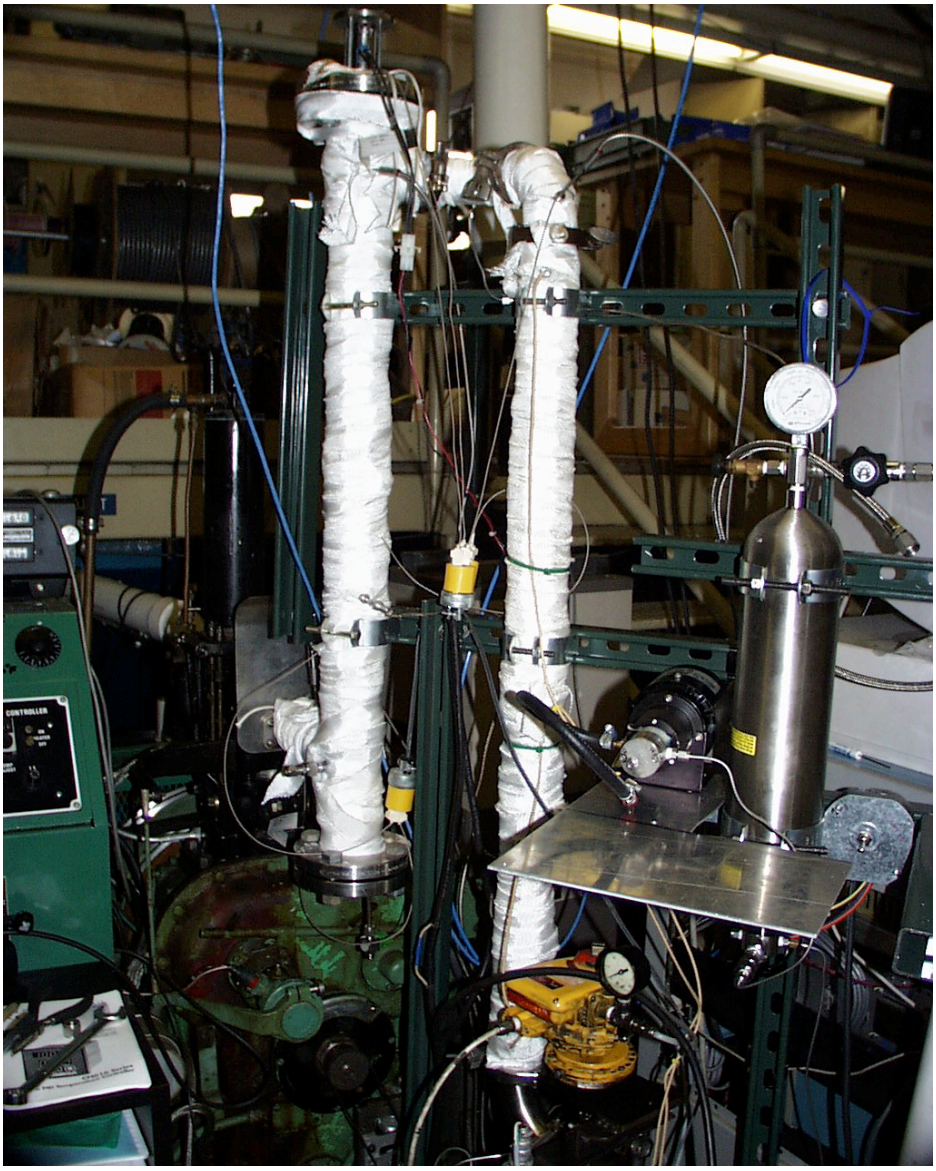

Figure 3 **Fuel Delivery Apparatus to Provide Premixed Prevaporized Fuel Samples to the CFR Octane Rating Engine for Ignition Studies**

Subtask 2.1.2 Impact on Chemical and Physical Properties

Under this subtask, detailed chemical analyses of fuel samples were performed. From several runs at PARC, fuel fractions were provided representing the gasoline and diesel fuel cuts. The fuel cuts were subjected to GC-MS analysis to determine the representative major compounds that could be used as surrogates in model compound mixtures. For the gasoline cut, the prominent coal-derived species are methyl cyclohexane, decalin, propenyl benzene and tetralin (only a small amout of tetralin was detected). We have assessed the impact of the coal-derived compounds, focusing on methyl cyclohexane, on the ignition chemistry of gasoline by performing extensive tests on model gasoline compounds and methyl cyclohexane. This work will extend into Year 2 by performing Octane rating measurements with the CFR Octane rating engine converted back to the standard ASTM testing configuration and through performance measurements in the Hydra engine.

Subtask 2.1.3 Impact on SI Engine Emissions and Performance

Since the work to date has focused in facility preparation, no data is available yet on this subtask. However, one aspect of preparation for Task 2.1.3 has been acquisition through a generous donation from Chevron Texaco of an AVL emissions analyzer for use on this project. The AVL emissions analyzer is projected to return to Penn State in October, at which point we will have all the instrumentation in place to perform this task.

Subtask 2.2 Impact on Diesel Fuel Quality and Performance

Under this subtask, we have focused on two activities, both related to facility development. One side of the work has been refinement and enhancement of two existing engine test stands, one housing a Navistar V-8 7.3L turbodiesel engine and the other housing a DDC 4-cylinder 2.5L turbodiesel engine. The other activity has involved developing ignition testing capabilities which involved purchase of new IQT instrument and development of an ignition test capability as an expansion of an existing CFR Octane Rating Engine.

2.2.1 Acquisition, Installation and Instrumentation of Ignition Test Equipment

At present, we are using the "IQT" ignition quality test instrument to examine the derived cetane number (DCN) of various diesel fuels, fuel blends and additized fuels. While we feel that there is room for improvement in the calibration of the IQT, it is giving reliable trends, measurements consistent with outside laboratories and useful data. We have begun tests on the impact of coal-derived compounds on the DCN of base diesel fuels.

In addition, a device to provide premixed prevaporized fuel samples to be fed to a CFR Octane Rating engine, operated with the spark plug deactivated, has been configured to serve as a "rapid compression machine" to study the elementary effects of fuel composition on the ignition process of hydrocarbons. Some preliminary data has been obtained for reference fuels and is presented below. **Figure 4** provides a sample of the type of data this experiment can provide. Here the ignition of n-heptane is examined,

at fixed inlet temperature and equivalence ratio (0.05) and with increasing compression ratio. In **Figure 4(iii)** the first evidence of 1st stage ignition is observed at roughly 680 K. In **Figure 4(iv),** 2nd stage ignition begins at roughly 800 K. These results are consistent with published experiments and numerical simulations of n-heptane ignition.

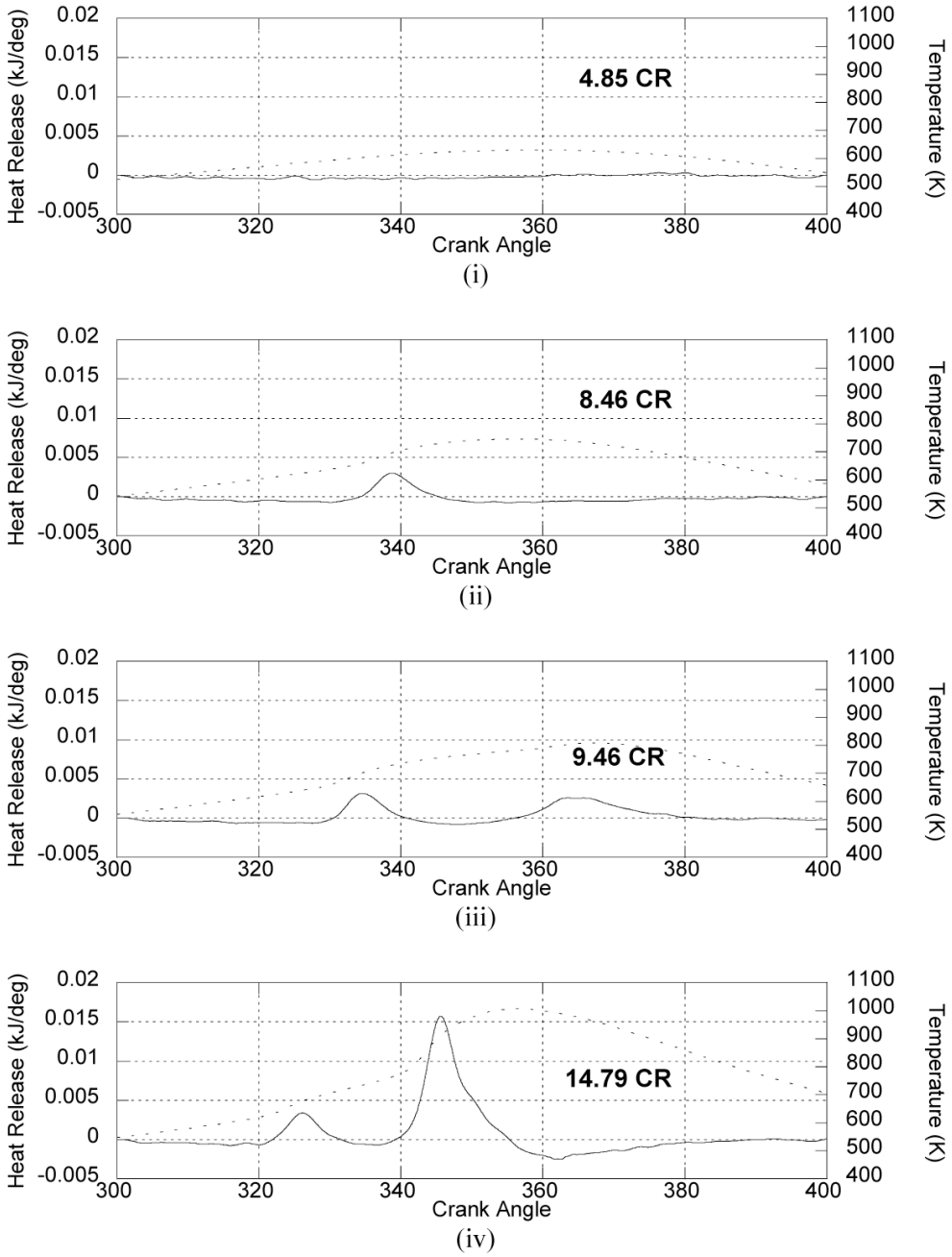

Figure 4 Ignition Process for n-Heptane at ϕ=0.05 and Increasing Compression Ratio. In Plot (iii) the First Evidence of 1st Stage Ignition is observed at roughly 680 K. In Plot (iv), 2nd Stage Ignition Begins at roughly 800 K.

2.2.2. Development of Analytical Methods and Test Procedures

The "IQT" apparatus is now covered under an ASTM test method so that its operation and application are considered standard practice. We have agreed to participate in round robin testing activities to help support the community's use of the IQT and to provide external comparison of our data.

The modification of the CFR Octane Rating engine to serve as a rapid compression machine for ignition studies represents a unique adaptation of a standard instrument and will provide a means of comparing experimental data with kinetic models of the ignition process.

2.2.3. Evaluation of Capabilities and Needs for Supplemental Measurements and Analyses

The analytical methods developed for the characterization of the fuel cuts from the PARC runs can now serve as the basis for subsequent fuel and SOF chemical analyses. We have developed procedures for use of an existing FTIR spectrometer to speciate the products of our ignition tests,which has already highlighted significant differences in the intermediate species present as we pass through first and second stage ignition for different fuels.

2.2.4. Impact on Chemical and Physical Properties

Two preliminary studies were completed. Both were based on the speciation of the diesel cut from the PARC run. The GC-MS data showed that two prominent and representative compounds were fluorene and phenanthrene. So, baseline diesel fuels were doped at 1 to 5 wt.% to simulate the diesel fuel. In one study, engine emissions tests were performed at Southwest Research Institute through a Penn State graduate who was at SwRI as an intern. Unfortunately, the experimental system at SwRI was not satisfactory for detailed emissions studies. Only qualitative trends were obtained from this collaboration. In the other study, an undergraduate student performed smoke point tests on doped diesel fuel samples to assess the impact of these coal-derived compounds on the sooting tendency of the diesel fuels. Smoke point observations were plotted versus weight percents of the aromatics to study the effects of increasing aromatic concentrations. The smoke point of pure BP 325 ranged from 15.7-16.2 mm. The resulting graphs are as follows:

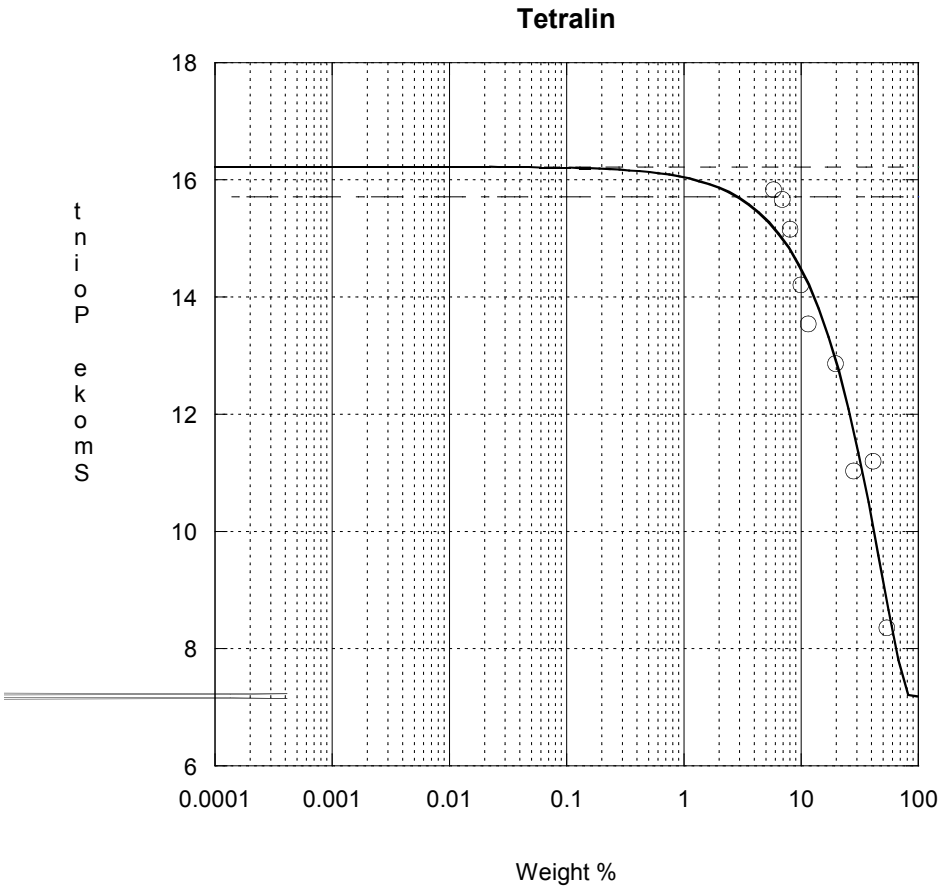

Figure 5: Tetralin Smoke Point vs. Weight %

The tetralin curve fit shows that tetralin begins to have an effect on the smoke point of BP 325 at concentrations near 3% by weight.

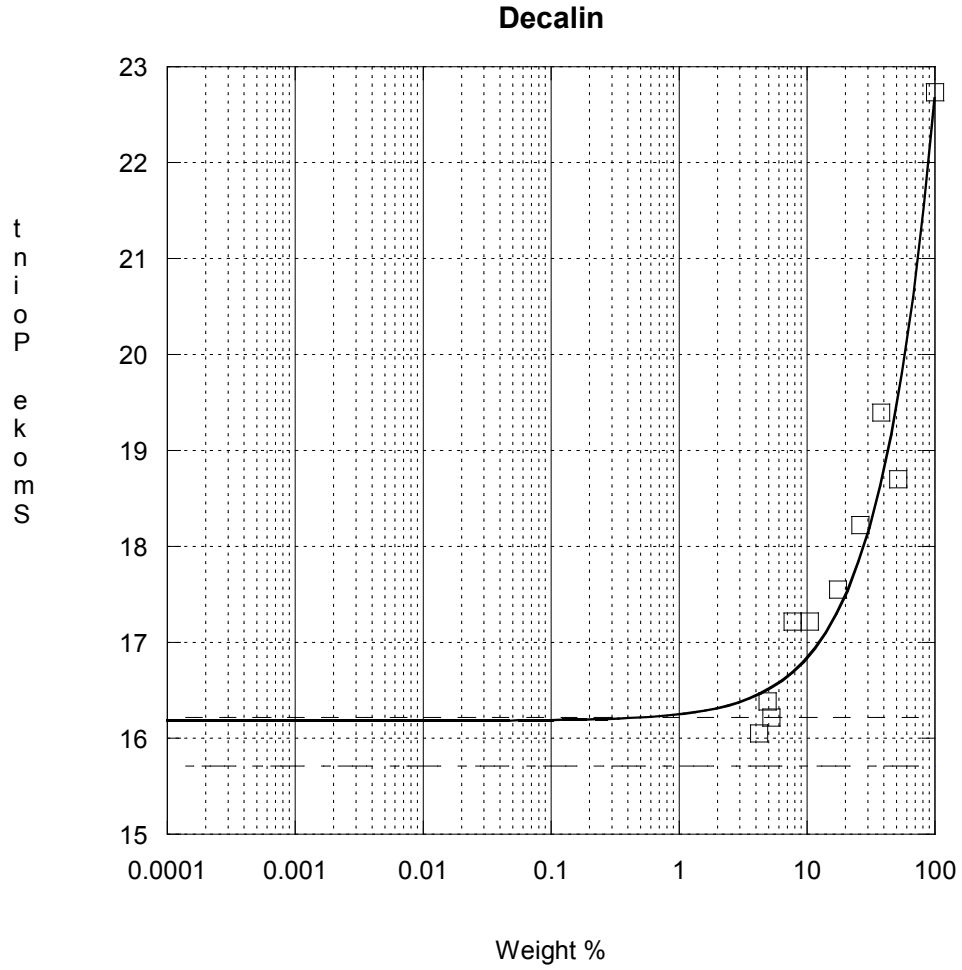

Figure 6: Decalin Smoke Point vs. Weight %

The decalin curve fit shows that decalin begins to affect the smoke point at 1% by weight. As opposed to the other chemicals in question, decalin has a positive effect on the smoke point of BP 325. Decalin's use as a stabilizing additive is supported by the findings of this study. Any concentration of decalin over 1% by weight can create a higher smoke point, which corresponds to less sooting tendency in the fuel.

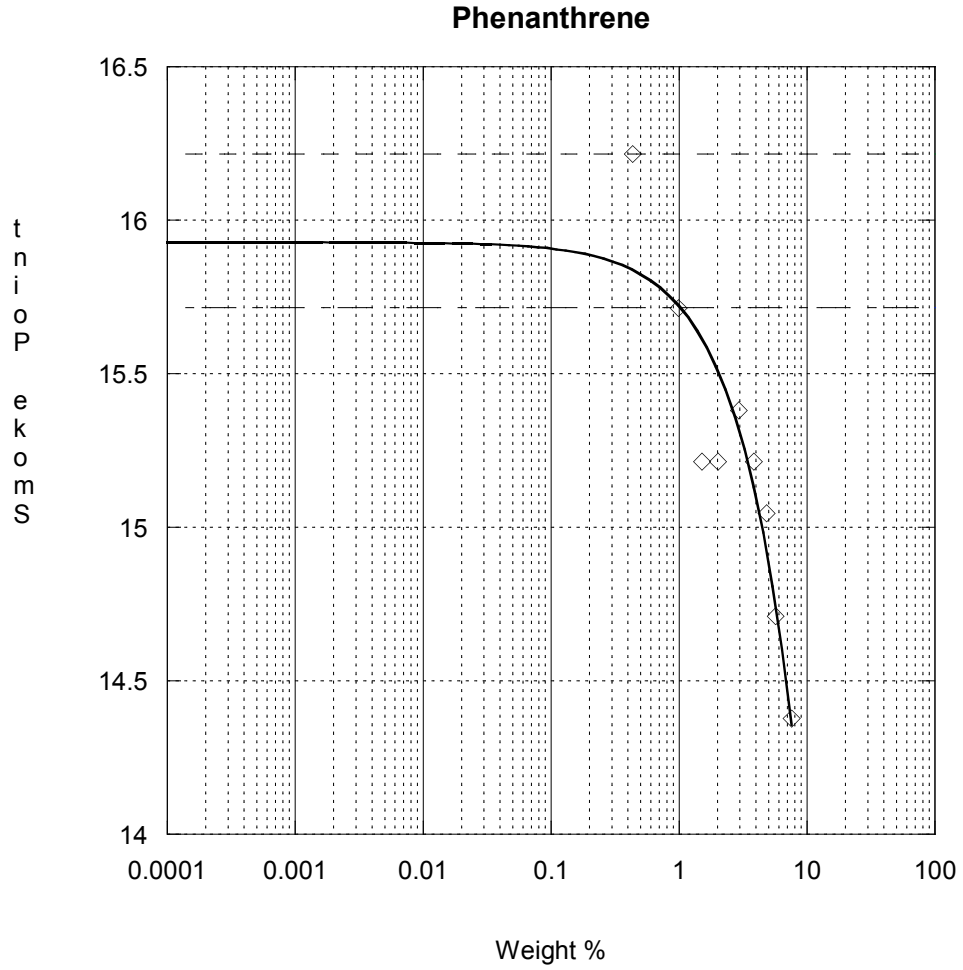

Figure 7: Phenanthrene Smoke Point vs. Weight %

The phenanthrene curve fit shows that the smoke point is affected by phenanthrene concentrations of 1% by weight or more.

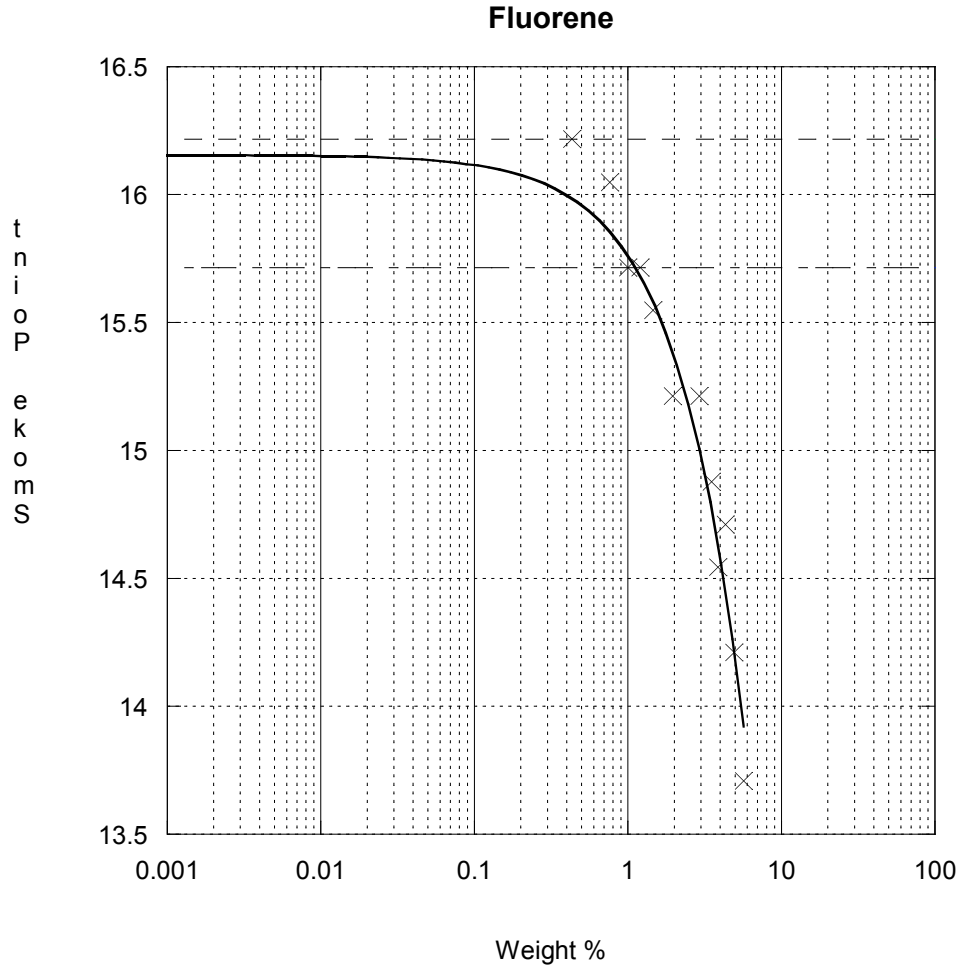

Figure 8: Fluorene Smoke Point vs. Weight %

The flourene curve fit shows that fluorene affects the smoke point of BP 325 when added at concentrations of about 1.25% by weight or greater.

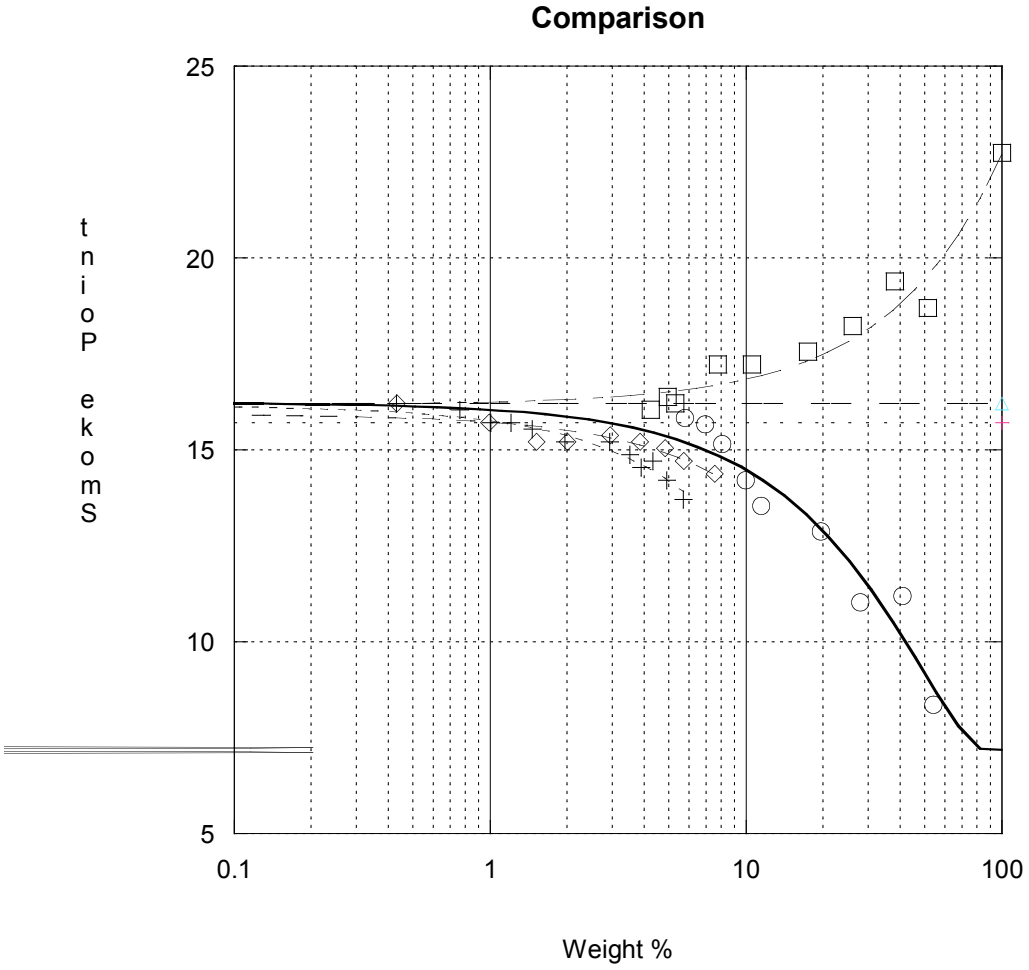

Figure 9: Comparison of Smoke Point vs. Weight %, tetralin (circle), decalin (square), phenanthrene (diamond), and Fluorene (plus sign)

This graph shows the degree of effect each of the chemicals has on the smoke point of BP 325. It can be seen that tetralin exhibits the highest threshold in the diesel fuel (Table 6). Phenanthrene and fluorene show negative smoke point effects at low concentrations, with fluorene showing a stronger effect as concentrations increase.

Compound	Threshold (wt %)
Tetralin	3
Decalin	1
Phenanthrene	1
Fluorene	1.25

Table 6: Thresholds Limits for Impact on Sooting Tendency

2.2.5 Impact on CI Engine Emissions and Performance

For the purpose of better understanding the impact of the coal-derived compounds on the injection, ignition and combustion of diesel fuels in a practical engine, we have developed an installation of an existing AVL 513D Engine Videoscope (purchased under an NSF Research Equipment Grant, # CTS-0079073) in our Navistar V-8 7.3L turbodiesel engine. This required design and machining access for an endoscope probe and a light guide to visualize the fuel spray and the spray flame. The modified cylinder head is ready for use and will be implemented after some other preliminary emissions studies are completed.

In parallel, we are adding instrumentation to an existing DDC 2.5L turbodiesel engine for examination of the impact of fuel composition of combustion and emissions. The instrumentation includes an AVL Indimodule combustion analysis system, which will permit highly accurate (true simultaneous) acquisition of fuel rail pressure, injection timing and cylinder pressure. At present we are installing the Indimodule hardware, we have received the pressure probe and are waiting for a revised design of a custom machined glow plug mounting adapter for the pressure probe. In addition, we have received from DDC a donation of an engine control interface that permits access to the engine control parameters. We now have the capability to perform precise experiments

on the impact of the coal-derived fuel compounds on emissions by maintaining control of engine operation parameters such as EGR rate and injection timing. A graduate student is presently performing fuel property measurements in preparation for a significant testing campaign using the DDC engine and Indimodule combustion analyzer to ascertain the effects on injection, ignition and heat release of coal-derived compounds in a state-of-the-art electronically controlled common rail turbodiesel engine.

Task 3. Desulfurization, Denitrogenation, Saturation of Aromatics, Chemicals from Coal

(Chunshan Song, Xiaochun Xu, Jae Hyung Kim, Brian Senger and Xiaoliang Ma)

This work relates to the integrated refinery processing of RCO and LCO for production of ultra-clean diesel fuels and for making value-added industrial aromatic chemicals. RCO is rich in naphthalene and also contains some nitrogen compounds such as quinoline. LCO is also rich in naphthalene structures but contains refractory sulfur compounds such as 4,6-dimethyldibenzothiophene.

This task deals with the following three subtasks, (1) deep desulfurization and denitrogenation, because LCO has a higher content of refractory sulfur compounds while RCO has a higher content of nitrogen compounds; (2) dearomatization of two-ring compounds, because both RCO and LCO are rich in aromatic structures; and (3) shape-selective conversion of naphthalene into 2,6-dimethylnaphthalene, because both RCO and LCO compositions are dominated by naphthalene structures, and a small fraction of them could be used for making value-added industrial chemicals.

Subtask 3.1: Desulfurization and Denitrogenation

As a part of the DOE refinery integration project, this sub-task aims at more effective deep desulfurization for obtaining ultra-clean diesel fuels which contain below 15 ppmw sulfur. For this purpose, the refractory sulfur compounds, particularly 4,6-dimethyldibenzothiophene (4,6-DMDBT), must be desulfurized or removed [26, 27]. General approaches to deep hydrodesulfurization include 1) improving the catalytic activity of the molybdenum sulfide-based catalysts used in the refining industry [28, 29]; 2) developing new catalysts [30-32]; 3) tailoring reaction and process conditions [33], and 4) designing new reactor configurations [33]. In general, deep hydrodesulfurization of dibenzothiophenes over heterogeneous catalysts proceeds through two reaction pathways. One is hydrogenation (HYD) pathway, involving aromatic ring saturation and the other is a hydrogenolysis pathway via direct C-S bond cleavage, which is also called the direct desulfurization (DDS) pathway [34, 35].

Figure 10 shows a schematic diagram for 4,6-DMDBT HDS showing hydrogenation/hydrogenolysis pathways [36]. To understand deep hydrodesulfurization mechanism and develop new type deep HDS catalysts, it is necessary to investigate the HDS activity kinetically for both reaction pathways (HYD and DDS pathways) as well as for overall reaction [36. 37].

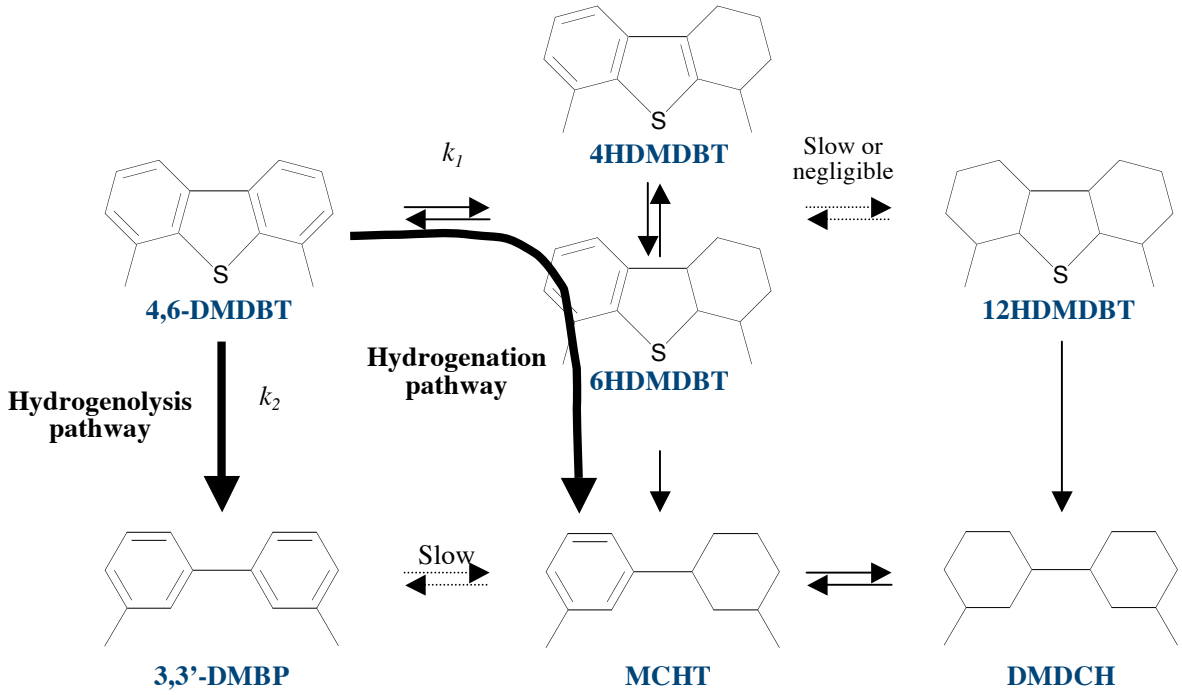

Figure 10. Scheme of 4,6-DMDBT HDS via ring hydrogenation (k_1) and direct C-S bond hydrogenolysis (k_2) pathways.

For production of clean fuels with low sulfur level, the effects of inhibitors, especially aromatic and nitrogen compounds, should be also considered and investigated. Recent study has indicated that some aromatic and nitrogen compounds present in the feed inhibit deep desulfurization significantly when the sulfur in feed is dropped to below 500 ppm level, since the aromatic and nitrogen compounds can compete with sulfur compounds on catalyst surface [38, 39]. Therefore, it is important to investigate deep HDS of refractory sulfur compounds and effects of inhibitors for developing catalysts which have high HDS activity of refractory sulfur compounds and high resistance for inhibitors (aromatic and nitrogen compounds).

Also, it was found by some researchers that the nitrogen compounds coexisting in middle–distillate oil inhibit the deep hydrodesulfurization and the removal of such

nitrogen compounds from the middle–distillate oil can improve significantly the deep HDS performance [40-42]. Recently, a new process, called PSU-SARS, is being explored in our laboratory. The idea in this process is to remove sulfur in the fuels by selective adsorption. The major advantages of this process are that the process can run at ambient temperature and pressure without using hydrogen gas and the spent adsorbents can be regenerated either by solvent washing or by oxidation using air. The idea in PSU-SARS process can be also applied to pre-denitrogenation of the middle–distillate oil to improve the deep hydrodesulfurization performance as shown in schematic diagram below.

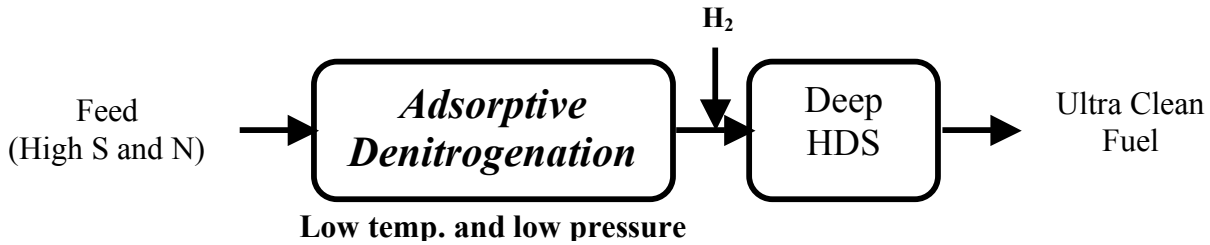

In this reporting period, we investigated the effect of nitrogen compounds on 4,6-DMDBT HDS over commercial catalysts and new catalysts prepared with mesoporous molecular sieve MCM-41. For adsorptive denitrogenation, two kind of model fuels, which were prepared with and without sulfur and aromatic compounds, were treated on zeolite-based and sulfide-based adsorbents in batch system and on zeolite-based, Ni-based and commercial adsorbents in flow system, respectively. Initially, we are focusing on adsorptive denitrogenation of basic or reactive nitrogen compounds such as quinoline or indole which inhibit hydrodesulfurization. It is expected that these nitrogen

compounds may be removed more easily by adsorption over certain adsorbents as compared with sulfur compounds.

3.1.1. Experimental

3.1.1.1. Hydrodesulfurization of 4,6-DMDBT

The reactant chemicals, 4,6-DMDBT, DBT, and decahydronaphthalene (decalin, used as solvent), were obtained from Aldrich Chemical Co. and were used without further purification. For the HDS of 4,6-DMDBT, its concentration was 1.23 wt% (0.81 mol%) in decalin. In order to examine the effect of aromatic compounds on HDS of 4,6-DMDBT, an equimolar amount of 1-methylnaphthalene (1-MN) and 4,6-DMDBT (or 0.74 mol of fluorene and 1.00 mol of 4,6-DMDBT) were added into the feed. For examination of nitrogen compound effect, 150 ppmw N (0.14 wt% quinoline) was added into the feed.

HDS was carried out in a batch reactor with a volume of 25 ml. The reactor was loaded with 0.1 g catalyst and 4.0 g decalin fuel containing 4,6-DMDBT or DBT, and was then purged with nitrogen and hydrogen five times, respectively, before being pressurized with hydrogen to the desired initial pressure. The reactor was placed in a fluidized sand bath, which was preheated to the desired temperature, and was agitated at 200 strokes/min. The temperature inside the reactor was monitored by a thermocouple. Following the reaction, the reactor was removed from the sand bath and was immediately quenched in a cold-water bath. A GC-MS (Shimadzu GC17A/QP-500) was used for identification of the products, while a gas chromatograph (SRI 8610C), equipped with an FID detector, was used for quantitative analysis of products.

Two commercial catalysts, $CoMo/Al_2O_3$ (Cr344) and $NiMo/Al_2O_3$ (Cr424), obtained from the Criterion Catalyst Co., were used for the HDS of 4,6-DMDBT and DBT. The chemical composition and textural properties of these catalysts are shown in **Table 7.** These two catalysts contained around 15 wt% MoO_3 and 3 wt% NiO or CoO. The $CoMo/Al_2O_3$ and $NiMo/Al_2O_3$ catalysts had surface areas of 190 and 155 m^2/g, and pore volumes of 0.56 and 0.45 cm^3/g, respectively. NiMo catalysts were also prepared on mesoporous molecular sieve MCM-41, and gamma-alumina with two-step impregnation method. High metal loaded NiMo catalysts contained around 40 wt% MoO_3 and 11 wt% NiO, and low metal loaded one did around 14 wt% MoO_3 and 3 wt% NiO which are the traditional metal amounts for commercial CoMo or NiMo catalysts.

The catalysts were presulfided at 350 °C for 4 h in a flow of 5 vol % H_2S-H_2 at a flow rate of 200 ml/min and were subsequently stored in decalin to minimize oxidation. Irreversible O_2 uptake measurement was carried out to estimate the number of active sites on the sulfide and phosphide catalysts, respectively. After pretreatment of the catalysts, calibrated pulses of O_2 in a He carrier flowing at 26.7 micromol/s ($40cm^3$ NTP min^{-1}) were injected at room temperature through a sampling valve and the mass 32 (O_2) signal was monitored with a mass spectrometer.

Table 7. Composition and properties of CoMo and NiMo sulfide and Ni phosphide catalysts

Catalyst	Content (wt%)		Support	Surface area (m^2/g)	Pore volume (cm^3/g)	Density (cm^3/g)	Active sites (μmol/g)
	MoO_3	Co or Ni					
Cr344	13.5 (9.0)	2.9 CoO	Al_2O_3	183.3	0.48	0.74	85.9[a]
Cr424	13.0 (8.7)	3.0 NiO	Al_2O_3	163.2	0.40	0.81	95.0[a]

[a] Measured by oxygen chemisorption

3.1.1.2. Adsorptive Denitrogenation

For adsorptive denitrogenation in batch system, a model fuel containing 150 ppmw of N as quinoline and 150 ppmw of N as indole in decline without aromatic and sulfur compounds was used in this study. The total nitrogen concentration in the fuel was 300 ppmw.

Metal ions (Cu, Ag, Ni, CuCe and NiCe) exchanged zeolites were prepared by ion exchange of commercially available NH_4Y- or NaY-zeolites with 5-fold excess of 0.1 M aqueous solution of respective metal nitrates at 80°C for 24 h. For exchanging with Ce^{3+}, a 2.5-fold excess of 0.1 M $Ce(NO_3)_3$ was used. After ion exchange, the zeolite suspension was filtered, washed thoroughly using deionized water, dried at 80 °C overnight, and then calcined at 450 °C for 6 h in air atmosphere employing a temperature ramp of 2 °C/min. These materials after calcination as adsorbents as such without any further treatment. Sulfided commercial catalysts as adsorbents were also used after presulfidation as mentioned in previous chapter.

The adsorptive denitrogenation of model fuel was performed in a batch reactor with a fuel/adsorbent ratio of 20 in weight, similar to the study reported in the literature [43]. The mixture of model fuel and adsorbent were stirred and kept at the temperature of 80 ˚C or at room temperature for 8 h.

For adsorptive denitrogenation in flow system, a model fuel containing 303 ppmw of N as same amount of quinoline and indole in the mixture solvent of decane and hexadecane was used. Total sulfur concentration was 686 ppmw of S as same amount of DBT and 4,6-DMDBT. **Table 8** shows the composition of model fuel for adsorptive denitrogenation in flow system.

Table 8 The concentration of each compounds in model fuel

Chemicals	Concentration		Molar concentration (mmol/l)
	(wt %)	ppmw S or N	
Sulfur compounds			
DBT(99+%)	0.20	343.3	8.2
4,6-DMDBT(97%)	0.23	343.4	8.2
Total		686.7	
Nitrogen compounds			
Quinoline	0.14	152.0	8.3
Indole	0.13	151.0	8.2
Total		303.0	
Aromatics			
Naphthalene	0.14		8.2
1-Methylnaphthalene	0.15		8.2
tert-Butylbenzene	9.92		
Total	10.21		
Paraffins			
n-Decane	44.01		
n-Hexadecane (99+%)	44.02		
n-Tetradecane (99+%)	0.06	(Internal standard)	
Total	100.00		

Analysis of fuel samples was conducted using Antek 9000 series nitrogen and sulfur analyzer for more accurate quantitative analysis and also SRI GC equipped with a capillary column (XTI-5, Restek) and a flame ionized detector (FID) for identification of each compound.

According to the results of adsorptive denitrogenation in batch system, zeolite Cu and CuCe adsorbents were selected and Ag/Y-zeolite was also chosen because it has been reported that Ag adsorbent interacts with aromatic compounds through π-complexation. These zeolite-based adsorbents were pretreated with He flow at 350 °C for 1 h for the reduction of metal. Also, activated alumina and activated carbon were tested because they are used widely for adsorption process in industries. The activated alumina was purchased form Aldrich Chemical Co. and has surface area of 155 m^2/g and pore size of

58 Å. In general, activated alumina can be used for removing nitrogen compounds and polar compounds in real fuels and is expected to show good adsorption properties of nitrogen compounds in the model fuel. The activated carbon was provided from Westvaco and has surface area of 1350 m^2/g and pore size of 15.7 Å. Both adsorbents were pretreated with nitrogen flow at 200 °C for 1 h in order to remove water adsorbed which might influence adsorption properties significantly. Also, A-2 (Ni-Al) and A-5 (Ni/Si-Al) adsorbents, which were developed in our lab, were also tested and compared with other adsorbents. These adsorbents were pretreated with H_2 flow at 200 °C for 1 h and cooled down to room temperature. The adsorptive denitrogenation of the model fuel on the adsorbents was performed in a flow system at room temperature with LHSV of 4.8 h^{-1}, as shown in **Figure 11**.

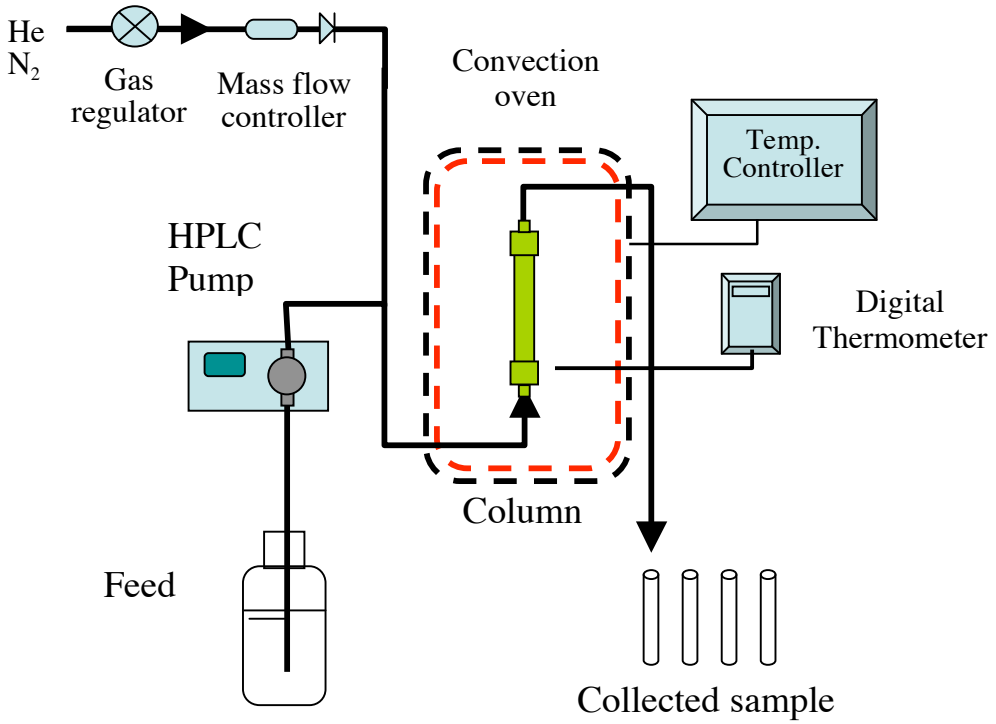

Figure 11. Schematic diagram of adsorptive denitrogenation apparatus.

3.1.2. Results and Discussion

3.1.2.1 The Effect of Nitrogen Compound on 4,6-DMDBT HDS

In order to get better kinetic data, the conversion of 4,6-DMDBT was kept below 20%. The main products from 4,6-DMDBT HDS were HDMDBT (hydrodimethyldibenzothiophene), MCHT (methyl cyclohexyltoluene) and. DMDCH (dimethyldicyclohexyl) was also detected at high conversion. During hydrotreating of 4,6-DMDBT and quinoline, the main product from quinoline hydrogenation (HYD) was 1,2,3,4-tetrahydroquiniline (1THQ) and 5,6,7,8-tetrahydroquinoline (5THQ) was detected in very small amount. Decahydroquinoline (DHQ) was not detected in this study. Hydrodenitrogenated products, propylcyclohexene (PCHE), proplycyclohexane (PCH) and propylbenzene (PB), were not detected because the concentration of quinoline added was very small and 1THQ and 5THQ were only converted very slowly to hydrodenitrogenated products.

The conversion of 4,6-DMDBT was very low over NiMo and CoMo sulfides catalysts at all reaction conditions when 4,6-DMDBT was hydrotreated in the presence of quinoline. It was under 6% after reaction of 47 minutes although the amount of quinoline added was very low, 150ppm N (0.15 wt % quinoline). At the beginning of reaction of 4,6-DMDBT and quinoline with hydrogen, the reaction rate of 4,6-DMDBT was very slow while that of quinoline was very fast. The conversion of quinoline was over 85% just 2 min after starting the reaction and most of the quinoline was converted after reaction time of 7 min.

In general, HDS of individual sulfur compound follows the pseudo-first-order kinetics, thus:

$$\ln(C_{DMDBT}/C_{DMDBT0}) = -(k_1 + k_2)\cdot t \qquad (1)$$

where k_1 is the pseudo first-order rate constant for the hydrogenation pathway, and k_2 is the pseudo first-order rate constant for the hydrogenolysis pathway. The value of (k_1+k_2), the overall rate constant, can be calculated from experimental data. **Figure 12** shows the pseudo first order kinetic profiles of 4,6-DMDBT HDS in the presence of and in the absence of quinoline over CoMo and NiMo sulfide catalysts.

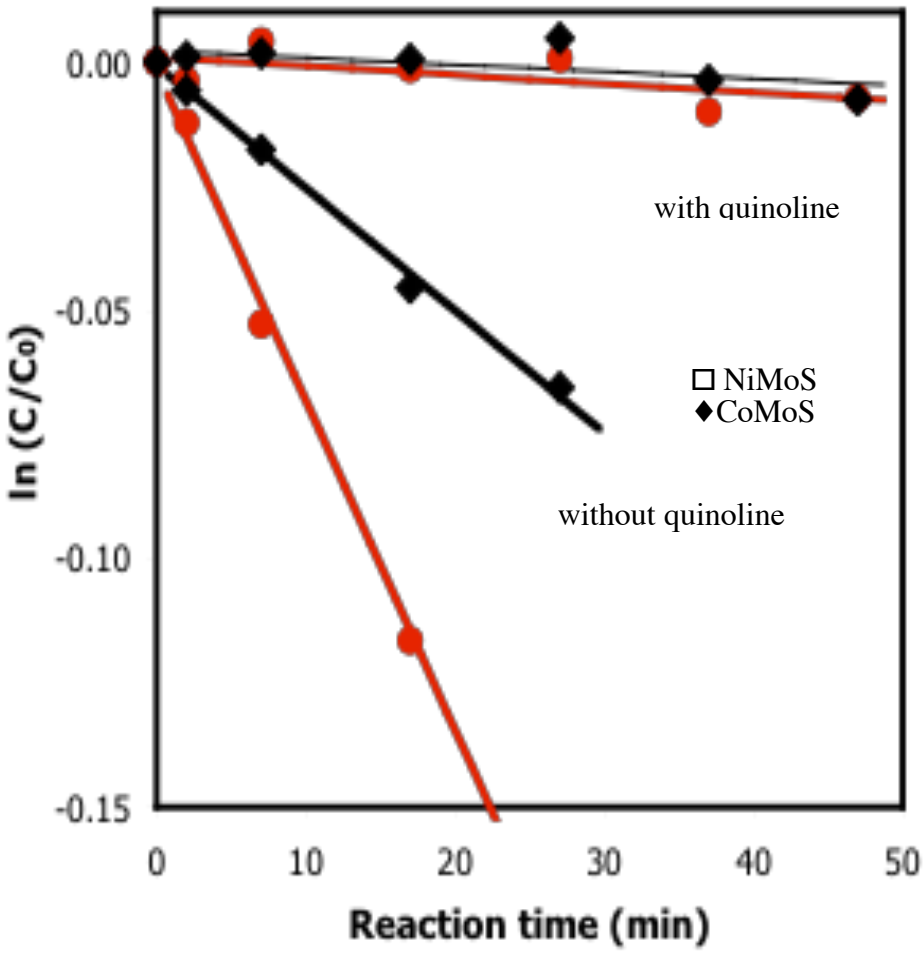

Figure 12. The effect of quinoline on hydrodesulfurization of 4,6-DMDBT over NiMo

The overall rate constants calculated on the basis of the experimental data are shown in **Table 9.** The overall rate constants over NiMo and CoMo sulfides were very low, 5.03×10^{-5} $s^{-1}g\cdot cat^{-1}$ and 3.39×10^{-5} $s^{-1}g\cdot cat^{-1}$, respectively.

Table 9. Kinetic Results for the Effect of Nitrogen Compounds on Hydrodesulfurization of 4,6-DMDBT

Inhibitor		Rate constant (10^{-5} s^{-1} g·cat^{-1})	
		Without N	Quinoline
NiMo Sulfide	k_1+k_2	117.21	5.03 (95.7%)[2]
	k_1/k_2[1]	5.36	5.06
	k_1	98.77	4.12 (95.8%)
	k_2	18.44	0.91 (95.0%)
CoMo Sulfide	k_1+k_2	44.15	3.39 (92.3%)
	k_1/k_2[1]	2.26	1.74
	k_1	30.60	2.16 (93.0%)
	k_2	13.55	1.24 (90.9 %)

[1] k_1/k_2 = [Initial selectivity of HDMDBT]/[Initial selectivity of DMBP]
[2] The data in parenthesis indicate the percentage loss of HDS activity after adding 150 ppmw N as quinoline.

In this study, the individual rate constants for each reaction pathway were calculated by using the method suggested in our previous work [36]. In this method, the ratio of k_1/k_2 was calculated by the ratio of the initial selectivity of primary products, as shown below:

$$\frac{k_1}{k_2} = \frac{[\text{Initial Selectivity of HDMDBT}]}{[\text{Initial Selectivity of DMBP}]} \qquad (2)$$

Table 9 lists the calculated rate constants for each reaction pathway with and without the presence of nitrogen compound (quinoline).

As shown in **Table 9**, the nitrogen compound quinoline is a very strong inhibitor on 4,6-DMDBT HDS. 4,6-DMDBT hardly converted to HDMDBT or DMBP in the presence of quinoline. After quinoline was converted to 1THQ which was main product from quinoline hydrogenation, the reaction rate of 4,6-DMDBT is still slow. This is

because 1THQ is also a basic nitrogen compound which is a strong inhibitor to HDS reaction on the catalysts [44, 45].

sulfide and Ni phosphide.

As shown in **Table 9,** quinoline significantly inhibited both reaction pathways over NiMo and CoMo sulfide catalyst. The loss of hydrodesulfurization activity was over 90% for hydrogenation pathway and hydrogenolysis pathway. Therefore, deep hydrodesulfurization needs more nitrogen tolerant catalysts than traditional NiMo and CoMo sulfide catalysts.

3.1.2.2 NiMo Supported on Mesoporous Support MCM-41

The prepared NiMo/MCM-41 catalyst contains around 40 wt% MoO_3 and 11 wt% NiO, which are very high metal amount as compared with traditional commercial CoMo and NiMo catalysts. The MCM 41 support, which was prepared with SiO_2/Al_2O_3 ratio of 50 in our laboratory, has surface area of 1113 m^2/g and pore volume of 1.33 ml/g, which is much higher than those of Al_2O_3. So, we loaded a higher amount of Ni and Mo metals on the MCM-41 supports. **Table 10 and Figure 13** show the overall and individual rate constant for each reaction pathway over NiMo catalysts in 4,6-DMDBT HDS. The overall rate constant over NiMo/MCM-41 was 40.18×10^{-5} $s^{-1}g\cdot cat^{-1}$ and was higher than those over $NiMo/Al_2O_3$ catalysts, which were 36.46×10^{-5} $s^{-1}g\cdot cat^{-1}$ on low metal loaded $NiMo/Al_2O_3$ and 37.07×10^{-5} $s^{-1}g\cdot cat^{-1}$ on high metal loaded $NiMo/Al_2O_3$. In the case of alumina supported catalysts, low metal loaded catalyst, which contains 14.0 wt% MoO_3 and 3.0 wt% NiO, has very similar overall rate constant to high metal loaded catalyst, which contains as the same metal amounts as NiMo/MCM-41.

Table 10. Rate constants of 4,6-DMDBT HDS over sulfided NiMo catalysts supported MCM-41 or Al_2O_3

Rate constant (10^{-5} s^{-1} g·cat^{-1})	NiMo/MCM-41 (SiO_2/Al_2O_3 = 50)	NiMo/Al_2O_3 (Low)	NiMo/Al_2O_3 (High)	Cr424	Cr344
k_1+k^2	40.18	36.46	37.07	117.21	44.15
k_1/k_2	3.30	8.74	6.90	5.36	2.26
k_1	30.84	32.72	32.38	98.77	30.61
k_2	9.34	3.74	4.69	18.44	13.55
NiO wt%	11.00	3.00	11.00	3.00	3.00
MoO_3 wt%	40.00	14.00	40.00	14.00	14.00

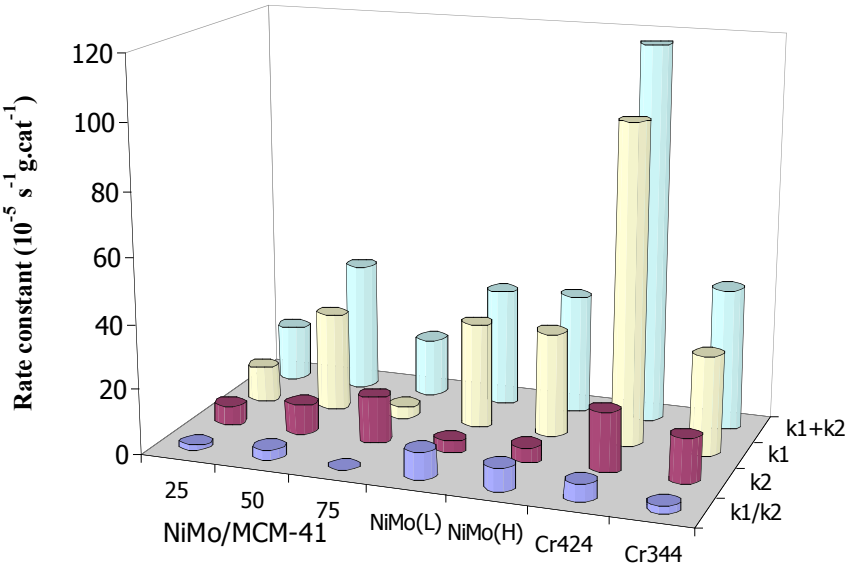

Figure 13. The comparison of the HDS rate constants over NiMo catalysts.

Therefore, the low metal loading is the optimum metal amount on alumina-supported catalyst as reported by many researchers. However, the high metal loaded NiMo/Al_2O_3

had higher k_1/k_2 ratio than the low metal loaded one. It may be because stacked NiMoS layer produce more active sites for DDS reaction pathway, but the effect was not much.

The NiMo/MCM-41 is more active on 4,6-DMDBT HDS than NiMo/Al_2O_3 catalysts, but still not better than commercial CoMo and NiMo catalysts. When the MCM-41 supported NiMo catalyst was prepared with two step method, the surface area of MCM-41 reduced significantly after the calcination of Mo/MCM-41, which was prepared at first step. MCM-41 needs to be treated carefully when it is used with aqueous solutions because its uniform pore structure may be destroyed even at low temperature (around 100 °C) due to water sensitivity [46]. Therefore, it is necessary to improve a metal impregnation method or this mesoporous support to be stable at high temperature.

3.1.2.3. Adsorptive Denitrogenation in Batch System

Figure 14 shows the adsorption amounts of quinoline and indole over the zeolite-based adsorbents and sulfide adsorbents at 80ºC.

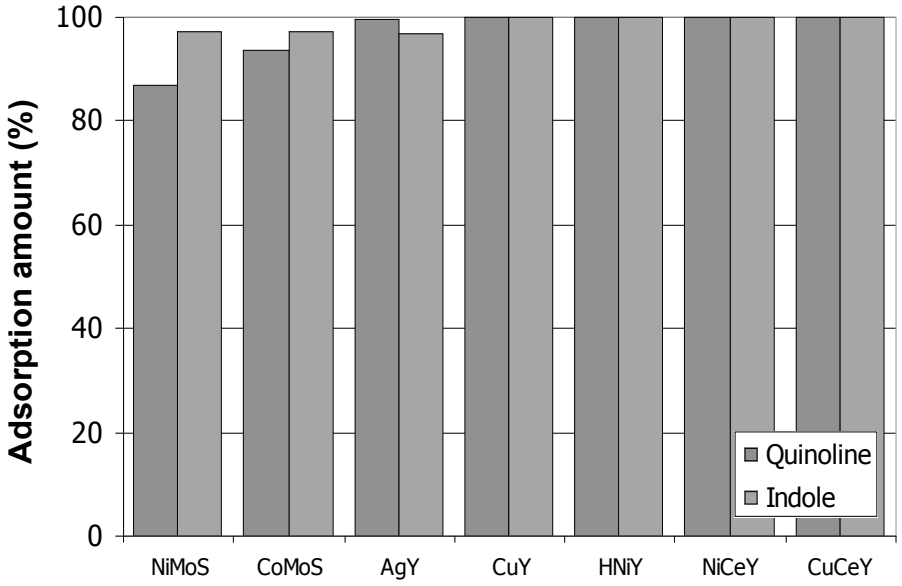

Figure 14. The adsorption amounts of nitrogen compounds over zeolite-based adsorbents and sulfide adsorbents at 80ºC in batch system.

All adsorbents showed very high adsorptive capacity of quinoline and indole. The nitrogen compounds were removed over 90% from the model fuel. The zeolite-based adsorbents exhibited better adsorptive performance than NiMoS and CoMoS adsorbents. In comparison of the adsorption amount, the metal sulfide adsorbents adsorb more indole than quinoline, while the adsorption amount of indole and quinoline was almost same on the zeolite-based adsorbents as shown in **Figure 15**.

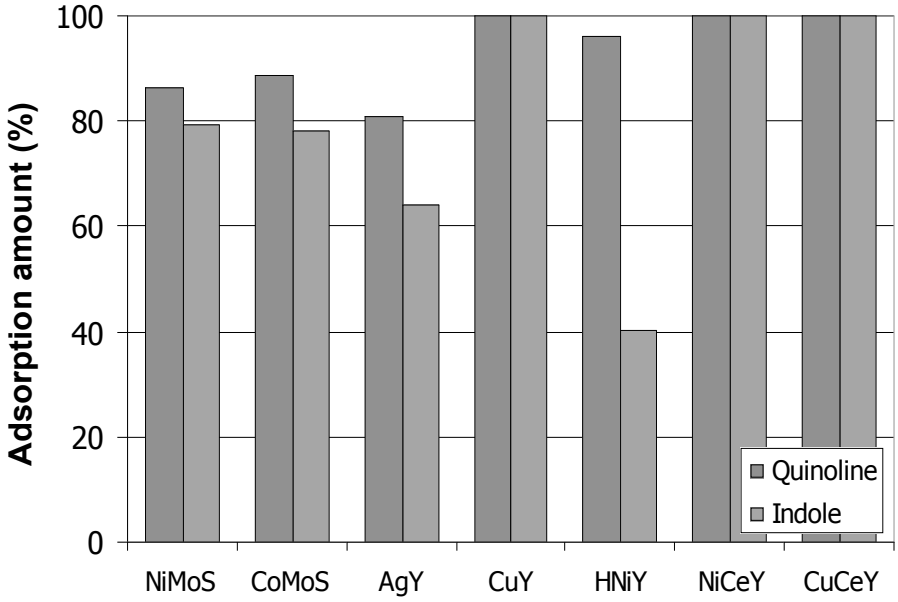

Figure 15. The adsorption amounts of nitrogen compounds over zeolite-based adsorbents and sulfide adsorbents at room temperature in batch system.

Indole and quinoline are two strong inhibitors on HDS of sulfur compounds. As shown in **Figure 15** the adsorptive amount of quinoline over CoMoS is higher than that over NiMoS, while the adsorptive amount of indole over the CoMoS and NiMoS is similar. This indicates that HDS over CoMoS might be affected more severely by quinoline than that over NiMoS, which is in agreement with our previous observation that quinoline inhibited more strongly HDS of 4,6-DMDBT over CoMoS than that over NiMoS [47].

The adsorptive denitrogenation were also tested at room temperature over the sulfide adsorbents and Ag, Cu CuCe and NiCe/Y-zeolite adsorbents as shown in **Figure 15**. Most adsorbents showed higher selectivity for quinoline to indole as shown in **Figure 16**. However, the adsorption capacity on Ag and Ni/Y-zeolite adsorbents was lower than those at 80˚C while the capacity on other zeolite-based adsorption was not changed at all and that on sulfide adsorbents was almost unchanged as shown in **Table 11.**

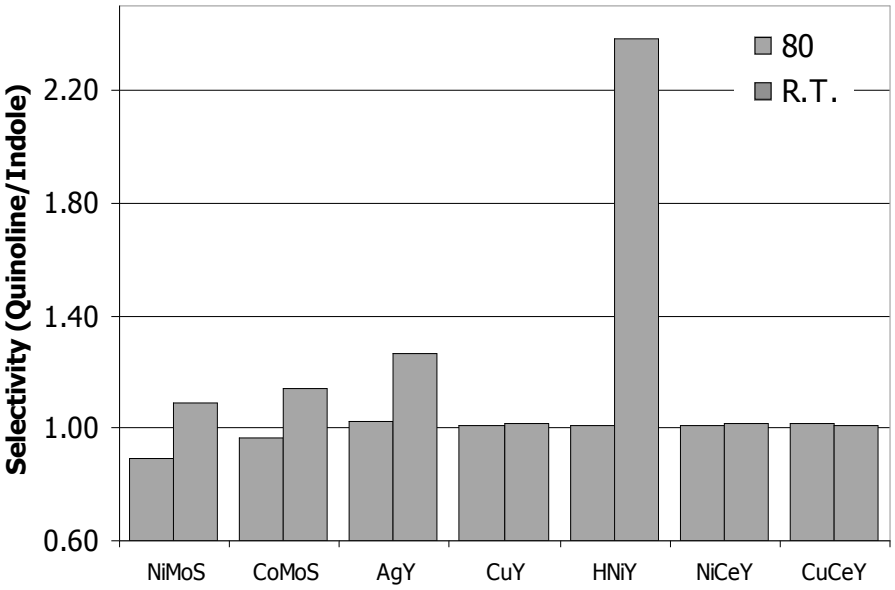

Figure 16. The selectivity between quinoline and indole over several adsorbents after denitrogenation.

Table 11. The capacity of nitrogen compounds over several adsorbents in batch system

	Capacity (mg-N/g)						Quinoline/Indole ratio	
	Quinoline		Indole		Total			
	80ºC	RT	80ºC	RT	80ºC	RT	80ºC	RT
NiMoS	2.5	2.5	2.9	2.4	5.4	4.9	0.9	1.1
CoMoS	2.7	2.6	2.9	2.3	5.6	4.9	1.0	1.1
AgY	3.0	2.2	3.0	1.6	6.0	3.8	1.0	1.3
CuY	3.0	3.0	3.0	3.0	6.0	6.0	1.0	1.0
HNiY	3.0	2.9	3.0	1.0	6.0	3.9	1.0	2.4
NiCeY	3.0	3.0	3.0	3.0	6.0	6.0	1.0	1.0
CuCeY	3.0	3.0	3.0	3.0	6.0	6.0	1.0	1.0

[1] The data in parenthesis indicate the nitrogen capacity at room temp.

As shown in the present results, Cu, CuCe and NiCe/Y-zeolite were the best adsorbent for nitrogen compounds (quinoline and indole) among the tested adsorbents. All of the zeolite-based adsorbents tested in this study were in oxidic state because they were not further treated after calcination. If they will be taken reduction pretreatment, they could have better adsorption property. At adsorptive denitrogenation in flow system, they were pretreated with He at 350 °C for 1 h for reduction. The better performance of CuCe and NiCe/Y-zeolite might be due to the synergistic interaction of Ce with Cu or Ni.

3.1.2.4. Adsorptive Denitrogenation in Flow System

Figure 17 shows the adsorption breakthrough of nitrogen concentration over zeolite-based adsorbents, Ni based adsorbents, activated alumina and activated carbon adsorbents.

The activated alumina and activated carbon showed better adsorption property for nitrogen compounds than zeolite-based adsorbents. **Table 12** shows the adsorption

capacity of nitrogen and sulfur on zeolite-based, Ni-based, activated alumina and activated carbon adsorbents.

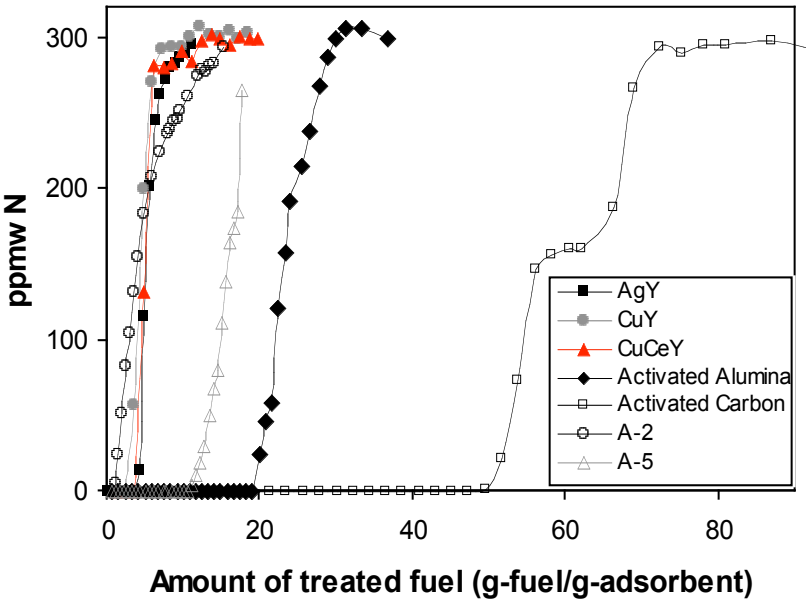

Figure 17. Breakthrough of nitrogen concentration on several adsorbents in flow system.

Table 12. The adsorption capacity on several adsorbents in flow system

	Adsorption capacity (mg/g)			Breakthrough volume of fuel (g-fuel/g)
	Nitrogen	Sulfur		
CuCeY	1.0	1.6[1]	(2.2)[2]	3.4
CuY	0.7	0.7	(1.2)	2.2
AgY	1.1	0.04	(0.5)	3.5
Activated Alumina	5.7	1.0	(2.2)	19.0
Activated Carbon	14.3	2.8	(16.3)	47.2
A-2	0.1	0.0	(0.3)	0.5
A-5	3.2	1.8	(3.2)	10.6

[1]Breakthrough capacity of sulfur until S compounds breakthrough
[2]Saturation capacity of sulfur until N compounds breakthrough

The breakthrough volume for activated carbon was 47.2 g-fuel/g and was much higher than those for the activated alumina, zeolite-based and Ni-based adsorbents. The

zeolite-based adsorbents had breakthrough volume of fuel less than 4.0 g-fuel/g. However, A-5 (Ni/Si-Al) had better adsorption property than the zeolite-based adsorbents as shown in **Table 12**.

In the adsorption capacity of nitrogen, the activated carbon had nitrogen capacity of 14.3 mg-N/g and the activated alumina had nitrogen capacity of 5.7 mg-N/g. Other adsorbents had around or less than 1.0 mg-N/g except A-5 which had nitrogen capacity of 3.2 mg-N/g. Based on this result, the activated carbon is the promising adsorbent for adsorptive denitrogenation.

One interesting thing over the activated carbon is two steps adsorption while the activated alumina and other adsorbents did not show this adsorption property. The nitrogen concentration over the activated carbon was steady for a while around 150 ppmw N after the fuel treatment of 55 g-fuel/g and then increased rapidly again after the fuel treatment of 60 g-fuel/g. The first breakthrough came from the adsorption of one of nitrogen compounds in model fuel and then the concentration increased until around 150 ppmw N. After analysis of the sample fuels by GC-FID, the first breakthrough was due to quinoline. The second step increase of nitrogen compounds appeared when indole was detected by GC-FID. Therefore, the activated carbon favors the adsorption of indole more than that of quinoline.

Figure 18 shows the breakthrough of sulfur compounds in the model fuel over zeolite-based, Ni-based, activated alumina and activated carbon adsorbents. The breakthrough of sulfur compounds appeared earlier than that of nitrogen compounds over all adsorbents in this study. It meant that the adsorption capacity of sulfur was much less

than that of nitrogen due to less adsorption strength of the sulfur compounds (DBT and DMDBT) than the nitrogen compounds (quinoline and indole).

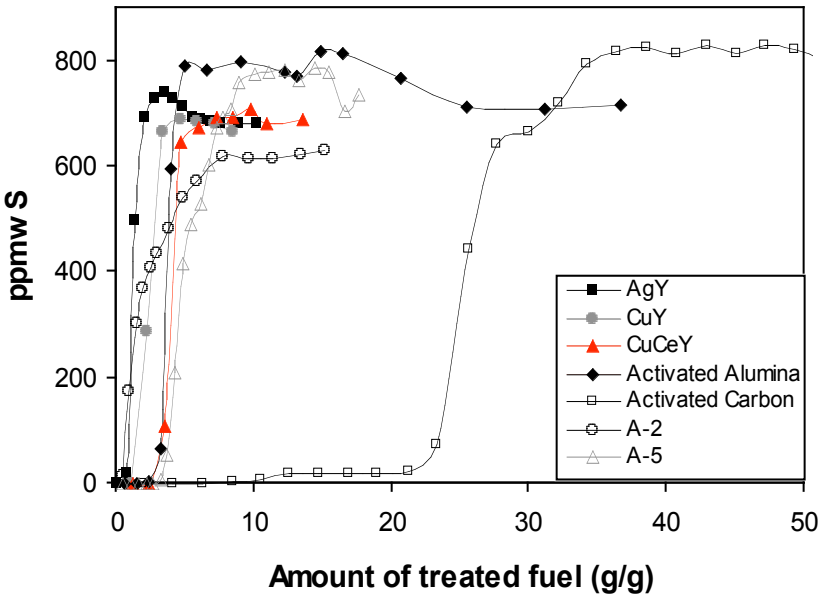

Figure 18. Breakthrough of sulfur concentration on several adsorbents in flow system.

The capacity of sulfur on the zeolite-based adsorbents was less than 1.0 mg-S/g except CuCe/Y-zeolte which had the sulfur capacity of 1.6 mg-S/g as shown in **Table 12**. This result is very similar to the previous results in batch system at room temperature. In the batch system at room temperature, Ag/Y-zeolite showed very low capacity of nitrogen compounds, especially of indole. The capacity of sulfur on Ag/Y-zeolite and Cu/Y-zeolite were 0.04 mg-S/g and 0.7 mg-S/g, respectively. However, CuCe/Y-zeolite had the sulfur capacity of 1.7 mg-S/g. It seems the Ce modification on Cu/Y-zeolite as mentioned in chapter 3.1.2.1. The capacity of sulfur on the activated carbon was 2.8 mg-S/g and higher than that on the zeolite-based, Ni-based and the activated alumina (1.0 mg-S/g). These sulfur capacity are much less than the nitrogen capacity in this study. It was expected the capacity of sulfur might be less in simultaneous adsorptive

denitrogenation and desulfurization than in only adsorptive desulfurization because some nitrogen compounds adsorb stronger on surface than sulfur compounds. The adsorption strength could represent reactivity in catalytic reaction. Most of basic nitrogen compounds, which have high basicity and high electron density on aromatic rings, have higher reactivity than sulfur compound. It may mean that they have higher adsorption strength than the latter. Therefore, they can inhibit the hydrodesulfurization of sulfur compounds in fuels. Quinoline and indole are very reactive nitrogen compounds due to their electronic properties in molecular.

The sulfur concentrations on Ag/Y-zeolite, A-5 (Ni-Al), activated alumina and activated carbon increased by around 800 ppmw S after the breakthrough of sulfur compounds that was higher than the initial concentration (686 ppmw S). The higher sulfur concentration returned to the initial sulfur concentration when nitrogen compounds were saturated on the surface of adsorbents. It means that some of sulfur and nitrogen compounds adsorbed same adsorption sites and nitrogen compounds helped elute out sulfur compounds on some adsorption sites because of their higher adsorption strength. It was similar phenomena on the adsorption of only sulfur compounds with sulfide adsorbents in our previous study [48]. DBT eluted out 4,6-DMDBT because the former adsorbed stronger on sulfide adsorbents than the latter.

As shown in this study, activated carbon is excellent adsorbent for adsorptive desulfurization as well as adsorptive denitrogenation. Therefore the activated carbon is the promising adsorbent for adsorption denitrogenation and desulfurization.

In the denitrogenation of a commercial diesel by Hernández-Maldonado and coworker [49], meanwhile, a thin guard bed of activated carbon (15% of the bed) for

Cu/Y-Zeolite extended the sorbent capacity of the main bed by adsorbing the largest molecules from the fuels and the sulfur capacity was also increased by about 20% for the desulfurization [50]. Based on the results in our group, activated carbon might have better adsorption properties than their zeolite-based adsorbents. In the desulfurization by Zhou and coworkers [51], activated carbon showed very excellent adsorption capacity of sulfur compounds in a model fuel and a commercial diesel as compared with other zeolite-based adsorbents that were prepared in our group.

Carbon materials have been used for adsorption of gas and liquid phases due to several merits related to surface properties. In the literature by Montes-Morán and coworkers [52], the important properties of activated carbon for adsorption behavior are the porous structure and surface chemistry that are determined by its raw material, activation process. The pore system of activated carbon is mainly consisted of micropore (≤2nm), mesopore (2 nm~50nm), macropore (>50nm), surface area is mainly contributed by micropore system. The micropore is more active to adsorption, but mesopore play important role in transferring adsorbates to active sites in surface of micropore. Among the surface groups on activated carbon, the acidic groups (carboxyl, lactone, phenol, lactol and so on) probably play an important role in adsorptive denitrogenation because some of nitrogen compounds have basic properties could interact with surface acidic groups. In the adsorptive denitrogenation by Sano and coworkers [53], it was also mentioned that the adsorption capacities of carbon materials for nitrogen species in gas oil are strongly dependent on their surface properties. The most important functional group of activated carbon to adsorb the nitrogen species is the CO producing group during temperature programmed desorption (TPD), whereas the CO_2 liberating group

seems to inhibit the adsorption of the nitrogen species. For clarifying the strong relationship of adsorptive denitrogenation and desulfurization with carbon materials, the extensive analysis of their surface properties is necessary.

3.1.3. Summary

3.1.3.1. Hydrodesulfurization of 4,6-DMDBT

1) Nitrogen compound, quinoline was a very strong inhibitor on 4,6-DMDBT HDS and 1THQ, which was main product from quinoline hydrogenation, was also strong inhibitor. The reaction rate of 4,6-DMDBT was still slow when quinoline was converted to 1THQ over 85%. This is because 1THQ is also a basic nitrogen compound which is a strong inhibitor to HDS reaction on the catalysts. In kinetic study, quinoline significantly inhibited both reaction pathways over NiMo and CoMo sulfide catalyst. The loss of hydrodesulfurization activity was significantly for HYD pathway and DDS pathway. Therefore, deep hydrodesulfurization needs more nitrogen tolerance catalysts than traditional NiMo and CoMo sulfide catalysts.
2) The NiMo catalyst, which was prepared on mesoporous support, MCM-41, was more active on 4,6-DMDBT HDS than NiMo/Al_2O_3 catalysts, but still not better than commercial CoMo and NiMo catalysts. The surface area of MCM-41 reduced significantly after the calcination of Mo/MCM-41, which was prepared at first step. Therefore, it is necessary to improve a metal impregnation method to avoid pore destruction or this mesoporous support to be stable at high temperature.

3.1.3.2. Adsorptive Denitrogenation for Deep Hydrodesulfurization

1) At the adsorption denitrogenation in batch system, Cu, CuCe and NiCe/Y-zeolite were the best adsorbent for nitrogen compounds (quinoline and indole) among the tested zeolite-based adsorbents. The better performance of CuCe and NiCe/Y-zeolite might be due to the synergistic interaction of Ce with Cu or Ni.
2) Cu and CuCe/Y-zeolite were selected for adsorptive denitrogenation in flow system according to the batch system results. CuCe/Y-zeolite showed better adsorption property of nitrogen and sulfur compounds than Cu/Y-zeoltie due to the synergistic interaction of Cu with Ce as mentioned in the batch system results. However, the zeolite-based adsorbents had very low nitrogen and sulfur capacity as compared with activated alumina and activated carbon. Among the tested adsorbents, activated carbon showed the best adsorption properties of nitrogen and sulfur compounds. It seems to be because carbon materials have very unique the surface properties and pore structure for adsorption behavior. Therefore, activated carbon may be a promising adsorbent for adsorptive denitrogenation and desulfurization.

3.1.4. Future work

3.1.4.1 Development of Deep Hydrodesulfurization Catalysts

1. New catalyst, such as NiMo/MCM-41 and metal phosphide, with improved catalytic performance for simultaneous deep desulfurization and deep denitrogenation will be explored, and compared with commercial HDS and HDN catalysts. Tests will be conducted using a high-pressure fixed-bed flow reactor. RCO-LCO blends (with

RCO:LCO ratios ranging from 3:1 to 1:1) will be used along with some model feeds containing sulfur, nitrogen and aromatics for fundamental comparison study.

2. To better understand the catalytic mechanism for deep desulfurization and deep denitrogenation and to develop new high performance catalysts, kinetic studies for the HDS and HDN reaction pathways, i.e., hydrogenation pathway and hydrolysis pathway, will be investigated.

3.1.4.2 Adsorptive Denitrogenation for Deep Hydrodesulfurization

a. High quality adsorbent which can selectively removal nitrogen compound from RCO/LCO will also be further explored. These adsorbents include zeolite/molecular sieve based material, carbon materials, metals and metal oxides, etc.
b. For further detail adsorption properties and selectivity of aromatic, sulfur and nitrogen compounds, each compounds contained in the model fuel will be analyzed by GC-FID.
c. Based on adsorptive denitrogenation of model fuel, adsorptive denitrogenation of LCO and RCO will be performed on activated carbon and modified carbon adsorbents at same adsorption conditions.
d. The desulfurization of the fuel streams from the RCO/LCO blends after adsorption removal of nitrogen compound will also be carried out and compared with that of RCO/LCO blends without pre-removal of nitrogen compounds.

Subtask 3.2. Saturation of Two-Ring Aromatics

As a part of the DOE refinery integration project, this sub-task aims at saturating aromatics for high-quality diesel and jet fuels. High aromatics content in distillate fuels is undesirable since it lowers the fuel quality and contributes to the formation of environmentally harmful emissions [54, 55]. In general, lower aromatics content leads to increased thermal stability, improved combustion characteristics and less soot formation. The conventional method of dearomatization is by aromatics saturation (hydrogenation) [54]. Typically, sulfided Co-Mo/Al_2O_3 or Ni-Mo/Al_2O_3 catalysts are employed for hydrogenation. However, these catalysts are most active at higher temperatures where equilibrium limitations may prevent complete hydrogenation. Noble-metal catalysts are active at lower temperatures, where equilibrium limitations can be overcome, however sulfur-tolerance is a major obstacle to their commercial application.

To meet the fuel performance and compositional specifications for diesel fuel, it is necessary for both RCO and LCO to be hydrogenated [56, 57]. This work focuses on the development of increasingly sulfur-tolerant, noble-metal catalysts for the low-temperature hydrotreating and dearomatization (LTHDA) of distillate fuels for the production of ultra-clean and low-aromatic diesel fuels. The objectives of this work are to examine the effects of the structure of catalyst support and the influence of metal species and bimetallic combinations on low-temperature dearomatization.

3.2.1 Experimental

3.2.1.1 Catalyst Preparation

In order to examine the effects of support type and structure of pore channels, a series of catalysts was prepared using Palladium as the metal on various supports. Support types used included Y zeolite, mordenite, HZSM-5, alumina, titania, and the mesoporous alumnosilicate of MCM-41 type. Each catalyst was prepared using the incipient wetness impregnation (IWI) technique, with $PdCl_2$ as the metal precursor. In all cases, the nominal metal loading was 2 wt% Pd, and HCl was added to form soluble Pd species. A summary of all relavent catalyst supports used is found in **Table 13.**

Table 13 Properties of Selected Catalyst Supports

Catalyst	Support Type	Support Code	Surface Area (m^2/g)	SiO_2/Al_2O_3 Ratio
Pd/HY(30)	Y Zeolite	CBV720	780	30
Pd/HY(80)	Y Zeolite	CBV780	780	80
Pd/HM(90)	Mordenite	CBV90A	500	90
Pd/HM(20)	Mordenite	CBV21A	500	20
Pd/HZSM-5(80)	ZSM-5	CBV8014	425	80
Pd/Al_2O_3	Alumina	UOP	170	-
Pd/TiO_2	Titania	Degussa P25	71	-
Pd/MCM-41(50)	Al-MCM-41(50)	MCM-41(50)	1289	50

3.2.1.2 Experimental

A fixed-bed, flow reactor has been designed and constructed to carry out low-temperature dearomatization experiments. It was determined that tetralin (1,2,3,4-tetrahydronaphthalene) be used as a model aromatic compound in this study because it has been shown that saturation of the second aromatic ring is more difficult and rate-limiting in the total hydrogenation process. As a model compound for diesel fuel,

hexadecane (cetane) is used as a carrier for the feedstock. Nonane is added as an internal standard for GC/MS analysis. Feedstock composition for the dearomatization experiments is 20 wt% tetralin, 75 wt% hexadecane and 5 wt% nonane, with ppm quantities of sulfur, as benzothiophene (BT), added for certain experiments.

For each experiment, 0.5g of catalyst was used. To this is added 3.0g of α-alumina as a diluent, and the catalyst/diluent is packed in the reactor. Prior to each experiment, catalysts are reduced in-situ under a flow of 100 mL/min hydrogen. The pressure is maintained at 100 psi. The temperature program is as follows: Beginning at room temperature, the temperature is increased at a rate of 2°C/min until the temperature reaches 225°C. The temperature is then maintained at 225°C for 2 hours before the pressure is increased to the reaction pressure of 600 psi. When the reaction pressure is reached, the hydrogen flowrate is decreased to 80 mL/min and the liquid feed is started. The liquid flowrate is 0.08 mL/min. This corresponds to a WHSV of approximately $8hr^{-1}$ and a gas-to-liquid ratio of approximately 1000. Reaction and reduction conditions are summarized in **Table 14**. For this study, the concentration of sulfur in the feedstock was either 37 ppm or 100 ppm sulfur as benzothiophene (BT).

3.2.2 Results and Discussion

A comparison of experiments performed using a zeolite support (CBV780) compared with the amorphous supports alumina and titania is shown in **Figure 19**. It can be seen that zeolite supports clearly have the potential to achieve increased sulfur-tolerance compared with conventional amorphous supports.

Table 14 Reduction and Reaction Conditions

	Reduction	Reaction
Temperature:	25°C - 2°C/min - 225°C - 120 min @ 225°C	225°C
Pressure:	100 psi	600 psi
Hydrogen Flowrate:	100 mL/min	80 mL/min
Liquid Flowrate:	-	0.08 mL/min
WHSV:	-	~8 hr^{-1}
G/L:	-	1000

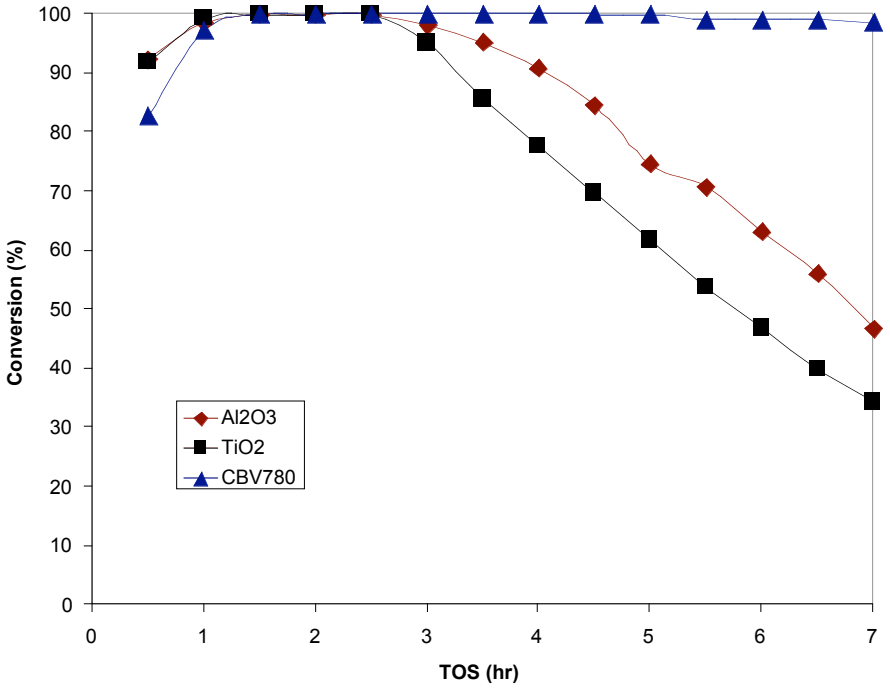

Figure 19 Conversion vs. TOS for the hydrogenation of tetralin over Pd catalysts on various supports at 225°C and 600 psig hydrogen pressure in the presence of 100 ppm benzothiophene.

The product distribution can yield potentially valuable information about the hydrogenation reaction of tetralin to decalins. The primary products are a mixture of trans- and cis-decalins. It is convenient to examine the ratio of trans- to cis-decalin. **Figure 20** shows the t-DHN/c-DHN ratio for the catalyst series CBV780/Al_2O_3/TiO_2. It

can be seen that as deactivation due to sulfur proceeds, the selectivity towards the product t-DHN decreases. This was observed with all of the Pd catalysts tested.

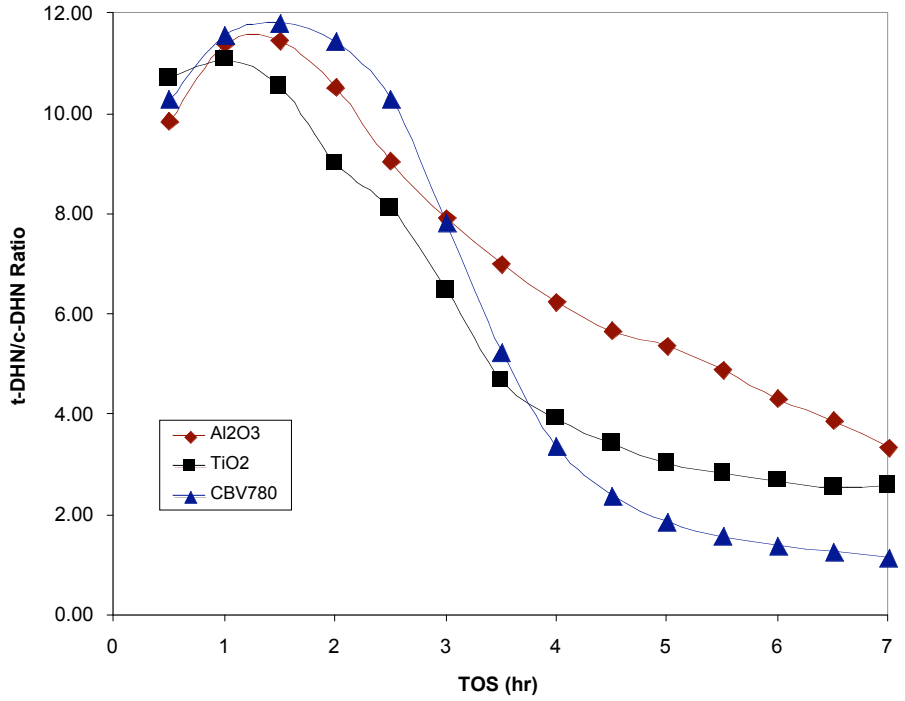

Figure 20 t-DHN to c-DHN ratio as a function of TOS for the hydrogenation of tetralin over Pd catalysts on various supports at 225°C and 600 psig hydrogen pressure in the presence of 100 ppm benzothiophene.

The results of hydrogenation experiments on various zeolite supports are shown in **Figure 21**. It is evident that zeolite structure has a significant impact on the sulfur tolerance of Pd catalysts. Under the reaction conditions and methods of catalyst preparation used in this study, Y-zeolite-supported catalysts exhibited the highest sulfur tolerance. It is interesting to note that the two mordenite-supported catalysts (CBV21A and CBV90A) performed almost identically, despite having much different SiO_2/Al_2O_3 ratios. It is thought that perhaps the more acidic support (as indicated by a lower SiO_2/Al_2O_3 ratio) might exhibit a higher sulfur tolerance due to a greater electron deficiency on the supported Pd metal particle [58], however, this was not observed in this

study. In fact, the Y-zeolite with the higher SiO_2/Al_2O_3 ratio (CBV780) performed better than its more acidic counterpart (CBV720) (See **Figure 19 and Figure 21**).

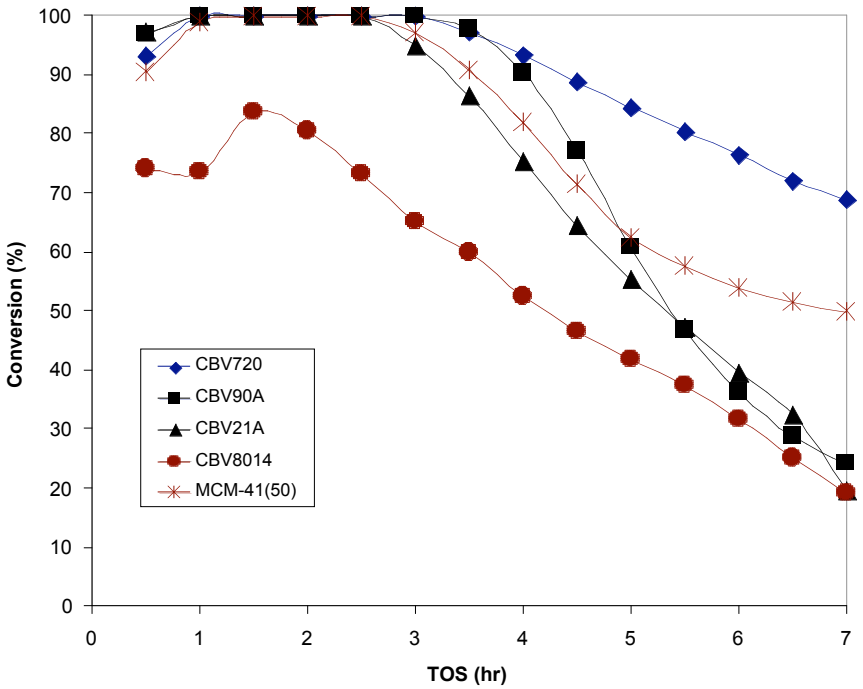

Figure 21 Conversion vs. TOS for the hydrogenation of tetralin over Pd catalysts on various supports at 225°C and 600 psig hydrogen pressure in the presence of 100 ppm benzothiophene.

The t-DHN/c-DHN ratios were also observed to be almost identical among the two mordenite supports, as shown in **Figure 22.** It is also seen in **Figure 22** that the selectivity towards t-DHN decreases as deactivation due to sulfur poisoning proceeds. It also appears that the t-DHN/c-DHN ratio is more sensitive to sulfur poisoning than is the conversion. This is more clearly illustrated in **Figure 23**, where the conversion and t-DHN/c-DHN ratio are shown on the same figure. Perhaps this is because isomerization sites are more susceptible to sulfur poisoning than hydrogenation sites.

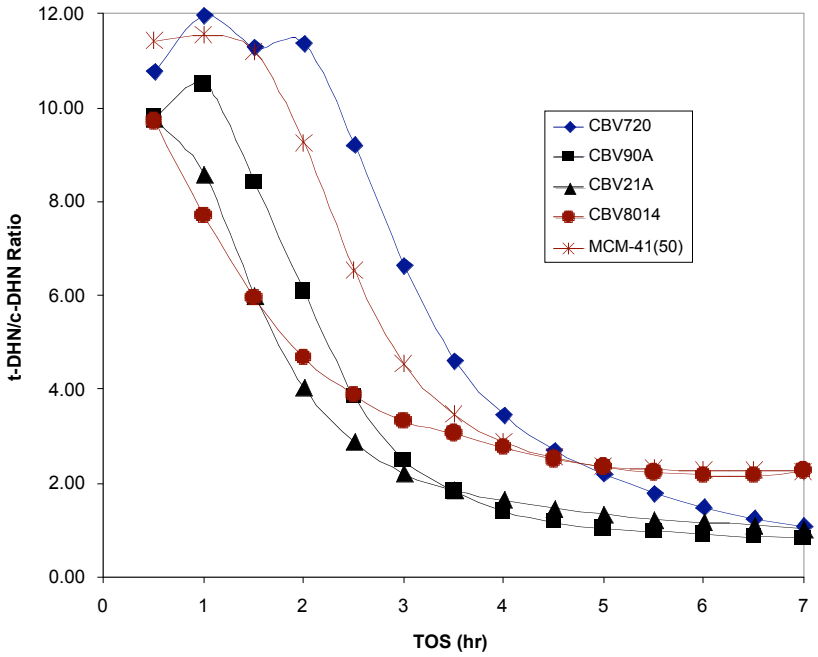

Figure 22 t-DHN to c-DHN ratio as a function of TOS for the hydrogenation of tetralin over Pd catalysts on various supports at 225°C and 600 psig hydrogen pressure in the presence of 100 ppm benzothiophene.

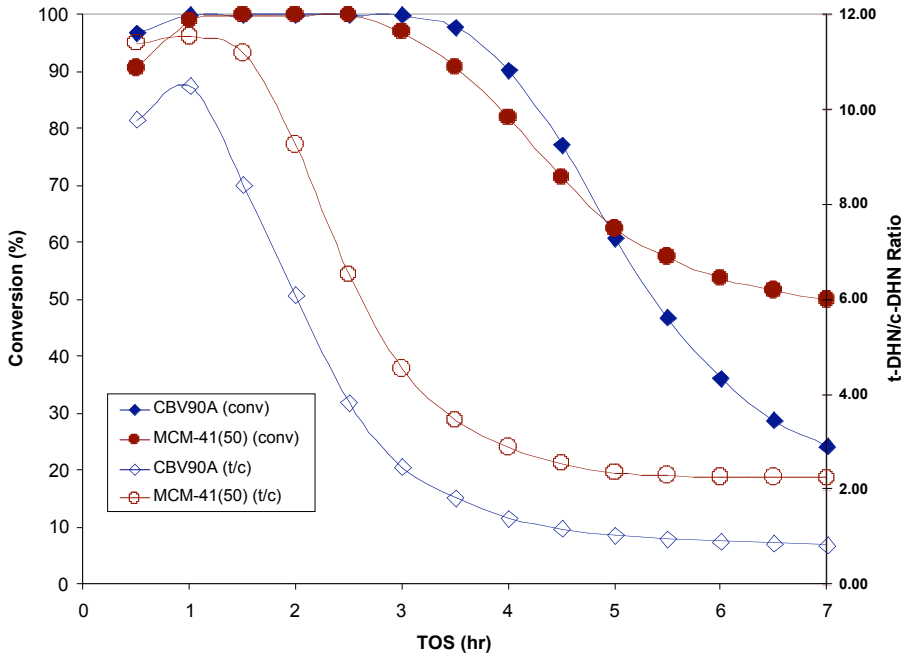

Figure 23 Conversion and t-DHN/c-DHN ratio vs. TOS for the hydrogenation of tetralin over Pd catalysts on CBV90A and MCM-41(50) supports at 225°C and 600 psig hydrogen pressure in the presence of 100 ppm benzothiophene.

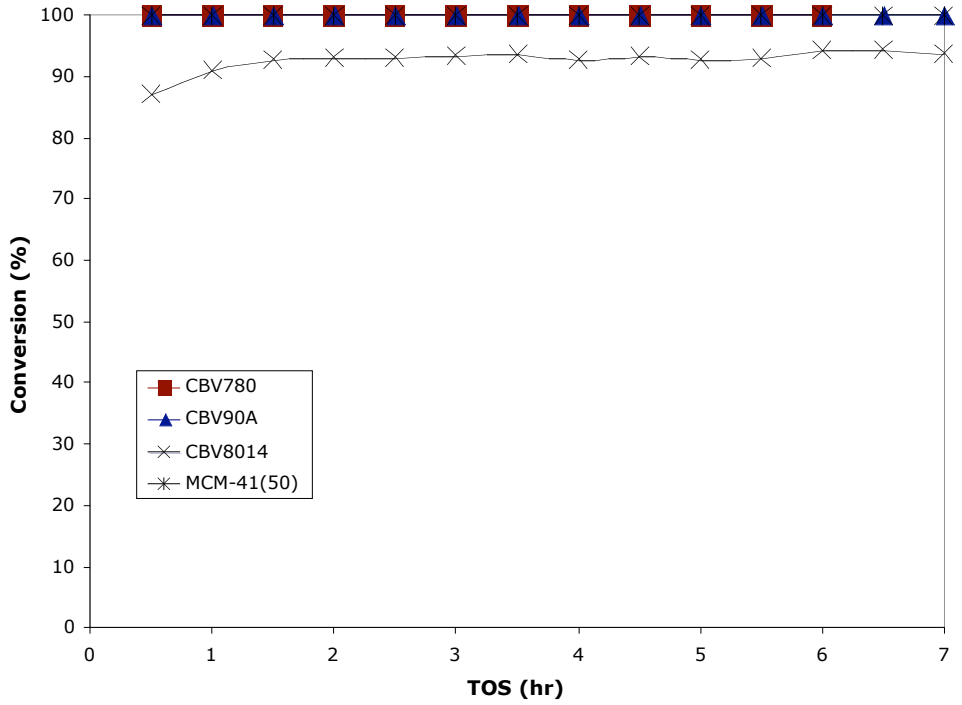

Figure 24 Hydrogenation of tetralin over Pd catalysts on various supports at 225°C and 600 psig hydrogen pressure in the presence of 37 ppm benzothiophene.

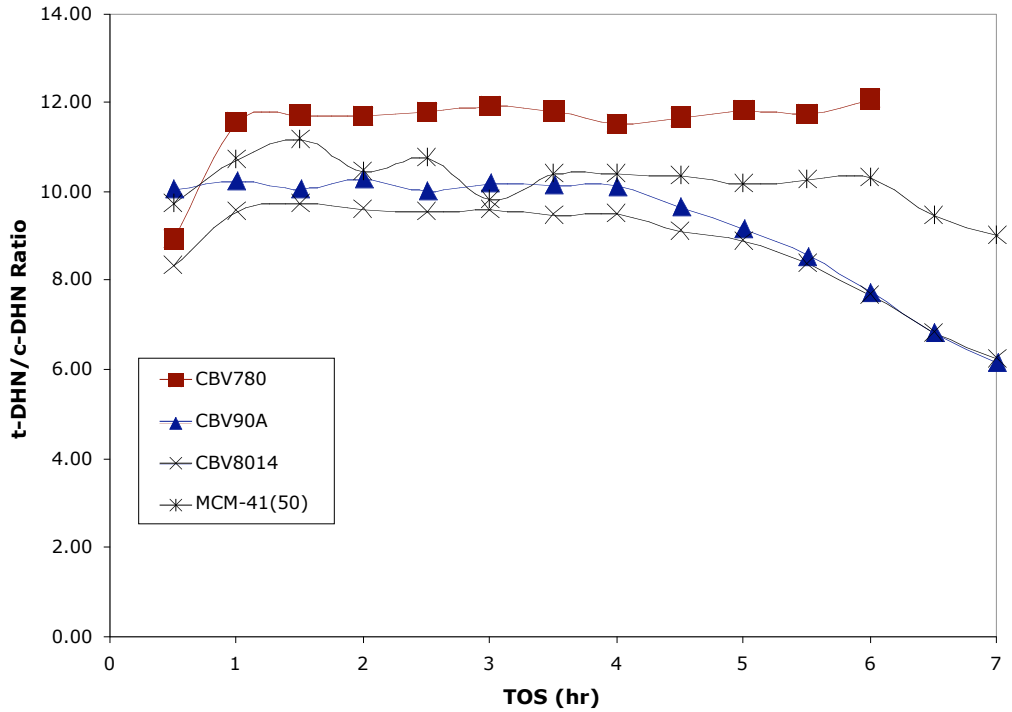

Figure 25 t-DHN to c-DHN ratio as a function of TOS for the hydrogenation of tetralin over Pd catalysts on various supports at 225°C and 600 psig hydrogen pressure in the presence of 37 ppm benzothiophene.

Experiments conducted using a feedstock with 37 ppm sulfur did not prove to be as useful as those conducted at 100 ppm. As shown in **Figure 24 and Figure 25**, the conversion was maintained at nearly 100% for all catalysts tested with this feedstock. However, a decrease in t-DHN/c-DHN ratio is observed, even though no deactivation is apparent by examining only the conversion.

3.2.3 Summary

A fixed-bed flow reactor was designed and constructed to carry out dearomatization experiments. A series of catalysts were prepared using Palladium as the active metal on various supports, including Y zeolite, mordenite and mesoporous aluminosilicate MCM-41, for the purposes of examining the effect of support type and structure of support pore channels. Dearomatization experiments were conducted using

the catalysts prepared. The initial experiments were conducted at a temperature of 225°C under a hydrogen pressure of 600 psi. The WHSV was approximately 8 hr^{-1} and the hydrogen to liquid ratio was approximately 1000. The feedstock contained 37 ppm or 100 ppm sulfur (as benzothiophene).

Based on the hydrogenation experiments conducted at 225°C and 600 psi hydrogen pressure, in the presence of benzothiophene, the following conclusions can be made:

- Zeolite structure has a significant impact on the sulfur tolerance of Pd catalysts.
- Y-zeolite-supported catalysts were shown to exhibit higher sulfur-tolerance than any of the other catalysts tested, with the conditions used for catalyst preparation.
- The effect of support acidity (as indicated by SiO_2/Al_2O_3 ratio) remains to be determined.
- As deactivation due to sulfur proceeds, the selectivity toward t-DHN decreases.
- The t-DHN/c-DHN ratio is more sensitive to sulfur poisoning than is the conversion.

3.2.4 Future Work

New catalysts with improved catalyst performance and sulfur resistance are currently being synthesized, characterized and tested. Some of these catalysts use other noble metals, such as Pt, Ru and Ni, as the active metal. Bimetallic catalysts with combinations of these metals will also be prepared and tested. Commercial hydrogenation catalysts will also be obtained and tested for comparison. With the aid of modern characterization methods, such as, XRD, N_2 adsorption/desorption, TPD, TPR, XPS, FT-IR, acidity measurement, TEM, etc., the effect of site distribution of noble

metals in different structures, the acidity of the molecular sieve support and the structure of support pore channels to the activity and sulfur tolerance of the dearomatization will be clarified. This allows us to design next generation dearomatization catalyst with better catalytic activity and better sulfur tolerance in years 3-4. Once the effects of all factors studied have been determined and the most promising catalysts have been identified, desulfurized and denitrogenated RCO and LCO will be used as the feedstock for dearomatization.

Subtask 3.3. Value-Added Chemicals from Naphthalene and Biphenyl

It is important to point out that refinery produces not only fuels, but also chemical feedstock for the chemical process industry that generate useful products such as plastics, fibers, and rubbers. While the bulk of RCO and LCO can be processed to make advanced thermally stable jet fuels, a part of the aromatics can be used for making value-added aromatic chemicals. Recent studies [59, 60] indicate that high-value chemicals can be obtained by selective conversion of polycyclic hydrocarbons such as naphthalene, biphenyl, and phenanthrene, over some zeolite catalysts. The products of such selective reactions are specialty chemicals, monomers of advanced polymer materials such as high-performance polyesters, advanced engineering plastics, and liquid crystalline polymers.

Chemical analyses of RCO and LCO clearly indicate that naphthalene is the representative structure of aromatics in these fractions, and at least over 60 % of RCO and LCO are aromatic components that have the naphthalene structure. Because 2,6-dialkylnaphtahlene is the intermediate of monomer for making engineering plastics such as polyethylene naphthalate, polybutylene naphthalate and liquid crystalline, selective

alkylation of naphthalene to 2,6-dialkylnaphtahlene is a highly value-added reaction. However, most literature studies deal with isopropylation. But methylation is more desirable for industrial applications although methylation is more difficult [61]. To realize the shape-selective methylation of naphthalene to produce 2,6-dimethylnaphthalene (2,6-DMN), shape-selective zeolite catalyst for selective reaction of naphthalene with methanol inside the channel was proposed. In this report period, a fixed bed flow reaction system for the methylation of naphthalene to produce 2,6-DMN was set up. The effect of types of zeolites and $SiO_2/Al2O_3$ ratio of zeolites on the methylation of 2-methylnaphthalene (2-MN) were investigated. Preliminary experiments on the modification of ZSM-5 zeolite were explored as high performance 2-MN methylation catalyst.

3.3.1. Experimental

3.3.1.1 Catalysts

Four types of zeolites, i.e., HY, H-Beta, H-Mordenite (HM) and HZSM-5, were used as catalysts. The $SiO_2/Al2O_3$ ratio of HY, H-Beta, H-Mordenite and HZSM-5 are 80, 50, 90 and 80, respectively. HZSM-5 with different the $SiO_2/Al2O_3$ ratio of 50, 80 and 280, respectively, were also tested. All the zeolite samples were obtained from Zeolyst International. Details on the physical properties of the catalyst are listed in **Table 15**. Zeolites with ammonium form were calcined at 450 ^oC for 6 hours to convert to hydrogen form.

Iron-substituted ZSM-5 was prepared by modifying the HZSM-5 (CBV5524G) with iron fluoride (FeF_3) and ammonium hydrogen fluoride (NH_4HF_2) at elevated

temperature. In a typical process, a solution containing 0.086 g of FeF_3 and 0.068 g of NH_4HF_2 was dissolved in 100 ml of deionized water to provide a solution having a molar ratio of FeF_3 to NH_4HF_2 of 2:3. This solution was added with rapid agitation over one hour at temperature 90-95 ^oC to a 10 weight percent slurry in water of HZSM-5. The slurry contained 5 g of HZSM-5 material. This mixture was refluxed for 24 hours, filtered, washed with deionized water, dried for 12 hours at 110 ^oC, and calcined at a temperature of 450 ^oC for 5 hours. Different iron sources, i.e., iron nitrate ($Fe(NO_3)_3$), and different fluorine source, i.e., ammonium fluoride (NH_4F), were used in the preparation of iron-substituted ZSM-5. In one experiment, the iron-containing ZSM-5 zeolite was prepared by mixing 5 g of HZSM-5, 0.086 g of FeF_3 and 0.068 g of NH_4HF_2. This mixture was calcined at 450 ^oC for 5 hours. The details on the catalysts and their corresponding preparation condition were listed in **Table 16**.

3.3.1.2 Catalyst Evaluation

Catalytic testing was carried out in a down-flow fixed bed reactor system as shown in **Figure 26**. In a typical run, 0.3 gram catalyst (10-18 mesh) loaded in reactor tube (Pyrex, I.D.: ½ inch) was placed in the furnace center. The catalyst was activated at 450 ^oC for 1 h under the inert N_2 gas flow (20 ml/min). Then the temperature was cooled down to the reaction temperature of 300 ^oC. Reactant dissolved in mesitylene solvent (2-methylnaphalene:methanol:mesitylene=1:5:5 mol ratio) was fed into reactor through a HPLC pump at the flow rate of 1.98 ml/min together with 20 ml/min carrier N_2 gas flow. The reaction product was collected at 1 hour interval. Both the reactants and products were analyzed by HP 5890 gas chromatography (GC) with a β-Dex 120 capillary column

(60m, 0.25 mm I.D. column with 0.25 micrometer coating film thickness). The ratio of 2,6-DMN/2,7-DMN will be determined and used as a key parameter to evaluate catalyst selectivity feature.

Table 15 Physical properties of the catalysts

Catalyst Type	Support Code	Na_2O (wt%)	Surface Area (m^2/g)
HY	CBV780	0.03	780
H-Beta	CP814Q	0.05	725
HM	CBV90A	0.05	500
NH_4ZSM-5	CBV8014	0.05	425
NH_4ZSM-5	CBV5524G	0.05	425
NH_4ZSM-5	CBV28014	0.05	400

Table 16 Iron modified ZSM-5 catalysts and their corresponding preparation conditions.

Catalyst ID	Preparation Method	Iron Source	Fluoride Source
M-Fe-01	Substitute	FeF_3	NH_4HF_2
M-Fe-11	Physical Mixture	FeF_3	NH_4HF_2
M-Fe-12	Substitute	$Fe(NO_3)_3$	NH_4HF_2
M-Fe-14	Substitute	FeF_3	NH_4F

Figure 26 Picture of the flow reaction system.

3.3.2 Results and Discussion

3.3.2.1 Types of zeolites on the methylation of 2-MN

Various large-pore (HY, H-Beta, and HM) zeolite and medium-pore (HZSM-5) zeolite were tested for the methylation of 2-MN. The changes in 2-MN conversion, 2,6-DMN selectivity and 2,6-DMN/2,7-DMN ratio with time on stream are shown in **Figure 27**. The initial reactivity of the catalysts decreases in the following order: HM>HY>HZSM-5. However, HY and HM deactivates faster than HZSM-5. HZSM-5 also shows a higher 2,6-DMN selectivity and 2,6-DMN/2,7-DMN ratio than HY and HM. Low 2,6-DMN selectivity and 2,6-DMN/2,7-DMN ratio of HY and H-M is believed to be caused by the large pore-port of these zeolites, which easily accommodate many competitive reaction product molecules, e.g., DMN isomers, ethylnaphthalene (EN) and trimethyl naphthalene, etc, and allow their rapid diffusion. Similar trend was reported in

the literature [62, 63]. Therefore, HZSM-5 shows a better catalytic effect on the methylation of 2-MN than the HY, H-beta and HM. In the following studies, we will focus on the ZSM-5 zeolite and its analogues.

3.3.2.2 SiO_2/Al_2O_3 Ratio of HZSM-5 on the Methylation of 2-MN

Besides the pore size, acidity also plays an important role on the methylation of 2-MN. The acidity of zeolites is generally determined by their SiO_2/Al_2O_3 ratio. The effect of SiO_2/Al_2O_3 ratio of HZSM-5 on the methylation of 2-MN was also investigated. **Figure 28** show the changes in conversion, 2,6-DMN selectivity and 2,6-DMN/2,7-DMN ratio with time on stream. HZSM-5 with SiO_2/Al_2O_3 ratio of 80 shows the highest and most stable catalytic activity among the HZSM-5 zeolites investigated. When the SiO_2/Al_2O_3 ratio of HZSM-5 is low, the catalyst has a strong acidity and therefore causes the quick coke deposition. The catalyst deactivates faster than that with high SiO_2/Al_2O_3 ratio. When the SiO_2/Al_2O_3 ratio of HZSM-5 is high, the catalyst has a weak acidity. Therefore, the catalytic activity for methylation of 2-MN is lower than that of the catalyst with low SiO_2/Al_2O_3 ratio. 2,6-DMN selectivity and 2,6-DMN/2,7-DMN ratio show a similar trend. HZSM-5 with medium acidity, i.e., SiO_2/Al_2O_3 ratio of 80, shows the best 2,6-DMN selectivity and highest 2,6-DMN/2,7-DMN ratio among the HZSM-5 zeolites investigated.

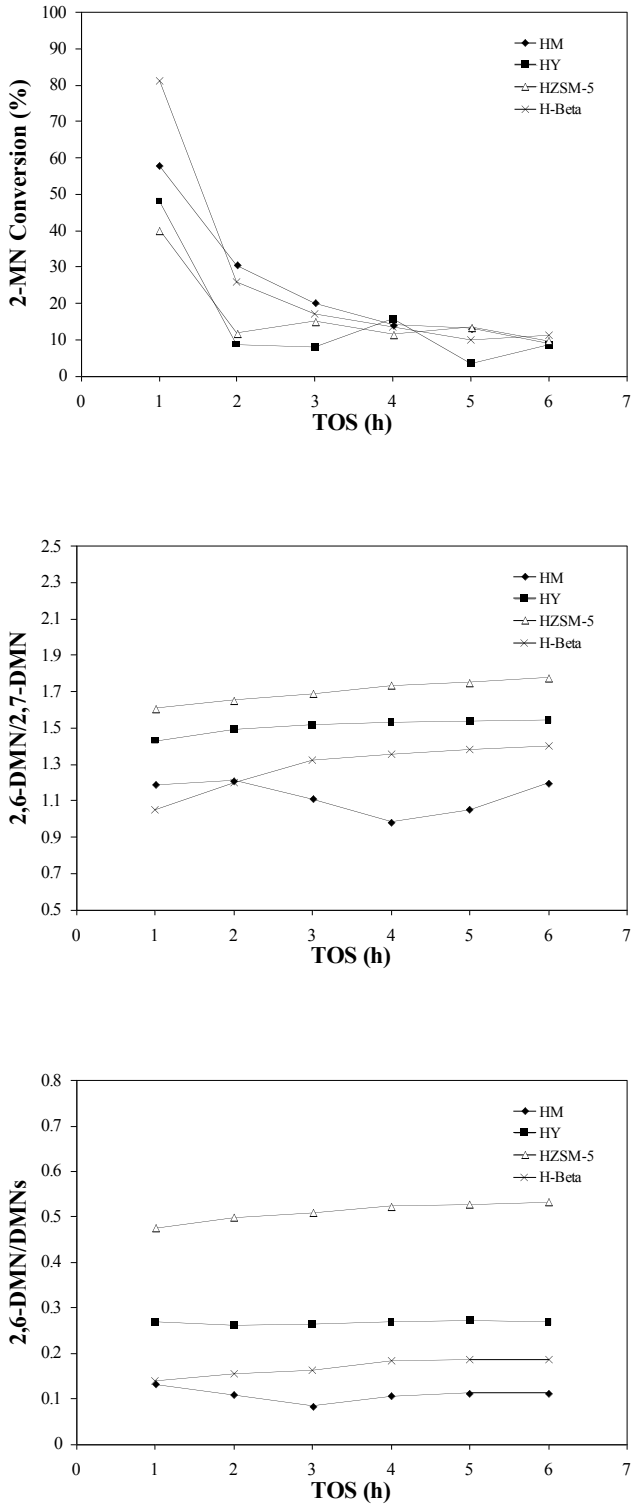

Figure 27 Effect of catalyst type in methylation of 2-MN with methanol. Reaction condition: temperature: 300 ^{o}C; Feed (2-MN:methanol: mesitylene=1:5:5 mol ratio): 1.98 ml/hr; Catalyst: 0.3 gram; Gas flow: 20 ml/min

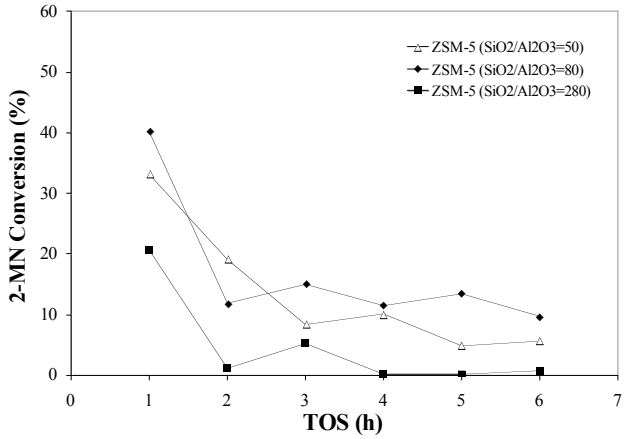

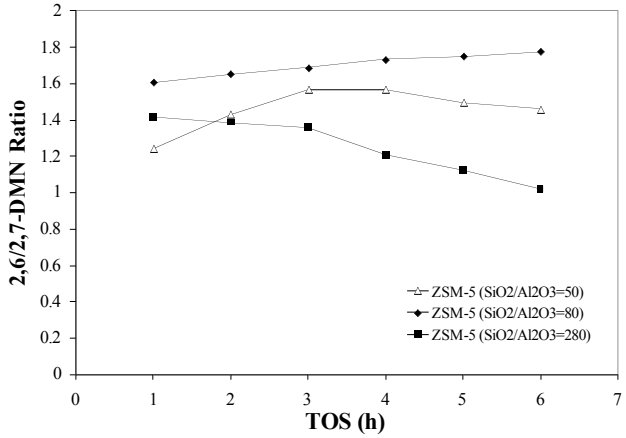

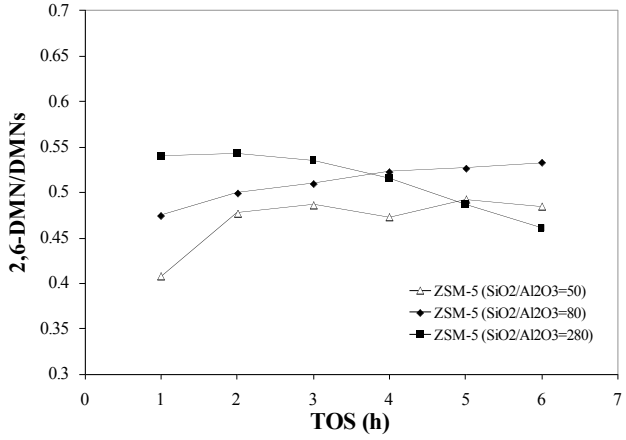

Figure 28 Methylation of 2-MN with methanol over HZSM-5 zeolite with different SiO_2/Al_2O_3 ratio. Reaction conditions: temperature: 300 ^oC; Feed (2-MN:methanol: mesitylene=1:5:5 mol ratio): 1.98 ml/hr; Catalyst: 0.3 gram; Gas flow: 20 ml/min

The 2,6-DMN selectivity and 2,6-DMN/2,7-DMN ratio increases with time on stream for HZSM-5 with SiO_2/Al_2O_3 ratio of 50 and 80, while the 2,6-DMN selectivity and 2,6-DMN/2,7-DMN ratio decreases with time on stream for HZSM-5 with SiO_2/Al_2O_3 ratio of 280.

3.3.2.3 Iron modification of HZSM-5 on the Methylation of 2-MN

3.3.2.3.1 Effect of Iron Modification

Figure 29 compares the conversion, DMN yield, 2,6-DMN/2,7-DMN ratio and DMN distributions for the HZSM-5 catalyst and Iron-substitute ZSM-5 molecular sieve catalyst (M-Fe-01). Although the 2-MN conversion slightly decreased, the DMN yield and 2,6-DMN/2,7-DMN ratio, which are the key parameters to evaluate the performance of the catalyst, substantially increased. It indicated that the catalytic performance of HZSM-5 was improved after modified with iron. Compared the DMN distribution, the formation of 2,6-DMN was promoted, while the formation of 1,2-, 1,6-, 1,7-, DMNs was inhibited, after the HZSM-5 was modified with iron. The amount of 1,6-, 1,7-, DMNs for M-Fe-01 was even below the detection limit of GC analysis. The formation of 1,3-, (2,3+1,4)-, 2,7-, DMNs remains almost unchanged. 1,5-DMN did not form for both catalysts. Therefore, the increase in 2,6-DMN/2,7-DMN ratio was mainly caused by inhibiting the formation of 1,2-, 1,6-, 1,7-, DMNs and promoting the formation of 2,6-DMN.

3.3.2.3.2 Effect of Preparation Method

Two different catalyst preparation methods, i.e., physical mixture and wet-chemistry substitution, were employed for the preparation of iron-modified MFI

molecular sieve catalyst. Their catalytic performance was compared in **Figure 30**. The catalyst prepared by physical mixing method (M-Fe-11) showed a lower catalytic activity than HZSM-5 and a higher catalytic activity than M-Fe-01. The yield of DMNs for M-Fe-11 is similar with that for M-Fe-01 and higher than that for HZSM-5. However, its 2,6-DMN/2,7-DMN ratio was close to HZSM-5 and significantly lower than M-Fe-01. For DMN distribution, 2,6- and 2,7- DMNs for M-Fe-11 did not change as compared with those for HZSM-5. This is the reason that 2,6-DMN/2,7-DMN ratio for M-Fe-11 was similar with that for HZSM-5. Therefore, the wet-chemistry substitution method was a better method than the physical mixing method.

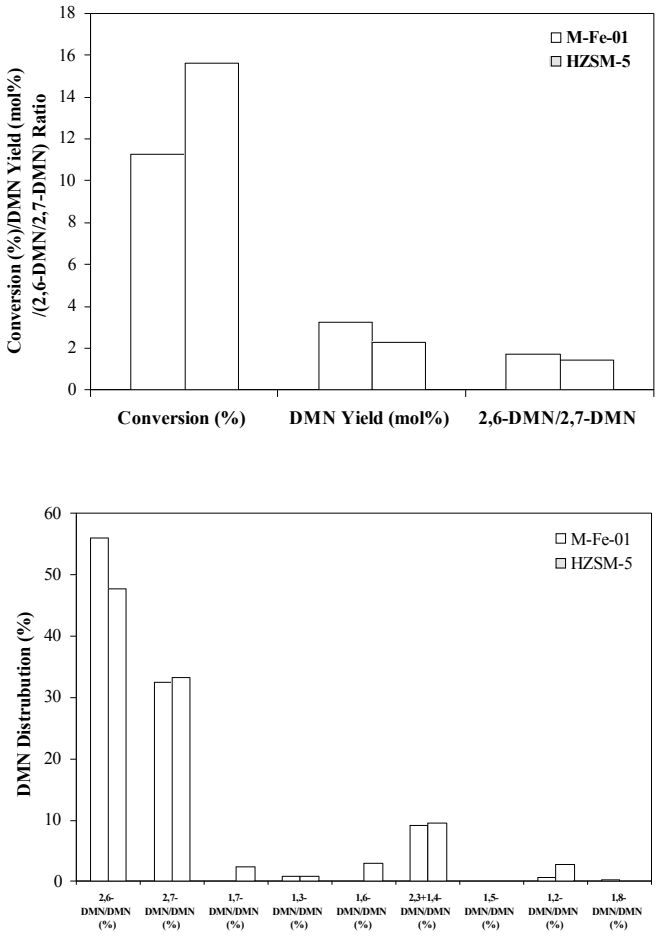

Figure 29 Methylation of 2-MN with methanol over HZSM-5 zeolite and Iron-substitute ZSM-5 molecular sieve catalyst (M-Fe-01). Reaction conditions: temperature: 300 ^{o}C; Feed (2-MN:methanol: mesitylene=1:5:5 mol ratio): 1.98 ml/hr; Catalyst: 0.3 gram; Gas flow: 20 ml/min

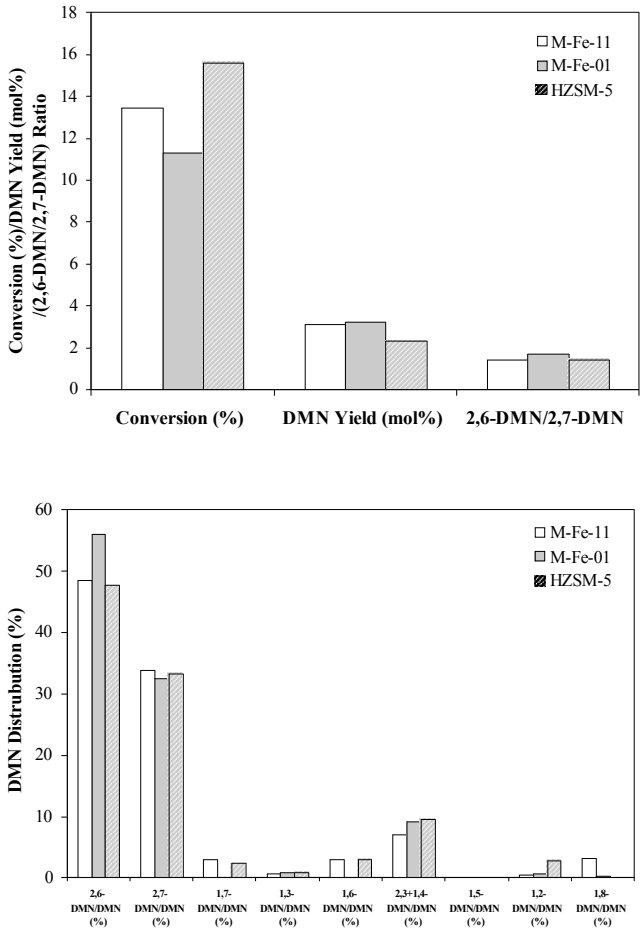

Figure 30 Effect of preparation method on the methylation of 2-MN with methanol over Iron-substitute ZSM-5 molecular sieve catalysts. Reaction conditions: temperature: 300 ^{o}C; Feed (2-MN:methanol: mesitylene=1:5:5 mol ratio): 1.98 ml/hr; Catalyst: 0.3 gram; Gas flow: 20 ml/min

3.3.2.3.3 Effect of Iron Source

Two iron sources, i.e., iron fluoride (FeF_3) and iron nitrate ($Fe(NO_3)_3$), were used for the preparation of iron-modified MFI molecular sieve catalyst by wet chemistry method. Their catalytic performance was compared in **Figure 31**. The catalyst prepared with $Fe(NO_3)_3$ (M-Fe-12) showed a higher catalytic activity than M-Fe-01. The catalytic activity of M-Fe-12 was even higher than the HZSM-5. The yields of DMNs for M-Fe-12 was slightly lower than M-Fe-01. However, it was still significantly higher than that for

HZSM-5. The 2,6-DMN/2,7-DMN ratio for M-Fe-12 was in between that for HZSM-5 and M-Fe-01. For DMN

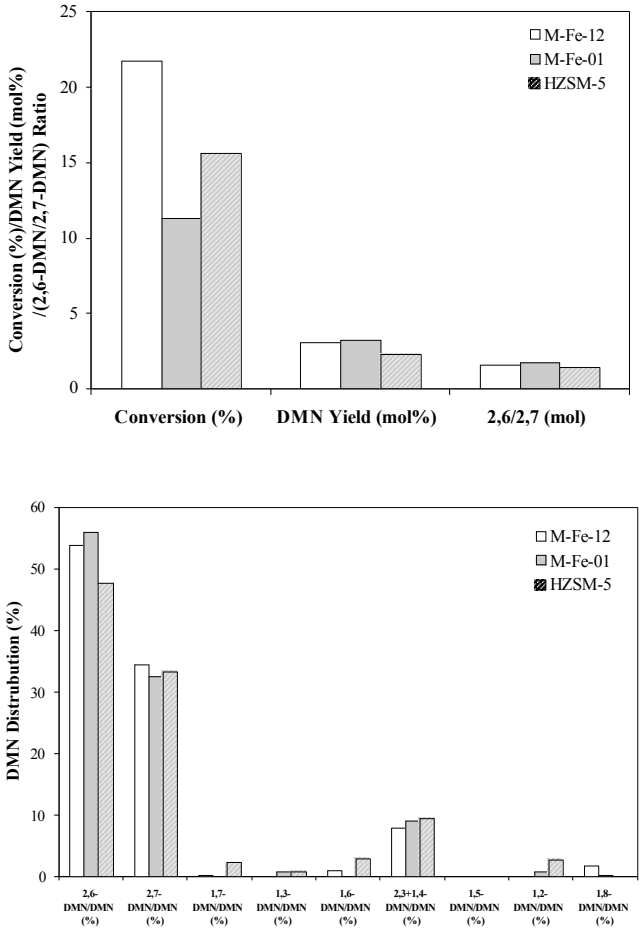

Figure 31 Effect of iron source on the methylation of 2-MN with methanol over Iron-substitute ZSM-5 molecular sieve catalysts. Reaction conditions: temperature: 300 ^{o}C; Feed (2-MN:methanol: mesitylene=1:5:5 mol ratio): 1.98 ml/hr; Catalyst: 0.3 gram; Gas flow: 20 ml/min

distribution, 2,6-DMNs yield for M-Fe-12 increased as compared with that for HZSM-5. However, the increase in 2,6-DMNs yield was less for M-Fe-12 than for M-Fe-01. The formation of 1,2-, 1,6-, 1,7-, DMNs was inhibited, which was similar with M-Fe-01. However, while the formation of 1,6-, 1,7-, DMNs for M-Fe-01 was fully inhibited

(below the detection limit of GC analysis), 1,6-, 1,7-, DMNs still synthesized for M-Fe-12 . The formation of 1,3-, (2,3+1,4)-, 2,7-, DMNs remains almost unchanged.

3.3.2.2.4 Effect of Fluorine Source

Two fluoride sources, i.e., ammonium hydrogen fluoride and ammonium fluoride, were used for the preparation of iron-modified MFI molecular sieve catalyst by wet chemistry method. Their catalytic performance was compared in **Figure 32**. The catalyst prepared with NH_4F (M-Fe-14) showed a significant higher catalytic activity than HZSM-5 and M-Fe-01. However, both the yields of DMNs and the 2,6-DMN/2,7-DMN ratio for M-Fe-14 was lower than those for M-Fe-01, which was prepared with NH_4HF_2. The yields of DMNs and the 2,6-DMN/2,7-DMN ratio were even lower than those for HZSM-5. The change of DMN distribution for M-Fe-14 catalyst was also opposite to that for M-Fe-01. 2,6-,

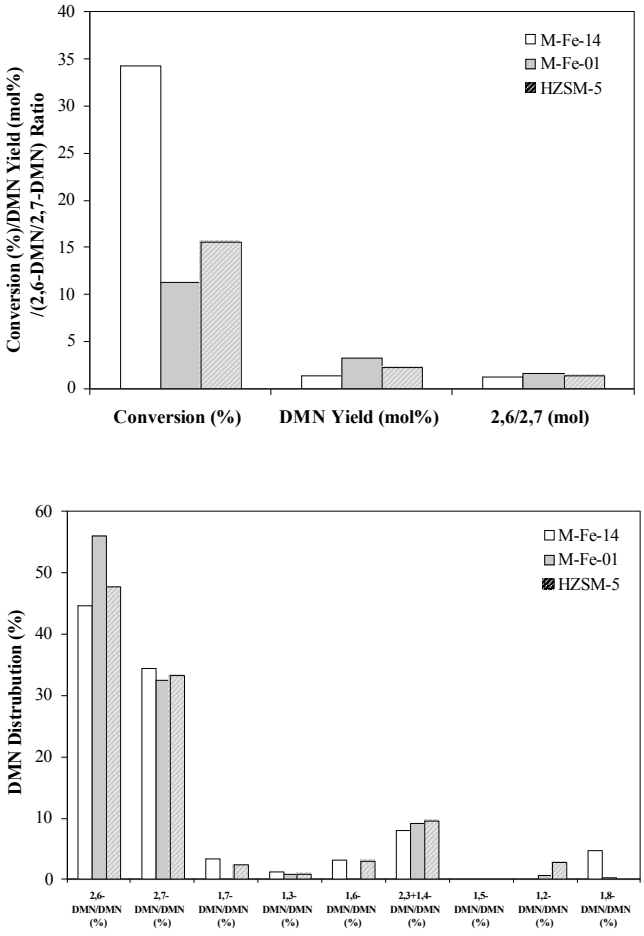

Figure 32 Effect of fluoride source on the methylation of 2-MN with methanol over Iron-substitute ZSM-5 molecular sieve catalysts. Reaction conditions: temperature: 300 ^{o}C; Feed (2-MN:methanol: mesitylene=1:5:5 mol ratio): 1.98 ml/hr; Catalyst: 0.3 gram; Gas flow: 20 ml/min

1,2-, (2,3+1,4)-, DMNs yield for M-Fe-12 decreased; 1,3-, 1,6-, 1,7- and 2,7- DMNs yield slightly increased; and only 1,8-DMN yield increased, as compared with those for HZSM-5. Therefore ammonium hydrogen fluoride was a better fluoride source for the preparation of iron-substituted MFI molecular sieve catalyst than ammonium fluoride.

3.3.3 Summary

1. HZSM-5 zeolite with medium pore size is a better catalyst than the HY, HM or H-Beta zeolites with large pore size for the selective methylation of 2-MN with methanol to produce 2,6-DMN; HZSM-5 with moderate acidity shows the best reaction activity, catalyst stability and 2,6-DMN selectivity.
2. Iron-modified MFI molecular sieve catalyst shows a better catalytic performance on the selective methylation of 2-MN to 2,6-DMN. Both the 2,6-DMN yield and 2,6-DMN/2,7-DMN selectivity are improved after the HZSM-5 zeolite catalyst is modified with iron.
3. For the modification of HZSM-5 with iron, wet chemistry substitution method is a better method than the physical mixing method; ammonium hydrogen fluoride is a better fluoride source than ammonium fluoride. The iron source shows different effect on activity and selectivity. The catalyst modified with iron nitrate shows a higher activity while the catalyst modified with iron fluoride shows a higher 2,6-DMN/2,7-DMN selectivity.

3.3.4 Future work

In year 2, we intend (1) to further explore new catalyst formulation with improved catalyst performance; (2) to identify the active species of transition metal in the selected catalyst; (3) to quantify the acidic sites on both the external and internal structures that are accessible to the reactant molecules and catalytically active, and attempt to passivate the non-selective sites on the external particle surfaces of molecular sieve catalysts, and (4) finally to clarify the relationship among acid property (strength, site, etc), transition metal species, pore structure and catalyst performance (activity and selectivity). MFI

molecular sieve catalyst with different Fe/Al ratio, different transition metal species, different iron status (isomorphrous substitute or bulk species) and different preparation methods will be prepared and tested for methylation of 2-MN with methanol. Acidity of the MFI type molecular sieves will be modified with base organic or inorganic compounds. To selectively passivate the non-selective acid sites on the external surface, organic or inorganic compounds with molecular size larger than the pore size of MFI type molecular sieve will be used. Catalysts will also be characterized by NMR, XPS, TEM, SEM, XRD, TGA, FT-IR, TPR, TPD, TEOM, selective adsorption separation of 2,6/2,7 and acidity measurements, etc., to measure the pore structure of the molecular sieve catalyst, to identify the active status (species) of transition metal, and to quantify the acidic sites on both the external and internal structures. Finally, the catalytic performance (in terms of activity and selectivity) of the molecular sieve catalyst will be related to the pore structure of the molecular sieve catalyst, the active status (species) of transition metal and to acidic properties. This would allow more selective synthesis of value-added chemicals from naphthalene and biphenyl.

Task 4. Evaluation of Coal-Based Fuel Oil Products

(Prepared by Bruce G. Miller, Sharon Falcone Miller and Ronald T. Wincek)

The objective of the Task 4 activities was to evaluate the effect of introducing coal into an existing petroleum refinery on the fuel oil product. The activities included analyzing a petroleum-based commercial heavy fuel oil, characterizing its atomization performance, and measuring its combustion performance and emissions, specifically major, minor, and trace elements when fired in a watertube boiler designed for natural gas/fuel oil. The No. 6 fuel oil used to generate the baseline data was obtained from an east coast supplier. A coal-based fuel oil product was not available during Year 1; therefore, activities focused on establishing the analytical/testing protocols using the baseline fuel oil in preparation of coal-based fuel oil testing to be performed in Year 2. This was especially necessary since it was found that not only is there insufficient information on major, minor, and trace elements in fuel oil, but there are few commercial laboratories that can satisfactorily analyze fuel oil for these constituents. It was found that using commercial laboratories is problematic and must be done with caution.

Subtask 4.1 Fuel Analysis

The No. 6 fuel oil used in the combustion and emissions tests was analyzed by a series of ASTM and other analytical procedures (**Table 16**). The analyses were performed to generate baseline data in order to compare commercial/petroleum-based fuel oil with the fuel oil produced during co-processing in Year 2. Analyses were selected that could be used to compare the co-processed fuel oil with a petroleum-based

commercial fuel oil. Specifically, they will be used to: 1) ensure that the samples meet standardized fuel oil specifications [64]; 2) determine the quantity of trace elements in the co-processed fuel oil; and 3) classify the co-processed fuel oil per established specifications [64].

The results are provided in **Table 17** with the exception of the major, minor, and trace element analyses (which are discussed in Section 4.1.1). The analysis provides a baseline composition to compare to co-processed fuels in Year 2. The baseline fuel oil, as observed in Table 1, is a typical No. 6 fuel oil based on conventional analyses.

Table 17. Analysis of the No. 6 Fuel Oil used in the Combustion/Emission Tests

Characteristic	ASTM Method	Value
Relative Density, 60/60°F	ASTM D 1298-97 e2	0.975 g/ml
Relative Density, 60/60°F, API	ASTM D 1298-97 e2	13.63° API
Viscosity, 100°F	ASTM D 445-03	3,195 ssu
Viscosity, 130°F	ASTM D 445-03	990 ssu
Viscosity, 210°F	ASTM D 445-03	138 ssu
Total Sulfur	ASTM D 4239-04a	0.93% (wt/wt)
Water	ASTM D 1796-97 (2002)	0% (vol/vol)
Sediment	ASTM D 1796-97 (2002)	0% (vol/vol)
Ash	ASTM D 482-03	0.06% (wt/wt)
Higher Heating Value	ASTM D 240-02	18,714 Btu/lb
Higher Heating Value	ASTM D 240-02	152,272 Btu/gal
Total Carbon	ASTM D 5373-02	87.12% (wt/wt)
Total Hydrogen	ASTM D 5373-02	11.44% (wt/wt)
Total Nitrogen	ASTM D 5373-02	0.22% (wt/wt)

4.1.1. Major, Minor, and Trace Elemental Analysis

It is necessary to quantify the emissions of inorganic hazardous air pollutants (IHAPs) during combustion of commercial fuel oil and heavy fuel oil produced during co-processing. This is especially important with the recent promulgation of national emission standards for hazardous air pollutants (NESHAP) for industrial, commercial,

and institutional boilers and process heaters [65]. Small (< 10 million Btu/h firing rate) and large (> 10 million Btu/h firing rate) units are affected.

It became apparent that it was necessary to develop an analytical protocol when determining the inorganic chemical analysis of oils since there is limited information available and there are few commercial laboratories that can satisfactorily analyze fuel oils for major, minor and trace elements, which are not traditionally present in fuel oils. Oils generally contain inorganic elements at the trace level. The most prominent elements are heavy metals such as vanadium and nickel. However, the introduction of coal as a feedstock in co-processing with petroleum will likely increase the amounts of other elements as well as trace elements (some classified as IHAPs) in the product. These metals could ultimately be present in stack emissions.

Traditionally, solid fuels are easily digested and analyzed via inductively coupled plasma atomic adsorption spectroscopy (ICP), cold vapor atomic adsorption spectroscopy (CVAAS) and graphite furnace atomic adsorption spectroscopy (GFAAS). Liquid fuels are not so easily analyzed due to their combustive nature in analytical techniques, which use flame spectroscopy. In addition, many of the elements traditionally analyzed in coal are not routinely analyzed in oil as they are either not present or present in minute quantities. It was decided that the oil would be analyzed by a commercial lab that routinely handles combustible liquids. The advantage of this is that any industry would have access to such a lab and that the analysis procedure would meet industry standards. The No. 6 fuel oil was sent to Staveley Services/CTC Analytical Services, Portland, OR for analysis. Duplicate fuel oil samples were analyzed in addition to NIST Standard Reference Material (SRM) 2722 (Mercury in Crude Oil-Heavy Sweet). Analysis of the

No. 6 fuel oil is given in **Table 18**. Analyses were conducted according to ASTM Method D5184 (Standard Test Methods for Determination of Aluminum and Silicon in Fuel Oils by Ashing, Fusion, Inductively Coupled Plasma Atomic Emission Spectrometry, and Atomic Absorption Spectrometry (ICP AAS)) [66].

Table 18. Chemical Analysis of the No. 6 Fuel Oil

Element	No. 6 Fuel Oil-1 (ppm)	No. 6 Fuel Oil-2 (ppm)
Al	34.0	31.6
As	3.63	<0.01
Ba	0.38	0.73
Be	NA	NA
Cd	0.27	0.2
Co	NA	NA
Cr	0.12	0.03
Cu	0.16	0.96
Hg	0.59	0.13
Mn	0.15	0.39
Mo	0.07	0.01
Ni	40.5	44.6
Pb	0.12	0.6
Sb	NA	NA
Se	1.40	2.18
Sr	NA	NA
V	116	129
Zn	1.46	2.08

NA - Not available

There is some question as to the accuracy of the fuel oil analysis since there is some discrepancy in the concentration reported for the two samples, *i.e.*, As, Hg, Cr, and Pb. In addition, the Hg concentration reported for the NIST SRM was 1,240 ppb; however, the certified value for the SRM is 129.2 ppb. It is no surprise that the Hg data was incorrect given that the commercial lab used ICP AAS to analyze for Hg. Traditionally, mercury is best analyzed by CVAA. ICP MS has also been used for mercury analysis. The poor agreement of As concentration can also be attributed to the

fact that As is best analyzed by GFAAS. We are finalizing the protocol to perform appropriate analyses in our lab, which will be used in Year 2 of the project.

While the analysis of the fuel oil is not ideal, it does not compromise the emissions data. It does limit our ability, however, to perform a material balance with confidence.

Subtask 4.2 Fuel Atomization

In this subtask, measurements of the atomization performance for the baseline No. 6 fuel oil were performed using a commercial fuel oil gun. It is expected that the quality of atomization will influence the combustion performance and emissions because the droplet size affects the subsequent rate of oil volatilization and combustion downstream of the atomizing nozzle. To quantify the atomization performance, a type-T oil gun manufactured by Faber Burner Company in Lock Haven, Pennsylvania was selected. The oil gun was used to evaluate the atomization quality for the baseline fuel oil and the subsequent combustion testing. A diagram of the Faber oil gun is provided in **Figure 33**.

A type SLC internal-mix atomizer was connected to the outlet end of the oil gun, which was drilled out to an angle of 30°. This spray angle was chosen to prevent impingement of the oil droplets on the refractory-lined burner throat (quarl) during the subsequent combustion testing. It is also important that the spray angle be chosen such that the fuel droplets are entrained in the swirling combustion air stream. This ensures that they are brought in contact with oxygen in the preheated air as well as with the hot recirculated products of combustion. The combination of oil gun and atomizer used in

this study was designed to atomize lighter fuel oils (No. 2, 4, and 5) in addition to the heavier No. 6 fuel oil.

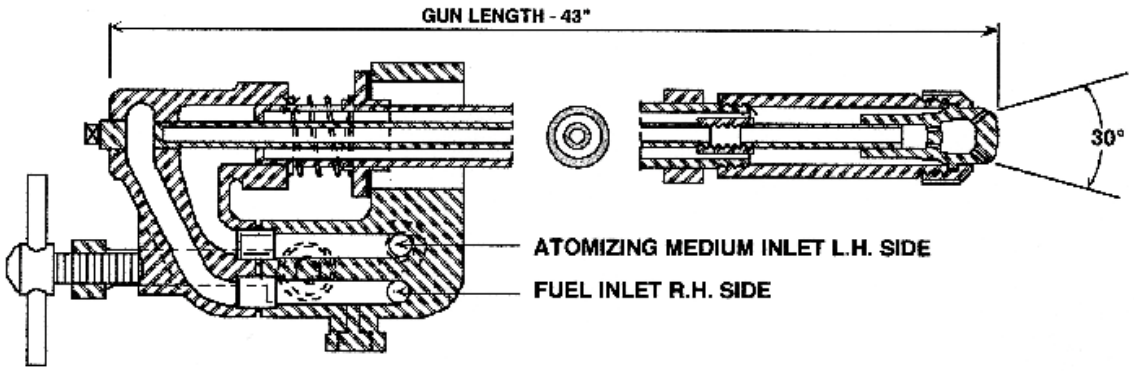

Figure 33. Schematic diagram of the Faber oil gun.

An atomization test facility (ATF) was used to measure the atomization characteristics of the baseline No. 6 fuel oil. A sketch of the ATF is given in **Figure 34**.

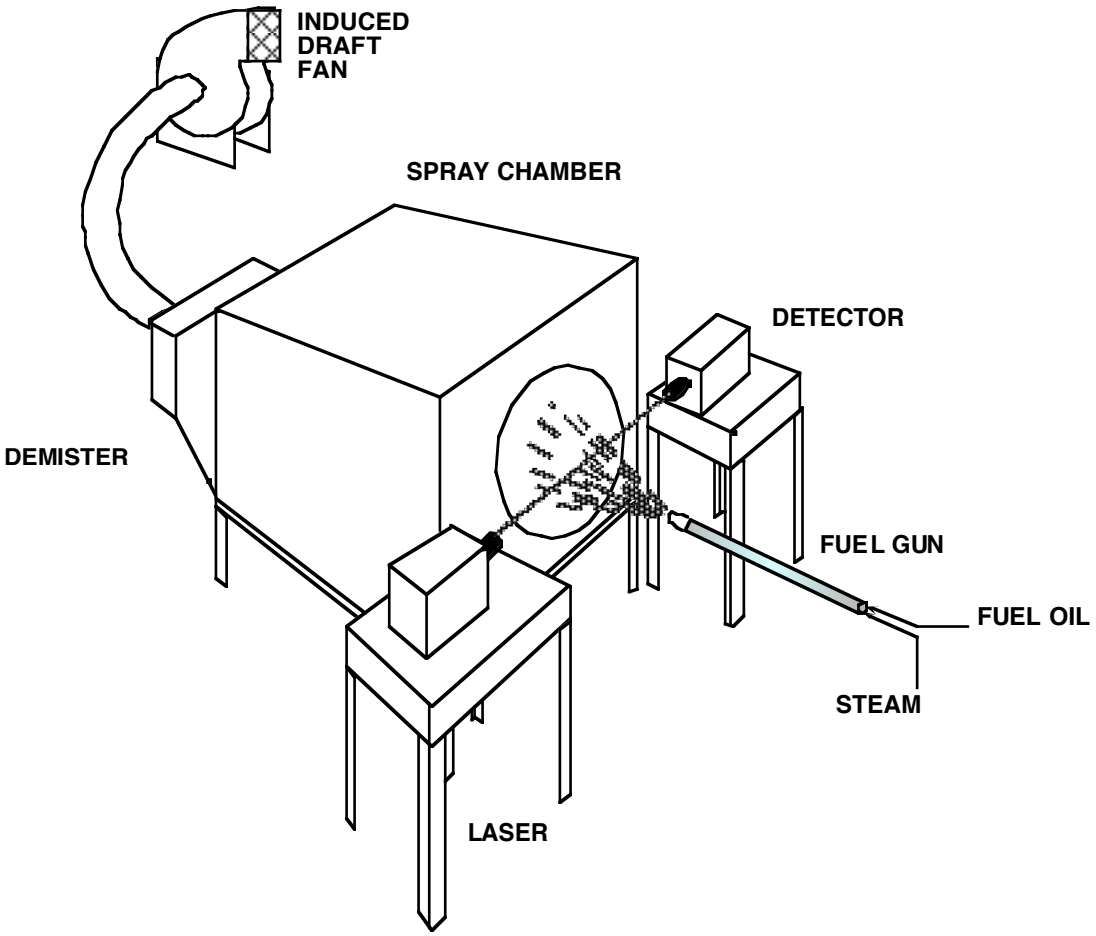

Figure 34. Sketch of the atomization test facility.

Central to the system is a spray chamber connected to an induced draft fan. Prior to entering the chamber, the spray is intersected by the laser beam from a Malvern 2600C Laser Diffraction Particle and Droplet Sizer. The analyzer includes a micro-computer which calculates the droplet size distribution and stores the data to disk. After being analyzed, the spray enters the chamber where most of the large droplets settle to the floor and are collected. The remaining fine droplets are then removed in the demister. A constant sweep of air provided by the induced draft fan ensures that few droplets pass through the laser beam volume more than once. The exhaust air containing very fine droplets is vented to the atmosphere.

As shown in **Table 16**, the viscosity of No. 6 fuel oil is very high (*i.e.*, 3,195 ssu), even at an elevated temperature of 100°F. To achieve acceptable atomization, No. 6 fuel oil must be heated thereby lowering the viscosity prior to introduction into the fuel gun. A temperature of 205 to 220°F, which is typical of industry, was maintained for both the atomization measurements and the combustion testing. Electrical drum heaters were used to heat the fuel prior to testing. Once the desired fuel temperature had been achieved, the fuel oil was delivered to the oil gun by a Moyno progressive cavity pump. The flow rate of both oil and steam were monitored by Micro Motion Mass Flow Meters. A complete schematic diagram of the flow system is shown in **Figure 35**.

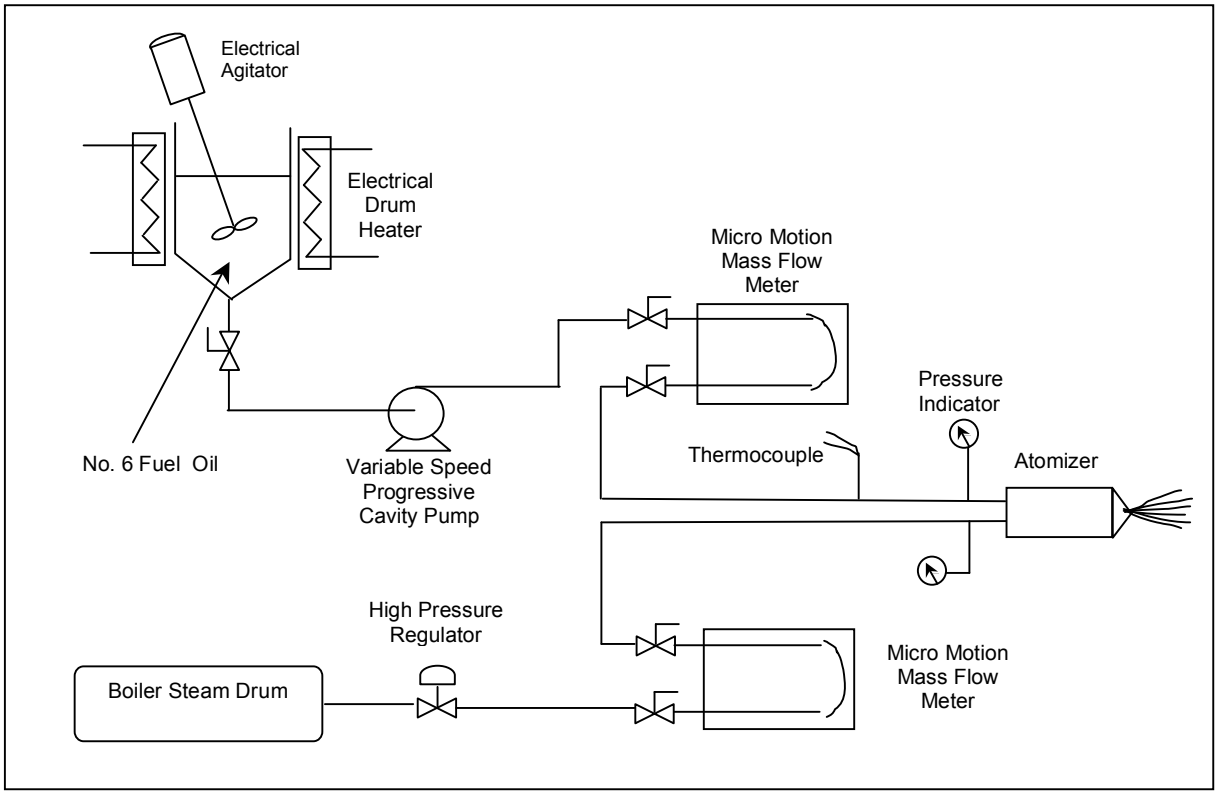

Figure 35. Flow diagram of the atomization test facility.

Spray quality is commonly expressed in terms of the Sauter Mean Diameter (SMD). The SMD is the diameter of the droplets whose ratio of volume to surface area is the same as that of the entire spray and can be defined as:

$$SMD = \frac{\sum n_i d_i^3}{\sum n_i d_i^2} \tag{4-1}$$

where n_i is the number of droplets in size d_i. This definition is derived from the realization that for a given quantity (volume) of fuel oil, the total surface area available for heating, evaporation, and other processes, to a large degree, controls the overall rate of combustion.

For a given fuel/nozzle combination, optimization of the operating parameters consists of determining the minimum flow rate and pressure of the atomizing media (an indication of the amount of energy used in the atomization process) required to achieve the target spray quality. The fuel pressure required to force a liquid through the discharge orifice increases with flow rate and also with the amount of resistance offered to the fuel by the atomizing medium (This applies to internal-mix nozzles; fuel and atomizing media interact external to the nozzle in external-mix designs.). The fuel is important since it may influence discharge characteristics of the fuel pump. As a corollary to the above, although the atomizing media flow rate is a function strictly of pressure when no fuel is flowing in the nozzle, it becomes dependent also on the fuel flow rate due to the interaction of the two fluids in an internal-mix nozzle [67].

Steam is commonly used as the atomizing media for applications burning No. 6 fuel oil because it can be readily supplied from the boiler's steam drum. Compressed air may be substituted during startup until sufficient steam pressure is available. Therefore, steam was used to atomize the baseline fuel oil in this evaluation.

The manufacturer of the fuel oil gun, *i.e.*, Faber, recommended that an atomizing pressure equal to 15 pounds per square inch (psi) greater than the oil delivery pressure be used to achieve sufficient atomization quality. Operating at a flow rate of 79.8 pounds of oil per hour (lb/h), equivalent to a firing rate of 1.5 million Btu per hour during the combustion testing, an atomization pressure of 60 psi was required. Using these conditions, the resulting droplet size distribution was measured and the results are provided in **Table 18**. The SMD ($D_{(4,3)}$) for the Faber oil gun was 114 µm. Inquiries to Faber and a literature search found no other studies contrasting the atomization quality of No. 6 fuel oil using the same oil gun design.

Upper	in	Lower	Under	Upper	in	Lower	Under	Upper	in	Lower	Under	Span 2.98
				346	2.2	299	97.8	58.9	3.6	50.8	37.6	
				299	10.9	258	87.0	50.8	3.6	43.8	34.0	D[4,3] 114.46µm
				258	8.7	222	78.2	43.8	3.6	37.8	30.4	
				222	3.1	192	75.2	37.8	3.6	32.6	26.8	
1128	0.0	973	100	192	3.3	165	71.9	32.6	3.9	28.1	22.9	D[3,2] 45.58µm
973	0.0	840	100	165	3.9	143	67.9	28.1	4.5	24.3	18.5	
840	0.0	724	100	143	5.0	123	62.9	24.3	5.4	20.9	13.1	
724	0.0	625	100	123	5.4	106	57.6	20.9	5.1	18.1	8.0	D[v,0.9] 266.98µm
625	0.0	539	100	106	4.7	91.7	52.8	18.1	3.9	15.6	4.2	
539	0.0	465	100	91.7	4.2	79.1	48.6	15.6	2.2	13.4	1.9	
465	0.0	401	100	79.1	3.8	68.2	44.8	13.4	0.9	11.6	1.0	D[v,0.1] 19.19µm
401	0.0	346	100	68.2	3.6	58.9	41.2	11.6	1.0	3.00	0.0	
Source = Data:refinin Record No. = 9 Focal length = 600 mm Presentation = lds				Beam length = 2.2 mm Log. Diff. = 3.585 Obscuration = 0.3341 Volume distribution				Model indp [2, 0] Volume Conc. = 0.2808% Sp.S.A 0.1316 m²/cc.				D[v,0.5] 83.16µm Shape OFF

Table 19. Droplet Size Distribution for No. 6 Fuel Oil Spray using the Faber Oil Gun

The steam-oil mass ratio for these conditions was 0.9. This ratio is probably excessive and unacceptable from an industrial point of view. However, this is typical of small, laboratory-scale processes. The efficiency of utilization of the atomizing medium generally increases with scale-up to larger units.

Subtask 4.3 Watertube Boiler Combustion Tests

The combustion performance attributes that boiler operators are most interested in are flame length, consumption of atomizing medium, turndown ratio, NO_x emissions, and particulate emissions [68]. The introduction of coal into the process streams of a petroleum refinery may result in changes to the fuel oil's composition. These changes may appear as differences in the API gravity, viscosity, or elevated levels of mercury and other metals. To evaluate whether these changes may affect the combustion performance and emissions of the No. 6 fuel oil, combustion testing was performed in Subtask 4.3. This testing was conducted in Penn State's watertube research boiler. A description of the boiler and ancillary equipment is provided in Section 4.3.1. While the coal-based No. 6 fuel oil was not available for testing, tests performed on the commercial No. 6 fuel oil did allow for the development of analyses protocols.

4.3.1. Description of the Research Boiler and Anciallary Equipment

Penn State's research boiler and ancillary equipment are shown in **Figure 36**. The 1,000 lb saturated steam (@ 150 psig)/h boiler is an A-Frame watertube boiler, designed and built by Cleaver Brooks. The combustion chamber is a 3x3x7 ft ($63ft^3$) chamber with a maximum heat release rate of 42,000 btu/ft^3-h. It contains 288 ft^2 of heating surface

and the maximum firing rate is two million Btu/h (60 Hp).

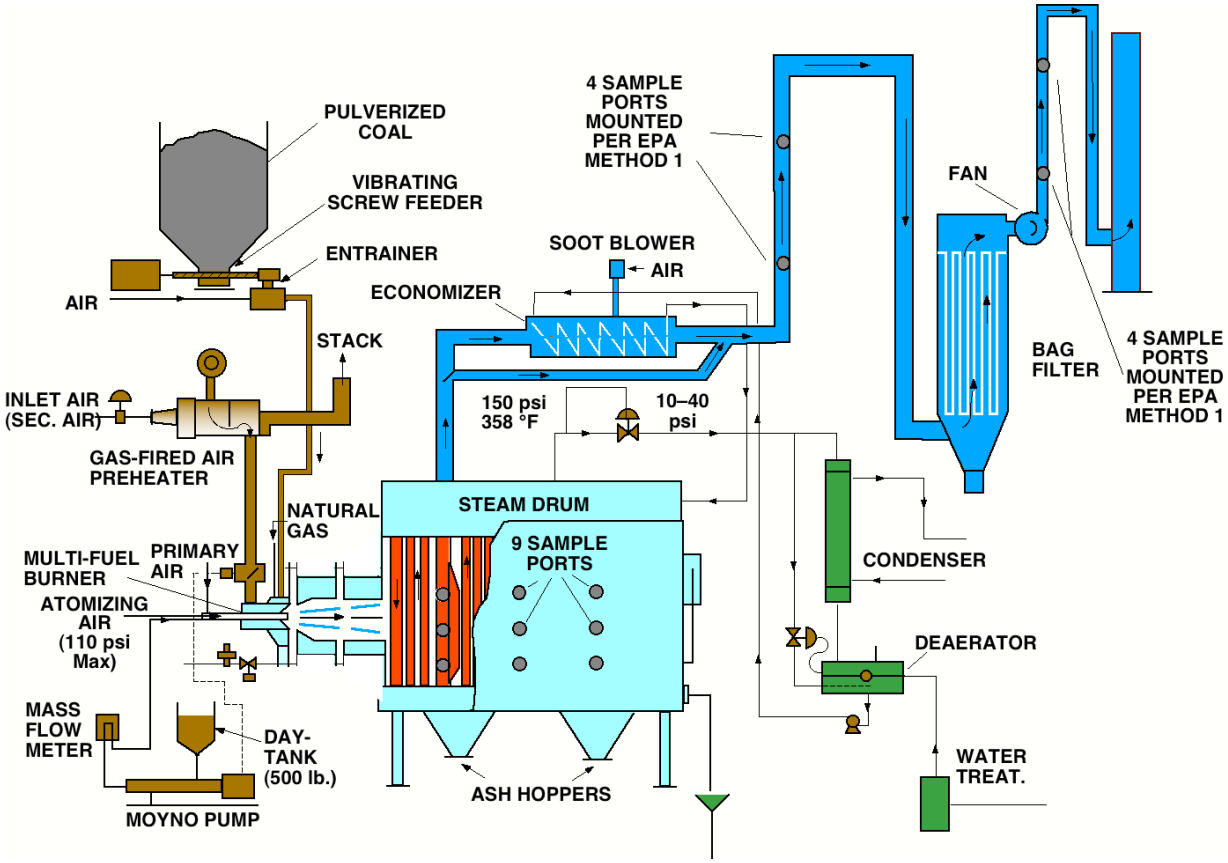

Figure 36. Schematic diagram of the research boiler system.

The boiler is equipped with eighteen side ports for gaseous and particulate sampling. Fourteen of the ports have diameters of 3 inches and four have diameters of 4 inches. The combustion gases split into two convective sections, one on each side of the radiant combustion chamber. There are access doors into each of the convective sections. There are also two ash hoppers under each convective section and a doorway giving access into the radiant combustion chamber.

During testing, the steam pressure is maintained constant at 150 psig by a back-pressure regulator. The steam flow rate is measured at the outlet of the steam drum by a steam flow meter before passing through a condenser. The condensed steam then flows into a feedwater tank before returning to the boiler.

To promote and enhance combustion, a ceramic burner throat extends the combustion chamber by two feet. This ceramic section, termed a quarl, is preheated by a natural gas flame prior to introducing the fuel oil. The quarl aids in the support of the fuel's ignition by storing some of the radiant heat energy released by the flame.

The No. 6 fuel oil was preheated and transported to the fuel oil gun via the same system used in the atomization testing (See Figure 4). The oil feed rate was monitored by a Micro Motion Mass Flow Meter, while the temperature was recorded by a thermocouple located at the inlet to the oil gun.

A gas-fired combustion air preheater supplied over 300,000 Btu/h to preheat up to 1,200 lb/h of air to 350°F. The preheated combustion air (primary air) was passed through a conventional swirl ring several inches before the gas distribution ring, both of which are 8 inches in diameter. A small portion of unheated primary air was fed through an annulus gap surrounding the nozzle. Preheated secondary air was introduced into the quarl tangentially through two headers that were balanced for uniform flow. The percentages of air introduced as cooling, primary, and secondary used in this study were approximately 2, 75, and 23, respectively.

The flue gas composition (O_2, CO_2, CO, NO_x, and SO_2) was monitored using a continuous emission monitoring system. After leaving the boiler, the combustion

products passed through an economizer and a baghouse for the removal of particulate matter. Additional sampling ports have been added to the inlet and outlet ducting of the baghouse per EPA Method 1. All instrumentation readings were recorded by a microcomputer data acquisition system.

4.3.2. Fuel Oil Combustion Test Results

Three combustion tests were performed firing the No. 6 baseline fuel oil at approximately 1.5 million Btu/h (~80 lbs oil/h) in the research boiler. The research boiler was fired on natural gas for a period of 4 hours to preheat the quarl. After the quarl temperature had reached approximately 1,200°F, the boiler was switched to firing the baseline fuel oil. Similar to the atomization measurements, the fuel oil was heated to between 205 and 220°F prior to being delivered to the fuel oil gun, and an atomization steam pressure of 60 psig was used. A summary of the average boiler operating and combustion data is provided in **Table 20**.

Table 20. Summary of the Average Boiler Operation and Combustion Data

	Test Number		
	1A	**2A**	**2B**
Flows			
Oil flow rate (lb/h)	79.8	79.8	79.8
Firing rate (million Btu/h)	1.49	1.49	1.49
Total Combustion Air (lb/h)	1,502	1,581	1,543
Primary Air	1,135	1,183	1,176
Secondary Air	343	374	343
Cooling Air	24	24	24
Steam Production (lb/h)	1,526	1,512	1,552
Atomizing Steam (lb/h)	71	75	74
Temperatures (°F)			
Primary Air	356	349	352
Secondary Air	618	582	599
Quarl	1,208	1,361	1,306
Boiler Outlet	455	460	459
Fuel Oil	208	211	206
Flue Gas Composition (dry)			
Oxygen (%)	3.8	4.0	3.9
Carbon Monoxide (ppm)	148	138	123
Carbon Dioxide (%)	14.8	13.4	13.9
Sulfur Dioxide (ppm)	553	302	306
Nitrogen Oxides (ppm)	539	582	NA

NA - Not available

Although the small-scale nozzle yielded a high steam-oil mass ratio, increased atomization steam pressures may provide for improved atomization quality (*e.g.*, finer droplet size). As observed with previous No. 6 fuel oil testing at Penn State's Demonstration Boiler (*i.e.*, firing rate of 20 million Btu/h), the reduction in droplet size produced a shorter flame [67]. Also observed was that the NO_x production generally increases with decreasing flame length. This is a direct result of rapid mixing of all the fuel with the combustion air close to the burner. The small droplets evaporate and burn more rapidly. As the droplets become larger, the flame becomes longer and mixing is

delayed, thereby producing a potential for sub-stoichiometric firing in the core of the flame structure. The flame length for the baseline fuel oil was approximately 36 inches. Thus, there was no risk of flame impingement on the back wall of the boiler.

Average NO_x emissions of 560 ppm (corrected to 3% O_2) were measured for the series of tests performed. It should be noted that while the burner installed on the research boiler was designed for firing natural gas and fuel oil, it has not been optimized for low NO_x production. Turndown was not measured since the primary goal of the testing was to operate under steady-state conditions allowing sufficient time to perform the trace element samplings.

An average oxygen level of 3.9% in the flue gas was used for the baseline fuel oil combustion tests. This amount of excess oxygen was established by slowly increasing the flow rate of combustion air until an acceptable level of CO was observed within the flue gas. The low concentrations of CO (123 to 148 ppm, corrected to 3% O_2) are not only evidence of good combustion efficiency, but also a general indicator of reduced particulate (soot) formation.

4.3.3. Determination of Metals Emissions and Form of Mercury from Stationary Sources

Trace element emissions are a function of combustion conditions, concentration and mode of occurrence of metals in the oil, and type of particulate control device (PCD), as they affect collection efficiency and particle size distribution. The behavior of various elements during coal combustion has been extensively studied. Categories regarding the

partitioning of elements between gas and solid phases have been devised based on the work of several researchers and reported by Clarke and Sloss [69], which are illustrated in **Figure 37**.

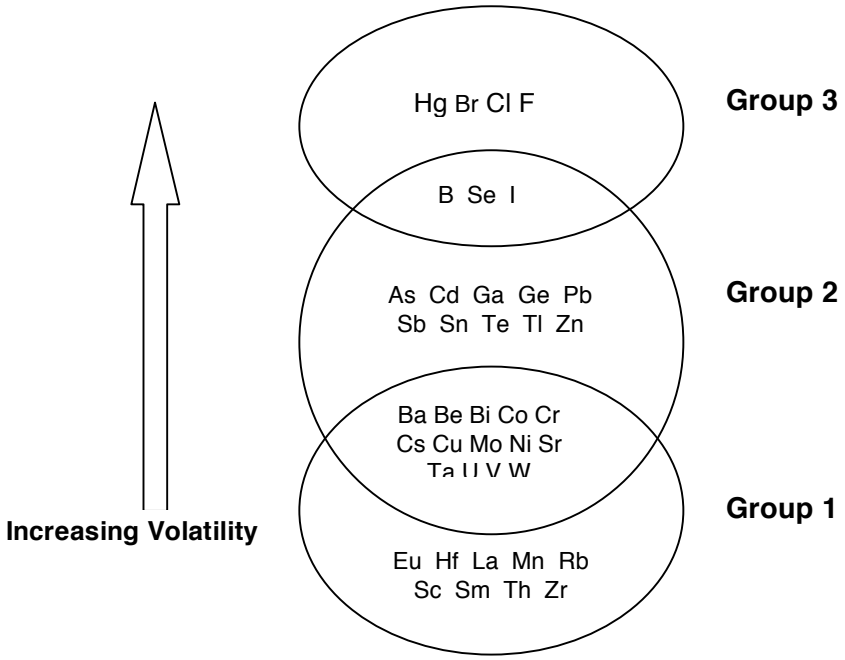

Figure 37. Classification of trace elements by their behavior during combustion and gasification. Taken from Clarke and Sloss [69].

> **Group 1**: Elements are concentrated in the bottom ash or equally partitioned between bottom ash and fly ash, which is usually trapped by PCDs.
> **Group 2**. Elements concentrated more in the fly ash than the bottom ash. They are also enriched on fine-grained particles, which may escape the PCD.
> **Group 3**. Elements that readily volatilize and are concentrated in the gas phase and depleted in the solid phase.

Some elements demonstrated partitioning behavior that is intermediate between groups. This is a reflection of the volatility of the element and its behavior in varying combustion systems. Although this classification was developed for solid fuels, they are applicable to oil-fired systems.

Operating variables that affect the behavior of inorganic elements (primarily Group 2 elements) during combustion include flame temperature and local O_2 concentration. These variables are especially affected when using low NO_x firing strategies. Lower combustion temperature may reduce the volatilization of Group 2 metals, thereby reducing their concentration in the fine particulates. Lower O_2 levels decrease the oxidation of volatile metals to less volatile oxides. Group 2 metals would remain in the vapor phase thereby increasing their concentration in the finer particulate. Group 1 and 3 elements would be unaffected. The partitioning behavior of the elements classified as intermediates may shift with changes in temperature and O_2 concentration.

According to a report titled "Compilation of Air Pollution Emission Factors" (AP-42) published by the U.S. EPA, Office of Air Quality planning and Standards (http://www.epa.gov/tnn/chief/ap42/ch01/) [70], metal behavior based on data obtained from oil-fired boilers were classified as follows (**Table 21**):

Table 21. Metal Partitioning in Oil-Fired Combustors

Class	Description	Elements
1	Equal distribution between fly ash and soot	Al, Co, Cr, Fe, Mn, Se, Ti
2	Enriched in fly ash relative to soot	As, Cd, Pb, Sb
3	Intermediate to Class 1 and 2; multiple behavior	Cr, Ni
4	Emitted in gas phase	Hg

4.3.3.1 Experimental Procedure

The metal emissions sampling and recovery were performed using the PSU Method, which is a combination of those used in the Method 29 and Ontario Hydro Mercury Speciation Methods [71; 72]. Modification of the Ontario Hydro train included

omission of one KCl impinger and one $H_2SO_4/KMnO_4$ impinger and the addition of a HNO_3/H_2O_2 impinger (**Figure 38**). The configuration was based on discussions with University of North Dakota Energy and Environmental Research Center (UNDEERC) and testing conducted at Penn State University. The recovery protocol for the filter, filter rinse, HNO_3/H_2O_2 and $H_2SO_4/KMNO_4$ samples are the same for Method 29 and the Ontario Hydro Mercury Speciation Method. The recovery and sample preservation of the KCl solution followed the Ontario Hydro Mercury Speciation Method.

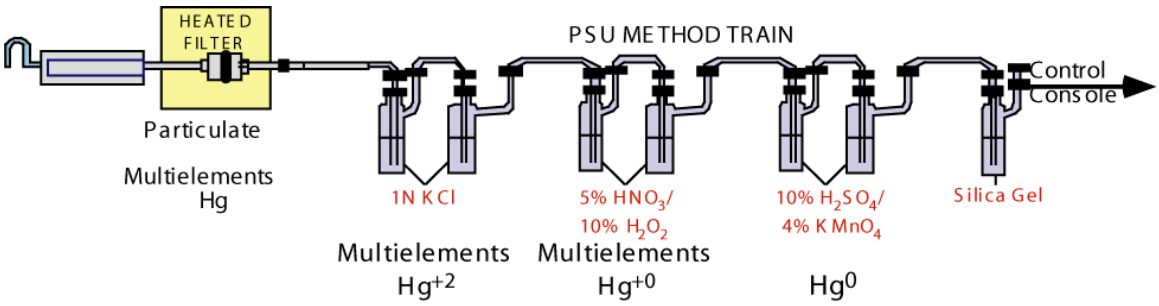

Figure 38. Modified Ontario-Hydro sample train.

The sample preparation, *i.e.*, digestion techniques, and analytical techniques for the multielements and mercury for the current PSU Method are shown in Figure 7. Numerous digestion and analytical techniques were tried that were not adopted into the current methodology and are not indicated in **Figure 39**. One solid and three liquid samples are generated during each test and analyzed as indicated in Figure 7. A detailed discussion of sample preparation and analysis for the PSU Method and EPA digestion methods is presented elsewhere [73-75].

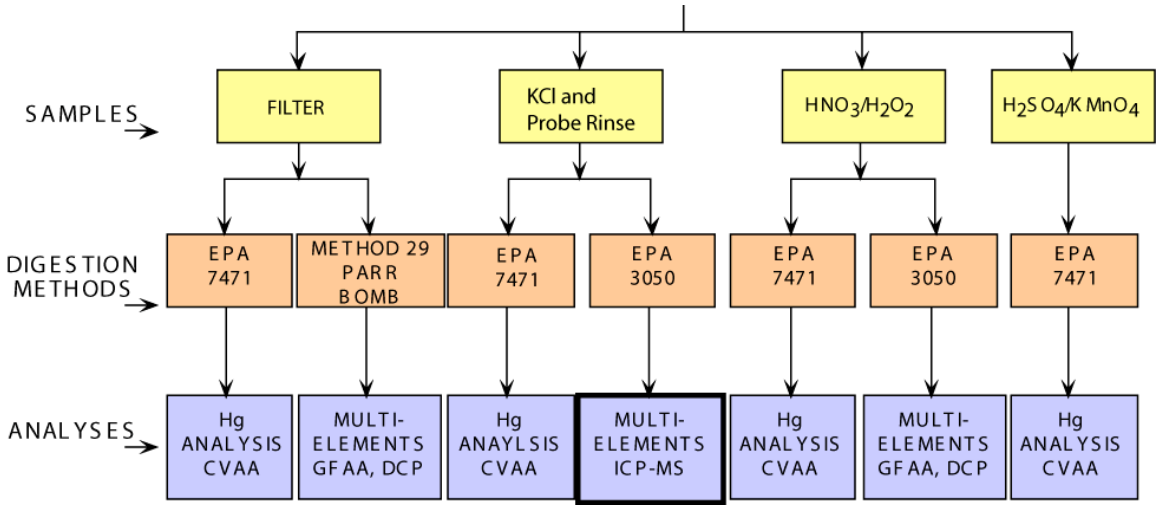

Figure 39. Analytical procedure for the PSU method

4.3.3.2. Emissions Results

Three sampling tests were performed (RI-PSU-1A, RI-PSU-2A, and RI-PSU-2B). The emission data sheets are given in Appendix A for each test. The sheets contain operational information as well as the analysis for the fuel oil and each portion of the train. The total emissions for each of the tests are given in **Table 22** and are reported in lbs/10^{12} Btu. In addition to the measured emissions, calculated emissions based on the emission factors published by the US EPA [76] are provided.

Table 22. Total Emissions Measured during Combustion Tests and Calculated Emissions Based on AP-42 Emission Factors

	Emissions (lb/10^{12} Btu)			
Element	**RI-PSU-1A**	**RI-PSU-2A**	**RI-PSU-2B**	***AP-42 Emission Factor Calculation**
Al	2809.33	918.70	1239.14	na
As	20.13	24.22	14.17	8.67
Ba	37.07	16.67	23.67	16.88
Be	0.42	0.16	0.23	0.183
Cd	0.41	0.14	0.19	2.61
Co	39.78	38.61	43.04	39.53
Cr	9.18	3.87	4.73	5.55
Cu	10.84	15.75	17.38	11.59
Hg	0.80	0.29	0.26	0.753
Mn	237.16	62.42	10541.12	19.7
Mo	3.27	4.47	2.88	5.17
Ni	892.00	991.93	1024.00	554.93
Pb	12.72	9.27	4.87	9.92
Sb	13.32	14.78	15.85	34.48
Se	7.78	1.94	3.27	4.49
Sr	43.61	13.23	23.37	--
V	2345.70	2311.23	2531.41	208.8
Zn	106.19	77.57	77.78	191.1

* Based on Revised Emission Factors [US EPA, 1996].
Na – not available

The United States EPA has published a document, "Compilation of Air Pollutant Emission Factors", referred to as AP-42, since 1972. Supplements to AP-42 have been routinely published to add new emissions source categories and to update existing emission factors. This document is also provided on EPA's website on their CHIEF [Clearinghouse for Inventories and Emissions Factors; www.epa.gov/ttn/chief/ap42] bulletin board. The emission factors used are given in **Table 7** and are taken from Report on Revisions to 5th Edition AP-12, Section 1.3 [76].

Emission factors may be appropriate to use in a number of situations such as source-specific emission estimates for area-wide inventories. These inventories have

many purposes including ambient dispersion modeling and analysis, control strategy development, in screening sources for compliance investigations, and in some permitting applications. Emission factors in AP-42 are neither EPA-recommended emission limits (*e.g.*, Best Available Control Technology (BACT), or Lowest Achievable Emission Rate (LEAR)) nor standards (*e.g.*, NSPS or NESHAP).

Table 23. Emission Factors for Metals from Oil-fired Combustors
[US EPA, 1996, Appendix A15-A16]

Element	Emission Factor (lb/1000 gallons)	Emission Factor Rating
As	1.32e-03	C
Ba	2.57e-03	D
Be	2.78e-05	C
Cd	3.98e-04	C
Cr	8.45e-04	C
Co	6.02e-03	D
Cu	1.76e-03	C
Pb	1.51e-03	C
Mn	3.00e-03	C
Hg	1.13e-04	C
Mo	7.87e-04	D
Ni	8.45e-02	C
Sb	5.25e-03	E
Se	6.83e-04	C
V	3.18e-02	D
Zn	2.91e-02	D

Emission factors and emissions inventories have long been fundamental tools for air quality management. Emission estimates are important for developing emission control strategies, determining applicability of permitting and control programs, ascertaining the effects of sources and appropriate mitigation strategies. Users include Federal, state, and local agencies, consultants, and industry. Data from source-specific emission tests or continuous emission monitors are usually preferred for estimating a source's emissions because those data provide the best representation of the tested

source's emissions. However, test data from individual sources are not always available and they may not reflect the variability of actual emissions over time. Consequently, emission factors are often the best or only method available for estimating emissions.

The calculated emissions for the fuel oil testingwere derived by the following equation:

$$(EF_{element})(1/HHV_{fuel\ oil})(1/10^{12}\ Btu) = Calculated\ Emissions \qquad (4\text{-}2)$$

where the units are as follows:

$$(lb/1{,}000\ gallons)(1\ gallon\ fuel/152{,}272\ Btu)(10^{12}\ Btu/10^{12}\ Btu) = lb/10^{12}\ Btu$$

Note that each average emission factor is given an "emission factor rating" (**Table 22).** The reliability of the AP-42 emission factors are rated from A (excellent) through E (poor), which is a general indication of the robustness of that factor. This rating is assigned based on the estimated reliability of the tests used to develop the factor. In general, factors based on many observations, or on more widely accepted test procedures, are assigned higher rankings with A being the best. All of the trace metal emission factors received a rating of C or less and are described as follows:

> C-Rating (average): developed only from A- and B-rated test data from a reasonable number of facilities. It is not clear if the facilities tested represent a random sample of the industry. The source category is specific enough so that variability within the source category population may be minimized.

D-Rating (below average): developed only from A- and B-rated test data from a small number of facilities and there is reason to suspect that these facilities do not represent a random sample of the industry. There is also evidence of variability within the source category population. This provides an order-of-magnitude calculation.

E-Rating (poor): emission factor developed from C- and D-rated test data and there is reason to suspect that these facilities do not represent a random sample of the industry. There is also evidence of variability within the source category population.

Graphic comparisons of the measured to the AP-42 calculated emissions are given in **Figures 40 and 41**. There was a significant amount of variability in the emissions measured and there are only three data points for each element, therefore, comparison of the AP-42 calculated emissions is based on whether the AP-42 value is within the range of the three measured values. Special consideration was taken in the case of elements having a D rating. If the calculated value was within an order of magnitude of the measured value than it was considered to meet the AP-42 standard.

Calculated emissions that were within the range of measured emission are as follows: Be, Hg, Mo, Se, Cr, Pb, Cu, Ba, and Co. Calculated emissions that were not within the range of measured emission are as follows: Cd, Sb, Zn, Mn, Ni, and V. Emission factors are not available for Al and Sr. Nine of the 15 elemental emissions for

which AP-42 emission factors exists were within the range of the three measured. Given the highly variable nature of the measured data it would be misleading to make any significant conclusions as to the usefulness of AP-42 emission factors in predicting emissions. In order to draw any further conclusions would necessitate conducting several more replicate test runs and doing a statistical analysis of the data. This comparison was made to highlight the need for stack testing to generate reliable metal emissions data.

In addition to the total emissions it is important to note the partitioning of the elements as discussed in the previous section. The average percent of each element in the solid and gas phase is given in **Table 24** and shown in **Figure 42**. The partitioning of the elements (% solid verses % gas phase) for each test is shown in **Figures 43 through 45**.

There is variability between the three tests; however, the average partitioning of the elements seems to follow the general pattern of behavior discussed earlier. The majority of the elements were concentrated in the solid phase, *i.e.*, particulate matter captured on the train filter. The elements that are of the greatest environmental concern are also those elements that have a significant occurrence in the gas phase, *i.e.*, Hg, As and Se.

The Group 3 element, Hg, occurred primarily as gas phase (75.5%). Selenium (Group 2-3 transition element) and As (Group 2 element) both have a significant portion in the gas phase (39.2 and 67%, respectively). The Group 1and 2 elements are concentrated in the particulate matter. The Group 2 elements occurred predominantly in

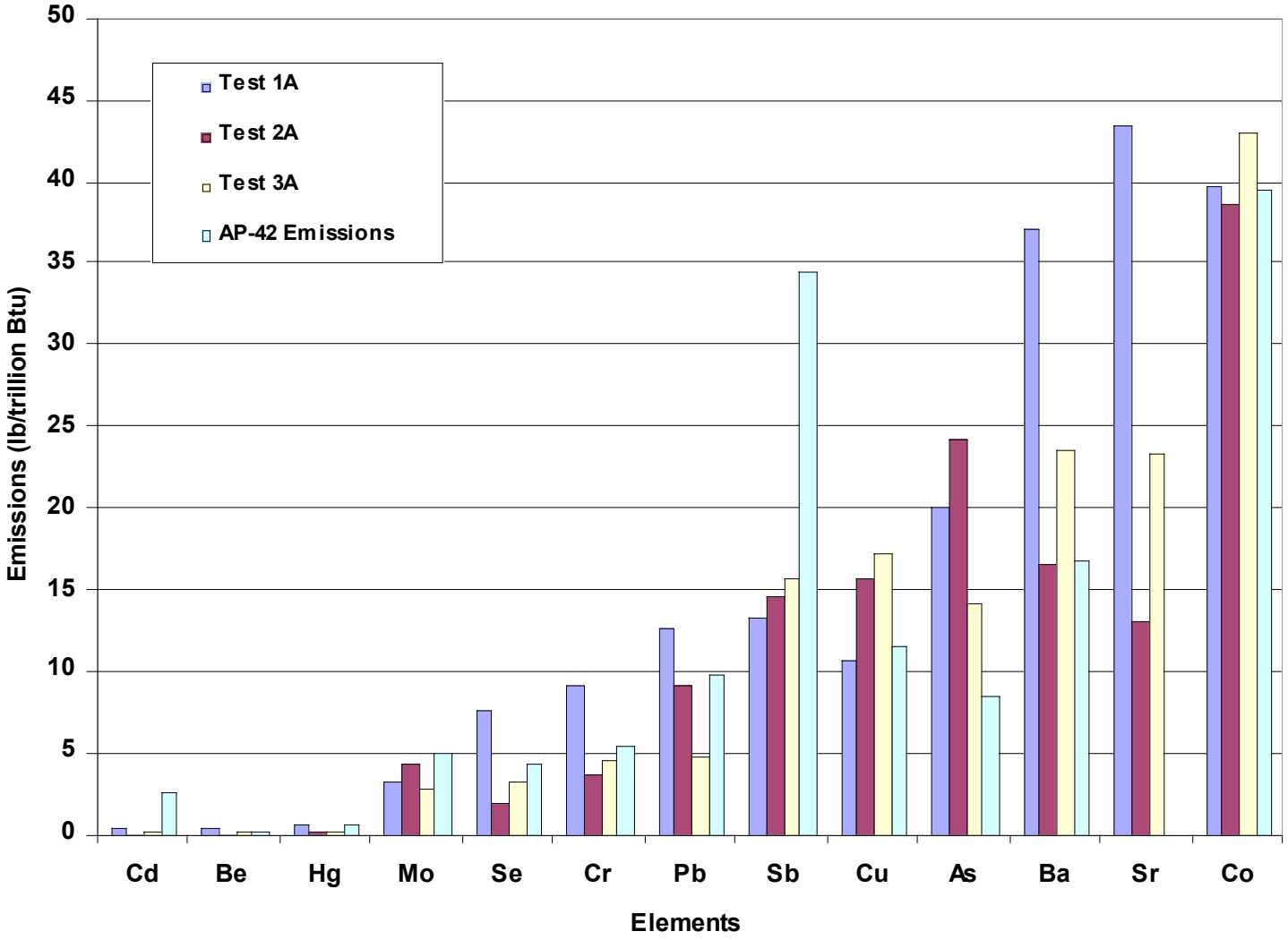

Figure 40. Measured and calculated emissions for selected elements.

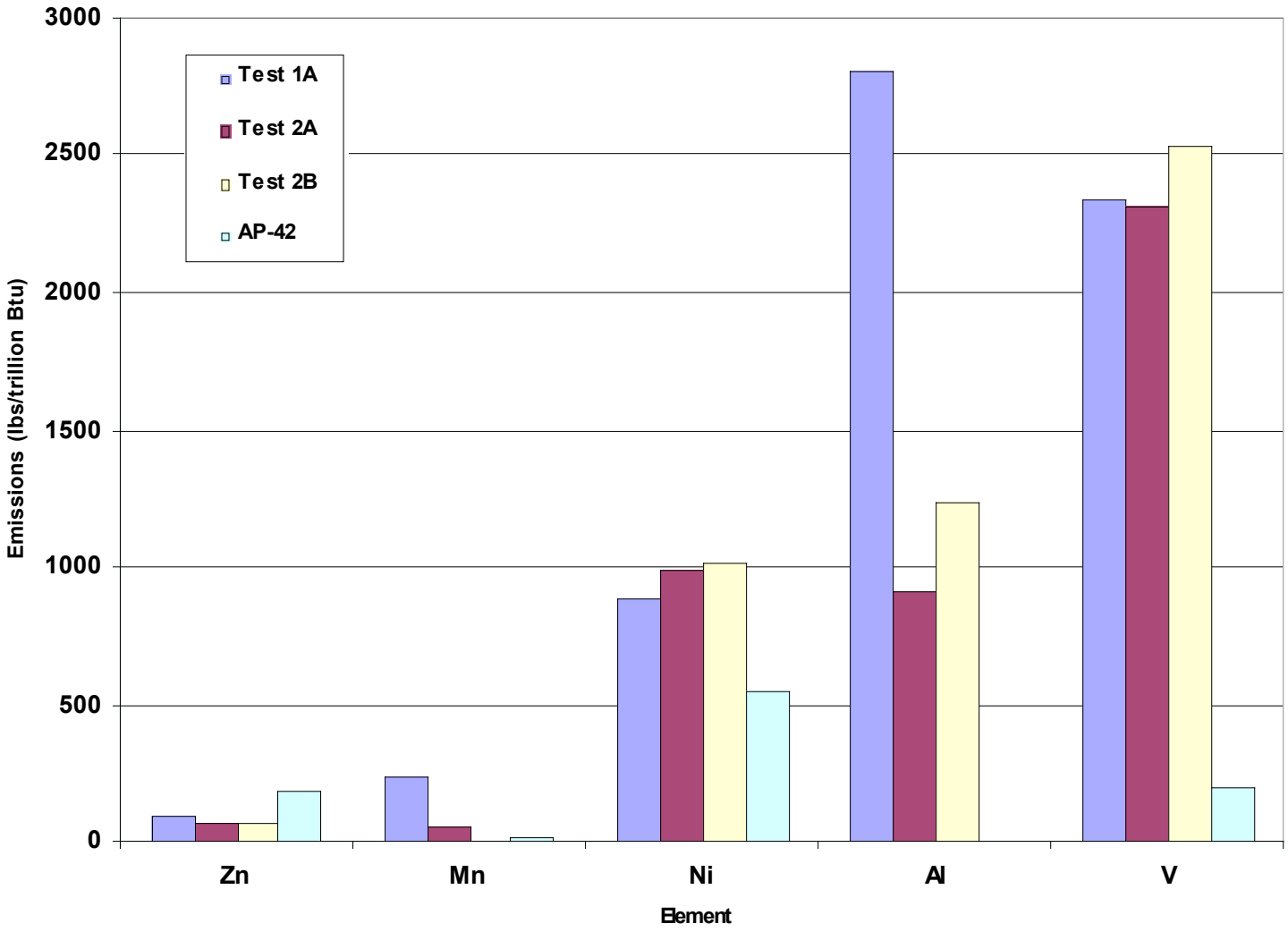

Figure 41. Measured and calculated emissions for selected elements.

Table 24. Average Weight % of Each Element in Solid and Gas Phase in Flue Gas Measured During Combustion Tests

	Avg Weight %	
Element	**Solid**	**Gas**
Al	93.3	6.7
As	33.0	67.0
Ba	91.6	8.4
Be	100.0	0.0
Cd	95.6	4.4
Co	100.0	0.0
Cr	80.5	19.5
Cu	43.7	56.3
Hg	24.5	75.5
Mn	9.9	90.1
Mo	84.0	16.0
Ni	98.2	1.8
Pb	99.3	0.7
Sb	100.0	0.0
Se	60.8	39.2
Sr	93.3	6.7
V	99.7	0.3
Zn	73.5	26.5

the solid phase as follows: 73.5% (Zn), 95.6% (Cd), 99.3% (Zn), to 100% (Sb). The exception is As. Arsenic has been shown to occur in the gas phase during coal combustion to a greater extent than other Group 2 elements. The concentration of Group 1 and Group 1-2 transition elements (Al, Ba, Be, Co, Mo, Ni, Sr, and V) in the solid phase ranged from 80.5% (Cr) to 100% (Be and Co). Copper and manganese are an exception in that they are concentrated in the gas phase (56.3 and 90.1%, respectively).

It is necessary to study elements that are not typically associated with fuel oils as fuels that are produced during co-processing of coal and petroleum-derived fuels. It is important to understand the effect of incorporating inorganic elements into an oil on gas and particulate emissions.

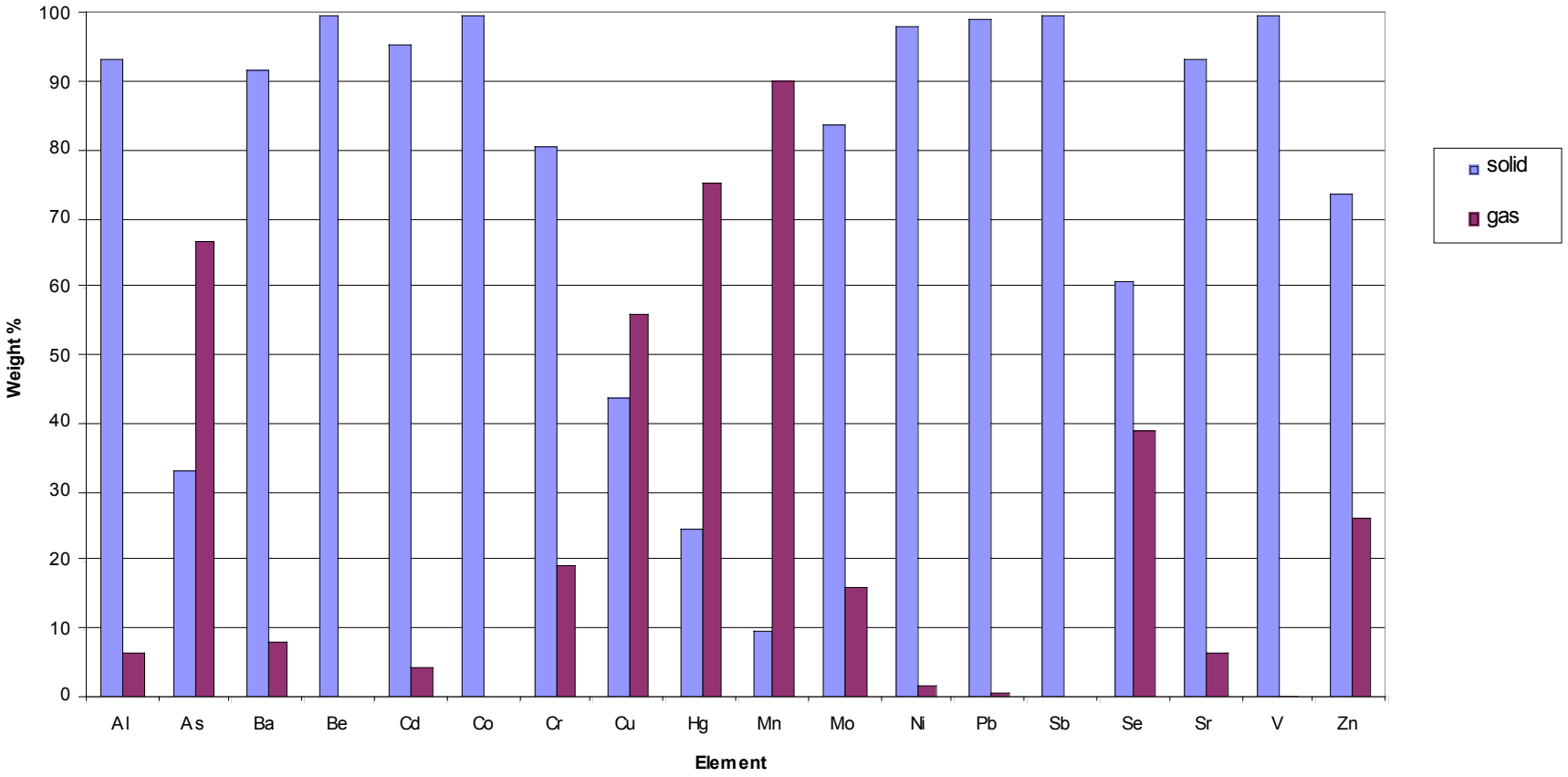

Figure 42. Average partitioning of elements between solid and gas phase by weight percent for tests 1A, 2A and 2B.

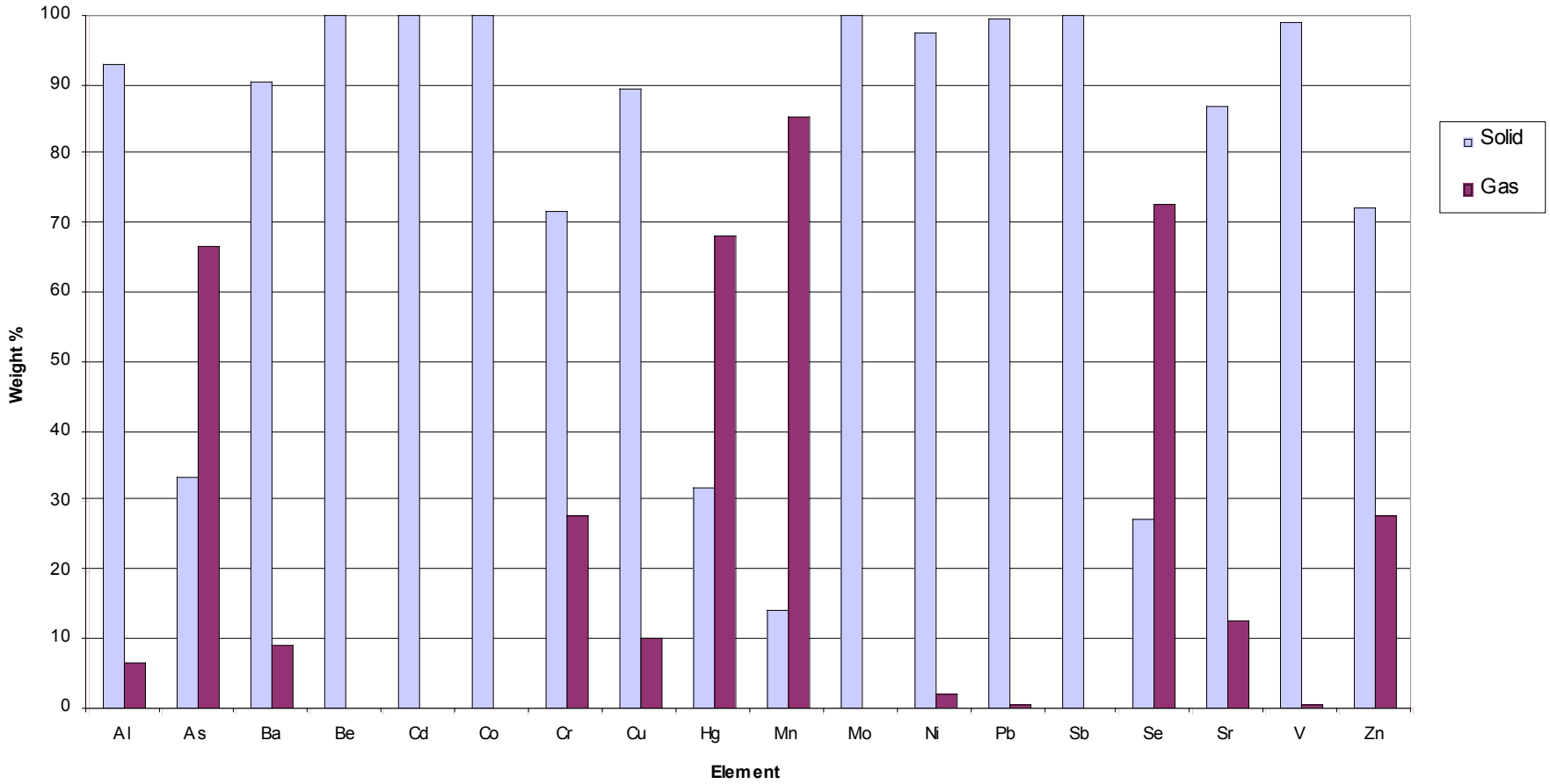

Figure 43. Partitioning of elements between solid and gas phase by weight % for test RI-PSU-1A.

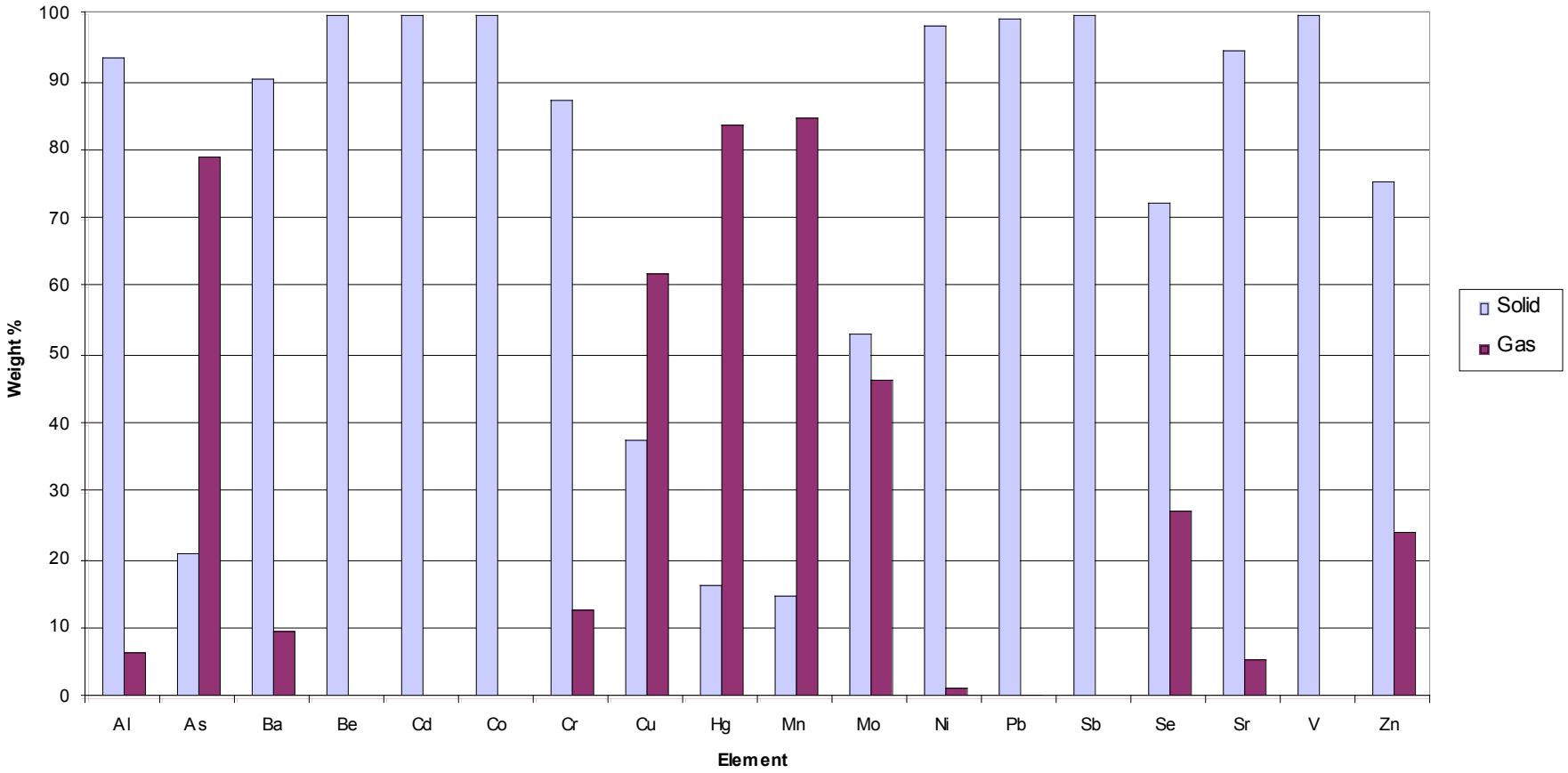

Figure 44. Partitioning of elements between solid and gas phase by weight % for test RI-PSU-2A.

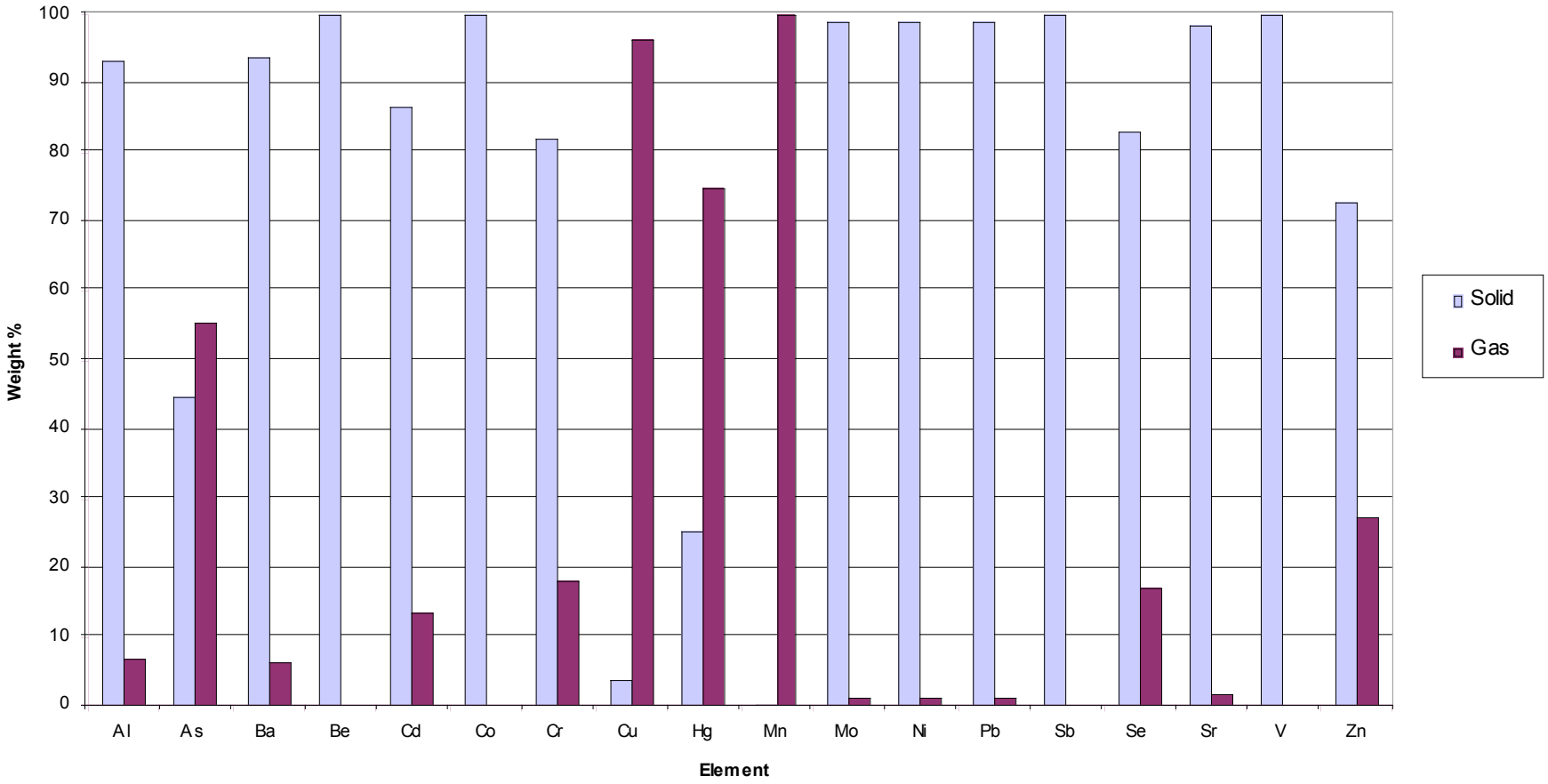

Figure 45. Partitioning of elements between solid and gas phase by weight % for test RI-PSU-2A.

Appendix A. Table 1A. Sampling Parameters and Sample Train Analysis for Test RI-PSU-1A

Test No:	RI-PSU-1A
Test Date:	6/15/2000
Fuel Type:	#6 Fuel Oil
Cal. Value	
(Btu/lb)	18,714
Firing Rate:	
lbs/hr	79.8
Btu/hr	1,493,377.0
PSU Method	Total Volume or
Sample Train	Weight Collected
Splits	(mL or g)
Rinse & KCl	1000
H_2O_2	500
$KMnO_4$	500
Filter	1.8747

Sampling Parameters	
Total H2O (g):	451.9
Total Dust (g):	**1.8747**
Pb (in Hg):	29.9
Delta H (in H2O):	0.696
Tm (R):	567
Ts (R):	808
Ps (in Hg):	29.2
Delta P (in H2O):	0.084
Cp:	0.99
Dn (in):	0.3125
Total Vm (ACF):	122.582
Sample Time (min):	245
Duct Dia: (ft)	0.625

Isokineticity Calc.	
Vw(std): SCF	21.420
VmC: ACF	123.379
Vm(std): SCF	115.422
Vt(std): SCF	136.842
% H2O:	15.65
Vs: FM	1436.295
Qn: ACFM	0.765
Qn(std): SCFM	0.489
% Isokinetic:	114.13
Dust Loading Calc.	
DCL: (grains/scf)	**0.2114**
Stack Flow: ACFM	440.426
Stack Flow: SCFM	281.879

Test 1A Lab Analysis Data - Uncorrected for Split Size (volume or mass)

Analyte	Rinse & KCl (µg/L)	H_2O_2 (µg/L)	$KMnO_4$ (µg/L)	Filter (µg/filter half)
Al	1030	14.6		7180
As	72.8	1.48		18.4
Ba	18.8	0.384		92.1
Be	ND	ND		1.14
Cd	ND	ND		1.11
Co	ND	ND		109
Cr	11.3	5.60		18.1
Cu	5.27	1.89		26.6
Hg	2	< 0.4	2	0.7031
Mn	886	454		93.4
Mo	ND	ND		8.95
Ni	108	1.75		2390
Pb	ND	0.614		34.7
Sb	ND	ND		36.5
Se	29.0	4.11		5.79
Sr	31.0	ND		104
V	95.7	1.12		6380
Zn	151	22.0		210

Test 1A Lab Analysis Data - Corrected Totals

Analyte	Rinse & KCl (µg)	H_2O_2 (µg)	$KMnO_4$ (µg)	Filter (µg)	Total (µg)	Total Emissions (lb/10^12 Btu)
Al	1030	7.30		14360	15397.30	2809.33
As	72.8	0.74		36.8	110.34	20.13
Ba	18.8	0.19		184.2	203.19	37.07
Be	ND	ND		2.28	2.28	0.42
Cd	ND	ND		2.22	2.22	0.41
Co	ND	ND		218	218	39.78
Cr	11.3	2.80		36.2	50.30	9.18
Cu	5.27	0.95		53.2	59.42	10.84
Hg	2	< 0.2	1	1.4062	4.4062	0.80
Mn	886	227.00		186.8	1299.80	237.16
Mo	ND	ND		17.90	17.90	3.27
Ni	108	0.88		4780	4888.88	892.00
Pb	ND	0.31		69.4	69.71	12.72
Sb	ND	ND		73.0	73.00	13.32
Se	29	2.06		11.58	42.64	7.78
Sr	31	ND		208	239	43.61
V	95.7	0.56		12760	12856.26	2345.70
Zn	151	11.00		420	582.00	106.19

	Test Oil -1		Test Oil - 2		Partitioning (%)	
Analyte	(mg/kg or ppm)	(lb/10^12 Btu)	(mg/kg or ppm)	(lb/10^12 Btu)	Solid	Gas
Al	34.0	1,817	31.6	1,689	93.3	6.7
As	3.63	193.97	0.01	0.53	33.4	66.6
Ba	0.38	20.31	0.73	39.01	90.7	9.3
Be					100.0	0.0
Cd	0.27	14.43	0.2	10.69	100.0	0.0
Co					100.0	0.0
Cr	0.12	6.41	0.03	1.60	72.0	28.0
Cu	0.16	8.55	0.96	51.30	89.5	10.5
Hg	0.59	31.53	0.13	6.95	31.9	68.1
Mn	0.15	8.02	0.39	20.84	14.4	85.6
Mo	0.07	3.74	0.01	0.53	100.0	0.0
Ni	40.5	2,164.2	44.6	2,383.2	97.8	2.2
Pb	0.12	6.4	0.6	32.1	99.6	0.4
Sb					100.0	0.0
Se	1.40	74.8	2.18	116.5	27.2	72.8
Sr					87.0	13.0
V	116	6,199	129	6,893	99.3	0.7
Zn	1.46	78.0	2.08	111.1	72.2	27.8

Table 2A. Sampling Parameters and Sample Train Analysis for Test RI-PSU-2A

Test No:	RI-PSU-2A				**Sampling Parameters**			**Isokineticity Calc.**					
Test Date:	7/6/2000				Total H2O (g):	459.4		Vw(std): SCF	21.776				
Fuel Type:	#6 Fuel Oil				Total Dust (g):	**0.4790**		VmC: ACF	132.847				
					Pb (in Hg):	29.9		Vm(std): SCF	125.273				
Cal. Value					Delta H (in H2O):	0.3303		Vt(std): SCF	147.049				
(Btu/lb)	18,714				Tm (R):	562		% H2O:	14.81				
					Ts (R):	815		Vs: FM	1612.767				
Firing Rate:					Ps (in Hg):	29.2		Qn: ACFM	0.859				
lbs/hr	79.8				Delta P (in H2O):	0.105		Qn(std): SCFM	0.545				
Btu/hr	1,493,377.0				Cp:	0.99		% Isokinetic:	74.98				
					Dn (in):	0.3125							
PSU Method	Total Volume or				Total Vm (ACF):	131.989		**Dust Loading Calc.**					
Sample Train	Weight Collected				Sample Time (min):	360		DCL: (grains/scf)	**0.0508**				
Splits	(mL or g)				Duct Dia: (ft)	0.625		Stack Flow: ACFM	494.540				
Rinse & KCl	1000							Stack Flow: SCFM	313.794				
H_2O_2	500												
$KMnO_4$	500												
Filter	1.8747												
Test 2A Lab Analysis Data - Uncorrected for Split Size (volume or mass)					Test 2A Lab Analysis Data - Corrected Totals								
													Total Emissions
Analyte	Rinse & KCl (µg/L)	H_2O_2 (µg/L)	$KMnO_4$ (µg/L)	Filter (µg/filter half)	Rinse & KCl (µg)	H_2O_2 (µg)	$KMnO_4$ (µg)	Filter (µg)	Total (µg)	(lb/10^12 Btu)			
Al	287	66.8		2270	287	33.40		4540	4860.40	918.70			
As	100	2.23		13.5	100	1.12		27.0	128.12	24.22			
Ba	8.03	0.758		39.9	8.03	0.379		79.8	88.21	16.67			
Be	ND	ND		0.42	ND	ND		0.84	0.84	0.16			
Cd	ND	ND		0.375	ND	ND		0.75	0.75	0.14			
Co	ND	0.501		102	ND	0.251		204	204.25	38.61			
Cr	ND	5.15		8.95	ND	2.58		17.9	20.48	3.87			
Cu	50.8	1.90		15.8	50.8	0.95		31.6	83.35	15.75			
Hg	0.9	<0.4	0.8	0.13	0.9	<0.2	0.4	0.2540	1.5540	0.29			
Mn	280	0.894		24.9	280	0.45		49.8	330.25	62.42			
Mo	10.8	0.39		6.32	10.8	0.19		12.64	23.63	4.47			
Ni	86.9	1.90		2580	86.9	0.95		5160	5247.85	991.93			
Pb	ND	0.527		24.4	ND	0.26		48.8	49.06	9.27			
Sb	ND	ND		39.1	ND	ND		78.2	78.20	14.78			
Se	ND	5.65		3.72	ND	2.83		7.44	10.27	1.94			
Sr	ND	7.55		33	ND	3.78		66	70	13.23			
V	6.93	1.51		6110	6.93	0.76		12220	12227.69	2311.23			
Zn	42.4	116.0		155	42.4	58.00		310	410.40	77.57			
	Test Oil - 1		Test Oil - 2		Partitioning (%)								
Analyte	(mg/kg or ppm)	(lb/10^12 Btu)	(mg/kg or ppm)	(lb/10^12 Btu)	Solid	Gas							
Al	34.0	1,817	31.6	1,689	93.4	6.6							
As	3.63	193.97	0.01	0.53	21.1	78.9							
Ba	0.38	20.31	0.73	39.01	90.5	9.5							
Be					100.0	0.0							
Cd	0.27	14.43	0.2	10.69	100.0	0.0							
Co					99.9	0.1							
Cr	0.12	6.41	0.03	1.60	87.4	12.6							
Cu	0.16	8.55	0.96	51.30	37.9	62.1							
Hg	0.59	31.53	0.13	6.95	16.3	83.7							
Mn	0.15	8.02	0.39	20.84	15.1	84.9							
Mo	0.07	3.74	0.01	0.53	53.5	46.5							
Ni	40.5	2,164.2	44.6	2,383.2	98.3	1.7							
Pb	0.12	6.4	0.6	32.1	99.5	0.5							
Sb					100.0	0.0							
Se	1.40	74.8	2.18	116.5	72.5	27.5							
Sr					94.6	5.4							
V	116	6,199	129	6,893	99.9	0.1							
Zn	1.46	78.0	2.08	111.1	75.5	24.5							

Table 3A. Sampling Parameters and Sample Train Analysis for Test RI-PSU-2B

Test No:	RI-PSU-2B				**Sampling Parameters**			**Isokineticity Calc.**					
Test Date:	7/6/2000				Total H2O (g):	402.1		Vw(std): SCF	19.060				
Fuel Type:	#6 Fuel Oil				Total Dust (g):	**0.5493**		VmC: ACF	114.907				
					Pb (in Hg):	29.9		Vm(std): SCF	106.669				
Cal. Value					Delta H (in H2O):	0.4094		Vt(std): SCF	125.728				
(Btu/lb)	18,714				Tm (R):	571		% H2O:	15.16				
					Ts (R):	819		Vs: FM	1561.900				
Firing Rate:					Ps (in Hg):	29.2		Qn: ACFM	0.831				
lbs/hr	79.8				Delta P (in H2O):	0.098		Qn(std): SCFM	0.525				
Btu/hr	1,493,377.0				Cp:	0.99		% Isokinetic:	74.84				
					Dn (in):	0.3125							
PSU Method	Total Volume or				Total Vm (ACF):	114.165		**Dust Loading Calc.**					
Sample Train	Weight Collected				Sample Time (min):	320		DCL: (grains/scf)	**0.0674**				
Splits	(mL or g)				Duct Dia: (ft)	0.625		Stack Flow: ACFM	478.942				
Rinse & KCl	1000							Stack Flow: SCFM	302.413				
H_2O_2	500												
$KMnO_4$	500												
Filter	1.8747												
Test 2B Lab Analysis Data - Uncorrected for Split Size (volume or mass)					Test 2B Lab Analysis Data - Corrected Totals								
													Total Emissions
Analyte	Rinse & KCl (µg/L)	H_2O_2 (µg/L)	$KMnO_4$ (µg/L)	Filter (µg/filter half)	Rinse & KCl (µg)	H_2O_2 (µg)	$KMnO_4$ (µg)	Filter (µg)	Total (µg)	(lb/10^12 Btu)			
Al	376	40.4		2710	376	20.20		5420	5816.20	1239.14			
As	35.8	2.19		14.8	35.8	1.10		29.6	66.50	14.17			
Ba	6.48	0.887		52.1	6.48	0.444		104.2	111.12	23.67			
Be	ND	ND		0.533	ND	ND		1.07	1.07	0.23			
Cd	ND	0.237		0.388	ND	0.119		0.78	0.89	0.19			
Co	ND	ND		101	ND	ND		202	202	43.04			
Cr	ND	7.93		9.11	ND	3.97		18.2	22.19	4.73			
Cu	77.3	2.55		1.5	77.3	1.28		3.0	81.56	17.38			
Hg	0.6	<0.4	0.6	0.15	0.6	<0.2	0.3	0.3020	1.2020	0.26			
Mn	49400	0.990		38.3	49400	0.50		76.6	49477.10	10541.12			
Mo	ND	0.378		6.66	ND	0.189		13.32	13.51	2.88			
Ni	64.6	3.57		2370	64.6	1.79		4740	4806.39	1024.00			
Pb	ND	0.551		11.3	ND	0.276		22.6	22.88	4.87			
Sb	ND	ND		37.2	ND	ND		74.4	74.4	15.85			
Se	ND	5.29		6.36	ND	2.65		12.72	15.37	3.27			
Sr	ND	3.74		53.9	ND	1.87		108	110	23.37			
V	ND	3.47		5940	ND	1.74		11880	11881.74	2531.41			
Zn	48.1	102		133	48.1	51		266	365.10	77.78			
	Test Oil - 1		Test Oil - 2		Partitioning (%)								
Analyte	(mg/kg or ppm)	(lb/10^12 Btu)	(mg/kg or ppm)	(lb/10^12 Btu)	Solid	Gas							
Al	34.0	1,817	31.6	1,689	93.2	6.8							
As	3.63	193.97	0.01	0.53	44.5	55.5							
Ba	0.38	20.31	0.73	39.01	93.8	6.2							
Be					100.0	0.0							
Cd	0.27	14.43	0.2	10.69	86.8	13.2							
Co					100.0	0.0							
Cr	0.12	6.41	0.03	1.60	82.1	17.9							
Cu	0.16	8.55	0.96	51.30	3.7	96.3							
Hg	0.59	31.53	0.13	6.95	25.1	74.9							
Mn	0.15	8.02	0.39	20.84	0.2	99.8							
Mo	0.07	3.74	0.01	0.53	98.6	1.4							
Ni	40.5	2,164.2	44.6	2,383.2	98.6	1.4							
Pb	0.12	6.4	0.6	32.1	98.8	1.2							
Sb					100.0	0.0							
Se	1.40	74.8	2.18	116.5	82.8	17.2							
Sr					98.3	1.7							
V	116	6,199	129	6,893	100.0	0.0							
Zn	1.46	78.0	2.08	111.1	72.9	27.1							

Task 5. Pitch and Coke Material

Many items that we take for granted have some relation to carbon, including aluminum based products where anode carbon is used to reduce the aluminum ore, steel from arc-furnaces using graphite electrodes, and even electric contacts on the key-boards [77]. However, the carbon we use is increasingly dependent on the availability of petroleum-derived streams or other foreign sources [78]. The decrease in domestic produced oil and the subsequent reliance on imported crude oil may have a serious impact on the future of carbon products and related materials in the US, since most carbon products are typically based on petroleum coke [79]. Further, petroleum-derived carbon is also marred by increasing hetero-atom, especially sulfur, and heavy-metal content, and a paradigm shift in the petroleum industry of moving away from producing coke by increasing the use of hydro-cracking and hydro-treatment [80]. Obviously, the introduction of coal-derived carbon precursors from co-coking, including carbon binders (pitch) and filler material (coke) can reduce the dependence of petroleum feedstocks for carbon materials.

Efforts to co-carbonize coal with petroleum residua under the conditions of a delayed coker to provide both aromatic carbon units necessary for thermally stable jet fuels and a valuable coke product represent a fundamental objective of this work. However, to introduce coal into a production-scale delayed coker requires some understanding of the range of problems that might be encountered, preferably on a laboratory scale. Recent changes in the design and operation of our 1 kg/hour laboratory-scale delayed coker have resulted in the ability to remove the entire coke product as a solid mass as compared to a

25 mm diameter core of coke that had been evaluated previously [81]. Indeed, optical microscopic investigations performed on cokes generated earlier this year from 100% decant oil and blends of 20% Pittsburgh seam coal / 80% decant oil provided a wealth of information regarding the identification of carbon materials derived from decant oil, coal and the interaction of the two components. These studies also showed that there was a tendency for the remnants of coal to be concentrated more toward the bottom and center of the reactor discharge.

Subtask 5.1: Sample Procurement and Preparation

Decant oil

A heavy petroleum stream, decant oil from United Refining, will be used for the co-coking experiments. Several drums of decant oil were obtained during this reporting period and shipped to PARC and Penn State.

Coal

During this report period an evaluation of coal mining/cleaning plant facilities in Pennsylvania was undertaken in an attempt to locate coals of high thermoplasticity, low ash yield (either natural or by advanced cleaning technology), low organic inert content and reasonably high production. Most raw coal has a fairly high ash yield and may be difficult to clean even with advance cleaning technology. In previous investigations it was determined that further processing of the coal fraction subjected to froth flotation can lower ash yield and maintain thermoplasticity.

Coal sample procurement was conducted on January 21, 2004 at Mine No 84/Eighty Four Mining owned by CONSOL Energy Inc. in Washington Co., PA. Mine No. 84 is an underground mine producing about 4.2 million short tons annually of a high volatile Pittsburgh seam and is ranked number 56 in U.S. among coal producers. The plant is equipped with a state-of-the-art coal cleaning facility and was chosen due to the commercial potential of the different coal-cleaning streams for co-coking. A conventional cleaned Powellton coal was added for comparison.

Arrangements were made for a three-member Penn State sampling team to collect a bulk coal sample and a sample from the froth flotation cells of the cleaning plant during a shift of operation that coal was being loaded for shipment on January 21, 2004. During our discussion with mine and cleaning plant personnel it was learned that a freeze-prevention agent was being applied to a portion of the coal. To avoid sampling coal containing this material we were directed to a belt drop area of 2 x 0 inch size coal coming from the cleaning plant and being placed on the belt containing coal with the additive applied. It was at this access point that cross-belt cuts of coal were collected over a three hour period to fill four 30-gallon steel drums (i.e., approximately 800 lbs). During this time two members of the team were sampling the two banks of four froth flotation cells. The froth effluent was collected across the full length of each cell and place in it own 10-gallon plastic drum. During the three hours of sampling eight drums were filled from the froth cells, eventually to be combined into one froth flotation cell sample.

The stream of highest interest was the froth flotation fraction. There are several benefits using this fraction for co-coking, including:

(i) no need for further grinding of coal prior to mixing with heavy oil residue;

(ii) it is likely that the highly thermoplastic vitrinite macerals will be concentrated in the light fines from froth flotation thereby increasing the liquid yield during co-coking and improve the properties of the resulting coke; and

(iii) greater possibility for further beneficiation of coal fines towards low ash co-coking coke.

The less than 2 inch clean coal fraction was procured as backup material.

Figure 46 shows the froth flotation setup of the plant and the corresponding ten samples taken. During the sampling operation the flotation cell was being operated with 96 cc/min of Freedom Industries, Inc. TF-944 froth agent (proprietary combination of alcohols and carboxylates) and 504 cc/min of diesel fuel as a collector agent. The froth generator to the left injected the froth into the middle of the left side of the froth cell. The froth was decanted off in eight chambers and one sample was taken from the entire side of each chambers using a quart size bucket. The samples were numbered 1 through 8 **(Figure 46).** An equal number of buckets was taken from each chamber and loaded into 20 gallons drums. Chamber 1 and 5, corresponding to Sample 1 and 5, contained the greatest amount of liquid while chamber 4 and 8 had the lowest amount of liquid and virtually consisted of froth. Correspondingly, the volume of sample was decreasing according to the arrows in **Figure 46**. In addition, two composit samples were generated

where Sample 9 contained about 14 buckets of each of the Sample 1 through 4 and Sample 10 about 14 buckets of Sample 5 through 8.

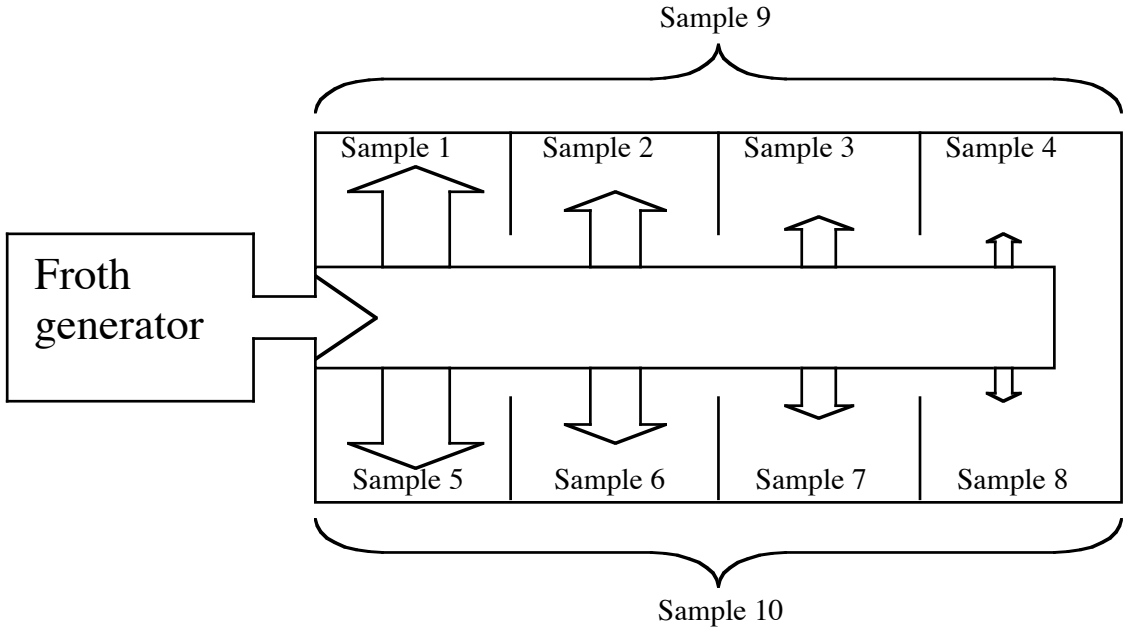

Figure 46. Froth flotation setup of the plant and the corresponding ten samples taken.

Small sub-samples of each drum have been removed for preliminary evaluation of solids content, proximate analysis, ultimate analysis, optical microscopy **(Table 25)** and particle size analysis.

Figures 47 through 56 compares the particle size distribution of Sample 1 through 10. Although there are some differences in the individual particle distributions between the different chambers, the overall particle size distribution seems to be similar for all the chambers. Indeed, this can be seen for Sample 9 and 10 **(Figures 54 and 55,**

respectively) where nearly identical distributions are obtained from the two composite samples (**see Figure 46**).

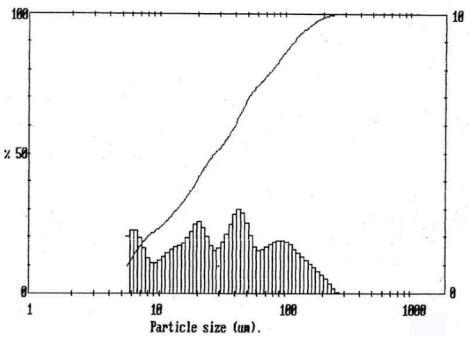

High Size	Under %	High Size	Under %	High Size	Under %	High Size	Under %	High Size	Under %	High Size	Under %	Span 3.96
564	100	254	100	114	89.8	51.3	70.2	23.1	45.4	10.4	24.2	D[4,3] 45.34µm
524	100	236	99.8	106	88.1	47.7	67.7	21.4	43.1	9.64	23.0	
488	100	219	99.4	98.6	86.2	44.4	64.8	19.9	40.5	8.97	21.9	D[3,2] 12.51µm
454	100	204	98.9	91.7	84.3	41.2	61.8	18.5	38.1	8.34	20.8	
422	100	190	98.2	85.3	82.4	38.4	58.9	17.2	35.8	7.76	19.5	
392	100	176	97.4	79.3	80.5	35.7	56.4	16.0	33.8	7.21	17.9	D[v,0.9] 115.02µm
365	100	164	96.5	73.8	78.8	33.2	54.3	14.9	32.0	6.71	15.9	
339	100	153	95.4	68.6	77.1	30.8	52.4	13.9	30.3	6.24	13.7	
315	100	142	94.2	63.8	75.5	28.7	50.8	12.9	28.6	5.80	11.4	D[v,0.1] 5.53µm
293	100	132	92.9	59.3	73.9	26.7	49.2	12.0	27.0			
273	100	123	91.4	55.2	72.2	24.8	47.5	11.2	25.5			

Source = :Sample	Beam length = 2.0 mm	Model indp		D[v,0.5] 27.63µm
	Log. Diff. = 3.209			
Focal length = 300 mm	Obscuration = 0.4524	Volume Conc. = 0.1256%		
Presentation = pil	Volume distribution	Sp.S.A 0.4796 m²/cc.		Shape OFF

Figures 47. Particle size distribution of Sample 1.

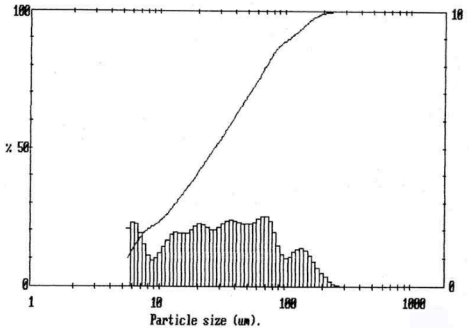

High Size	Under %	High Size	Under %	High Size	Under %	High Size	Under %	High Size	Under %	High Size	Under %	Span 3.73
564	100	254	100	114	91.0	51.3	69.9	23.1	45.4	10.4	24.1	D[4,3] 42.76µm
524	100	236	99.9	106	89.9	47.7	67.7	21.4	43.2	9.64	22.9	
488	100	219	99.7	98.6	88.9	44.4	65.4	19.9	40.9	8.97	21.9	D[3,2] 12.26µm
454	100	204	99.4	91.7	87.8	41.2	63.1	18.5	38.7	8.34	20.9	
422	100	190	98.9	85.3	86.3	38.4	60.8	17.2	36.7	7.76	19.8	
392	100	176	98.2	79.3	84.3	35.7	58.4	16.0	34.8	7.21	18.3	D[v,0.9] 106.52µm
365	100	164	97.3	73.8	82.0	33.2	56.0	14.9	32.9	6.71	16.4	
339	100	153	96.2	68.6	79.5	30.8	53.7	13.9	31.0	6.24	14.1	
315	100	142	94.9	63.8	77.0	28.7	51.6	12.9	29.0	5.80	11.8	D[v,0.1] 5.44µm
293	100	132	93.6	59.3	74.5	26.7	49.6	12.0	27.2			
273	100	123	92.2	55.2	72.2	24.8	47.5	11.2	25.5			

Source = :Sample	Beam length = 2.0 mm	Model indp		D[v,0.5] 27.09µm
	Log. Diff. = 3.194			
Focal length = 300 mm	Obscuration = 0.2754	Volume Conc. = 0.0659%		
Presentation = pil	Volume distribution	Sp.S.A 0.4893 m²/cc.		Shape OFF

Figures 48. Particle size distribution of Sample 2.

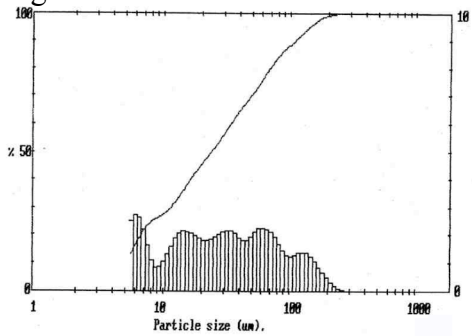

High Size	Under %	High Size	Under %	High Size	Under %	High Size	Under %	High Size	Under %	High Size	Under %	Span 4.31
564	100	254	100	114	91.0	51.3	71.1	23.1	49.2	10.4	28.3	D[4,3] 41.01µm
524	100	236	99.9	106	89.7	47.7	69.2	21.4	47.3	9.64	27.2	
488	100	219	99.7	98.6	88.5	44.4	67.3	19.9	45.5	8.97	26.3	D[3,2] 10.72µm
454	100	204	99.4	91.7	87.3	41.2	65.5	18.5	43.8	8.34	25.5	
422	100	190	98.9	85.3	85.7	38.4	63.6	17.2	41.6	7.76	24.3	
392	100	176	98.3	79.3	84.0	35.7	61.5	16.0	39.5	7.21	22.7	D[v,0.9] 107.76µm
365	100	164	97.4	73.8	82.1	33.2	59.3	14.9	37.4	6.71	20.5	
339	100	153	96.4	68.6	80.0	30.8	57.2	13.9	35.2	6.24	17.8	
315	100	142	95.1	63.8	77.7	28.7	55.0	12.9	33.1	5.80	15.1	D[v,0.1] 4.95µm
293	100	132	93.8	59.3	75.5	26.7	53.0	12.0	31.2			
273	100	123	92.4	55.2	73.2	24.8	51.0	11.2	29.6			

Source = :Sample	Beam length = 2.0 mm	Model indp		D[v,0.5] 23.84µm
	Log. Diff. = 3.310			
Focal length = 300 mm	Obscuration = 0.5922	Volume Conc. = 0.1604%		
Presentation = pil	Volume distribution	Sp.S.A 0.5595 m²/cc.		Shape OFF

Figures 49. Particle size distribution of Sample 3.

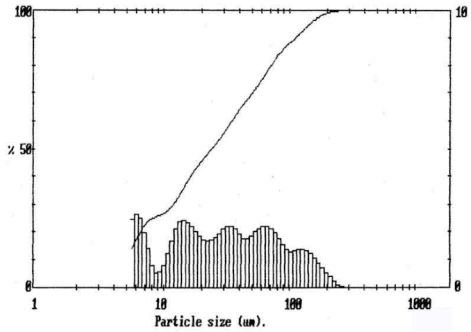

High Size	Under %	High Size	Under %	High Size	Under %	High Size	Under %	High Size	Under %	High Size	Under %	Span 4.37
564	100	254	100	114	90.7	51.3	70.7	23.1	49.1	10.4	27.4	D[4,3] 41.71µm
524	100	236	99.9	106	89.4	47.7	68.8	21.4	47.4	9.64	26.5	
488	100	219	99.7	98.6	88.1	44.4	67.0	19.9	45.7	8.97	26.0	D[3,2] 10.57µm
454	100	204	99.3	91.7	86.7	41.2	65.2	18.5	43.8	8.34	25.5	
422	100	190	98.7	85.3	85.2	38.4	63.3	17.2	41.8	7.76	24.6	
392	100	176	98.0	79.3	83.4	35.7	61.1	16.0	39.5	7.21	23.2	D[v,0.9] 109.71µm
365	100	164	97.1	73.8	81.4	33.2	58.9	14.9	37.2	6.71	21.2	
339	100	153	96.1	68.6	79.2	30.8	56.7	13.9	34.8	6.24	18.7	
315	100	142	94.8	63.8	77.0	28.7	54.6	12.9	32.4	5.80	16.0	D[v,0.1] 4.77µm
293	100	132	93.5	59.3	74.8	26.7	52.6	12.0	30.2			
273	100	123	92.1	55.2	72.7	24.8	50.8	11.2	28.6			

Source = :Sample	Beam length = 2.0 mm	Model indp		D[v,0.5] 23.99µm
	Log. Diff. = 3.178			
Focal length = 300 mm	Obscuration = 0.3758	Volume Conc. = 0.0830%		
Presentation = pil	Volume distribution	Sp.S.A 0.5678 m²/cc.		Shape OFF

Figures 50. Particle size distribution of Sample 4.

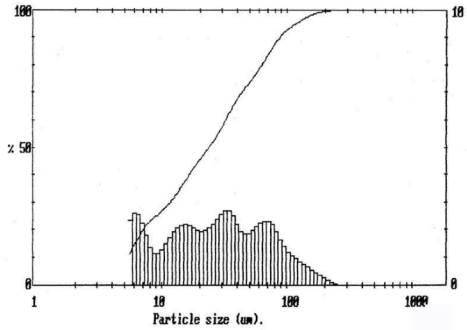

High Size	Under %	High Size	Under %	High Size	Under %	High Size	Under %	High Size	Under %	High Size	Under %	Span 3.47
564	100	254	100	114	94.9	51.3	74.4	23.1	49.4	10.4	27.6	D[4,3] 36.64µm
524	100	236	99.9	106	93.8	47.7	72.6	21.4	47.5	9.64	26.3	
488	100	219	99.9	98.6	92.6	44.4	70.7	19.9	45.5	8.97	25.1	D[3,2] 11.12µm
454	100	204	99.7	91.7	91.2	41.2	68.8	18.5	43.5	8.34	24.0	
422	100	190	99.4	85.3	89.6	38.4	66.5	17.2	41.4	7.76	22.6	
392	100	176	99.1	79.3	87.6	35.7	64.0	16.0	39.2	7.21	20.8	D[v,0.9] 86.86µm
365	100	164	98.7	73.8	85.4	33.2	61.3	14.9	37.0	6.71	18.6	
339	100	153	98.1	68.6	83.1	30.8	58.6	13.9	34.8	6.24	16.0	
315	100	142	97.5	63.8	80.8	28.7	56.1	12.9	32.7	5.80	13.4	D[v,0.1] 5.21µm
293	100	132	96.7	59.3	78.5	26.7	53.7	12.0	30.8			
273	100	123	95.8	55.2	76.4	24.8	51.5	11.2	29.1			

Source = :Sample	Beam length = 2.0 mm	Model indp	D[v,0.5] 23.53µm
	Log. Diff. = 3.200		
Focal length = 300 mm	Obscuration = 0.3011	Volume Conc. = 0.0664%	
Presentation = pil	Volume distribution	Sp.S.A 0.5395 m²/cc.	Shape OFF

Figures 51. Particle size distribution of Sample 5.

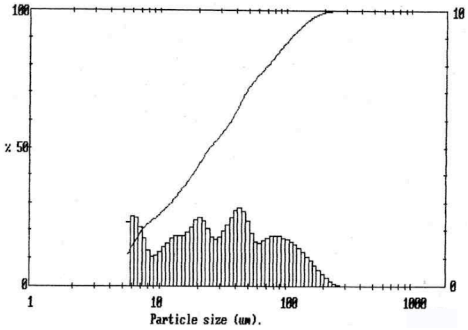

High Size	Under %	High Size	Under %	High Size	Under %	High Size	Under %	High Size	Under %	High Size	Under %	Span 4.08
564	100	254	100	114	91.6	51.3	72.7	23.1	48.1	10.4	26.6	D[4,3] 41.42µm
524	100	236	99.9	106	90.0	47.7	70.3	21.4	45.7	9.64	25.4	
488	100	219	99.7	98.6	88.3	44.4	67.6	19.9	43.2	8.97	24.3	D[3,2] 11.53µm
454	100	204	99.4	91.7	86.6	41.2	64.8	18.5	40.8	8.34	23.2	
422	100	190	99.0	85.3	84.8	38.4	62.0	17.2	38.7	7.76	21.9	
392	100	176	98.4	79.3	82.9	35.7	59.5	16.0	36.8	7.21	20.2	D[v,0.9] 106.06µm
365	100	164	97.7	73.8	81.1	33.2	57.3	14.9	34.9	6.71	18.0	
339	100	153	96.8	68.6	79.4	30.8	55.3	13.9	33.1	6.24	15.5	
315	100	142	95.7	63.8	77.7	28.7	53.6	12.9	31.3	5.80	13.0	D[v,0.1] 5.26µm
293	100	132	94.5	59.3	76.2	26.7	51.9	12.0	29.6			
273	100	123	93.1	55.2	74.6	24.8	50.1	11.2	28.0			

Source = :Sample	Beam length = 2.0 mm	Model indp	D[v,0.5] 24.69µm
	Log. Diff. = 3.299		
Focal length = 300 mm	Obscuration = 0.4316	Volume Conc. = 0.1087%	
Presentation = pil	Volume distribution	Sp.S.A 0.5202 m²/cc.	Shape OFF

Figures 52. Particle size distribution of Sample 6.

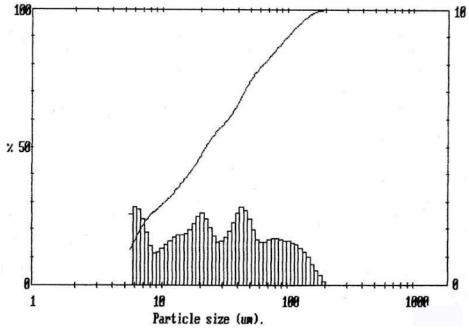

High Size	Under %	High Size	Under %	High Size	Under %	High Size	Under %	High Size	Under %	High Size	Under %	Span 4.24
564	100	254	100	114	93.2	51.3	75.1	23.1	51.6	10.4	29.7	D[4,3] 37.47µm
524	100	236	100	106	91.7	47.7	72.7	21.4	49.2	9.64	28.4	
488	100	219	100	98.6	90.1	44.4	70.0	19.9	46.6	8.97	27.2	D[3,2] 10.62µm
454	100	204	100	91.7	88.5	41.2	67.2	18.5	44.1	8.34	26.0	
422	100	190	99.9	85.3	86.8	38.4	64.6	17.2	41.9	7.76	24.6	
392	100	176	99.5	79.3	85.2	35.7	62.3	16.0	39.9	7.21	22.7	D[v,0.9] 98.15µm
365	100	164	99.0	73.8	83.5	33.2	60.3	14.9	38.1	6.71	20.3	
339	100	153	98.2	68.6	81.9	30.8	58.6	13.9	36.3	6.24	17.5	
315	100	142	97.2	63.8	80.3	28.7	57.0	12.9	34.5	5.80	14.7	D[v,0.1] 5.03µm
293	100	132	96.0	59.3	78.8	26.7	55.5	12.0	32.7			
273	100	123	94.7	55.2	77.1	24.8	53.7	11.2	31.1			

Source = :Sample	Beam length = 2.0 mm	Model indp	D[v,0.5] 21.97µm
	Log. Diff. = 3.412		
Focal length = 300 mm	Obscuration = 0.6381	Volume Conc. = 0.1800%	
Presentation = pil	Volume distribution	Sp.S.A 0.5651 m²/cc.	Shape OFF

Figures 53. Particle size distribution of Sample 7.

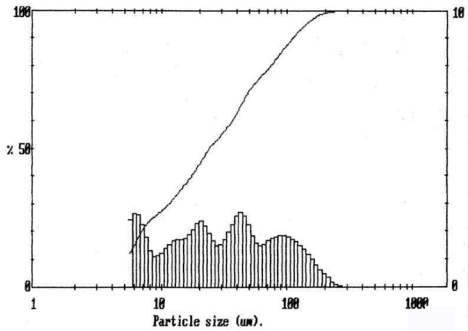

High Size	Under %	High Size	Under %	High Size	Under %	High Size	Under %	High Size	Under %	High Size	Under %	Span 4.40
564	100	254	100	114	90.8	51.3	71.8	23.1	49.0	10.4	28.2	D[4,3] 42.18µm
524	100	236	99.9	106	89.0	47.7	69.5	21.4	46.7	9.64	26.9	
488	100	219	99.7	98.6	87.2	44.4	66.9	19.9	44.3	8.97	25.8	D[3,2] 11.12µm
454	100	204	99.4	91.7	85.4	41.2	64.2	18.5	42.0	8.34	24.7	
422	100	190	98.9	85.3	83.5	38.4	61.6	17.2	39.9	7.76	23.3	
392	100	176	98.3	79.3	81.7	35.7	59.4	16.0	38.0	7.21	21.5	D[v,0.9] 110.35µm
365	100	164	97.5	73.8	79.9	33.2	57.4	14.9	36.3	6.71	19.3	
339	100	153	96.5	68.6	78.3	30.8	55.6	13.9	34.5	6.24	16.6	
315	100	142	95.3	63.8	76.7	28.7	54.1	12.9	32.8	5.80	14.0	D[v,0.1] 5.13µm
293	100	132	93.9	59.3	75.2	26.7	52.6	12.0	31.1			
273	100	123	92.4	55.2	73.6	24.8	50.9	11.2	29.6			

Source = :Sample	Beam length = 2.0 mm	Model indp	D[v,0.5] 23.93µm
	Log. Diff. = 3.242		
Focal length = 300 mm	Obscuration = 0.5321	Volume Conc. = 0.1409%	
Presentation = pil	Volume distribution	Sp.S.A 0.5394 m²/cc.	Shape OFF

Figures 54. Particle size distribution of Sample 8.

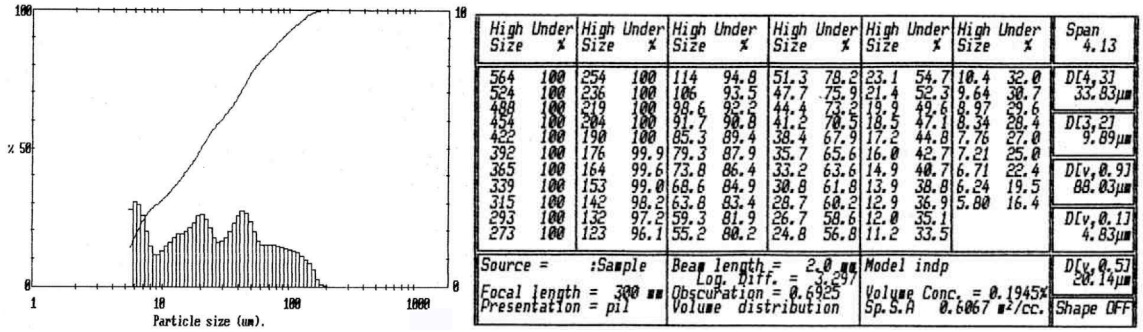

High Size	Under %	High Size	Under %	High Size	Under %	High Size	Under %	High Size	Under %	High Size	Under %	Span 4.13
564	100	254	100	114	94.8	51.3	78.2	23.1	54.7	10.4	32.0	D[4,3] 33.83µm
524	100	236	100	106	93.5	47.7	75.9	21.4	52.3	9.64	30.7	
488	100	219	100	98.6	92.2	44.4	73.2	19.9	49.6	8.97	29.6	D[3,2] 9.89µm
454	100	204	100	91.7	90.8	41.2	70.5	18.5	47.1	8.34	28.4	
422	100	190	100	85.3	89.4	38.4	67.9	17.2	44.8	7.76	27.0	D[v,0.9] 88.03µm
392	100	176	99.9	79.3	87.9	35.7	65.6	16.0	42.7	7.21	25.0	
365	100	164	99.6	73.8	86.4	33.2	63.6	14.9	40.7	6.71	22.4	D[v,0.1] 4.83µm
339	100	153	99.0	68.6	84.9	30.8	61.8	13.9	38.8	6.24	19.5	
315	100	142	98.2	63.8	83.4	28.7	60.2	12.9	36.9	5.80	16.4	
293	100	132	97.2	59.3	81.9	26.7	58.6	12.0	35.1			
273	100	123	96.1	55.2	80.2	24.8	56.8	11.2	33.5			

Source = :Sample	Beam length = 2.0 mm	Model indp	D[v,0.5] 20.14µm
Focal length = 300 mm	Log. Diff. = 3.297	Volume Conc. = 0.1945%	
Presentation = pil	Obscuration = 0.6925	Sp.S.A 0.6067 m²/cc.	Shape OFF
	Volume distribution		

Figures 55. Particle size distribution of Sample 9.

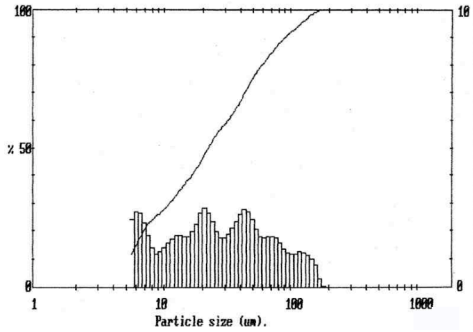

High Size	Under %	High Size	Under %	High Size	Under %	High Size	Under %	High Size	Under %	High Size	Under %	Span 3.83
564	100	254	100	114	94.1	51.3	76.4	23.1	51.7	10.4	28.7	D[4,3] 35.72µm
524	100	236	100	106	92.9	47.7	74.0	21.4	49.1	9.64	27.3	
488	100	219	100	98.6	91.7	44.4	71.3	19.9	46.3	8.97	26.0	D[3,2] 10.85µm
454	100	204	100	91.7	90.5	41.2	68.6	18.5	43.6	8.34	24.8	
422	100	190	100	85.3	89.1	38.4	65.9	17.2	41.4	7.76	23.4	D[v,0.9] 89.37µm
392	100	176	100	79.3	87.5	35.7	63.6	16.0	39.4	7.21	21.6	
365	100	164	99.7	73.8	85.7	33.2	61.5	14.9	37.6	6.71	19.3	D[v,0.1] 5.14µm
339	100	153	98.9	68.6	83.9	30.8	59.6	13.9	35.8	6.24	16.6	
315	100	142	97.8	63.8	82.1	28.7	57.8	12.9	33.9	5.80	13.9	
293	100	132	96.6	59.3	80.4	26.7	56.0	12.0	32.0			
273	100	123	95.4	55.2	78.5	24.8	54.1	11.2	30.3			

Source = :Sample	Beam length = 2.0 mm	Model indp	D[v,0.5] 21.98µm
Focal length = 300 mm	Log. Diff. = 3.289	Volume Conc. = 0.0363%	
Presentation = pil	Obscuration = 0.1817	Sp.S.A 0.5529 m²/cc.	Shape OFF
	Volume distribution		

Figures 56. Particle size distribution of Sample 10.

Figures 47 through 56 indicate that the froth section has no particle size higher than 250 µm, about 90% is below 110µm, 50% is below 70µm and 10% is below 25µm. This particle size distribution indicates that the fraction can be a good starting point for co-coking. As shown in **Table 25**, ash yield of the froth flotation samples are rather high (< 17%) which suggest that secondary cleaning procedures may be necessary.

Table 25. Properties of Froth Effluent Samples

Sample Id.	Sample Type Location	Volume Collected (Liter)	% Solids (As Recd.)	% Moist. Sample (Dried)	% Ash (Dry) Coal	% V.M. (Dry)	% F. C. (Dry)	Carbon (Dry)	Hydrogen (Dry)	Nitrogen (Dry)	Sulfur (Dry)	Oxygen (Dry)
01	Froth Effluent 1	36.0	14.18 ± 0.19	0.89 ± 0.06	13.53 ± 0.06	30.83 ± 0.35	55.64	73.20 ± 0.07	4.68 ± 0.09	1.35 ± 0.02	1.87 ± 0.01	5.37
02	Froth Effluent 2	28.3	15.58 ± 0.28	0.91 ± 0.05	12.50 ± 0.01	30.88 ± 0.49	56.62	74.15 ± 0.29	4.69 ± 0.13	1.35 ± 0.05	1.90 ± 0.01	5.40
03	Froth Effluent 3	23.7	13.86 ± 0.08	0.90 ± 0.04	13.86 ± 0.18	30.93 ± 0.50	55.21	72.26 ± 0.10	4.50 ± 0.16	1.30 ± 0.00	2.12 ± 0.01	5.96
04	Froth Effluent 4	20.6	15.07 ± 0.09	0.81 ± 0.01	13.29 ± 0.09	30.60 ± 0.12	56.11	73.07 ± 0.14	4.19 ± 0.20	1.34 ± 0.02	2.26 ± 0.01	5.85
05	Froth Effluent 5	40.7	12.45 ± 0.10	0.82 ± 0.03	17.61 ± 0.04	29.48 ± 0.04	52.91	69.21 ± 0.05	4.09 ± 0.01	1.28 ± 0.01	1.96 ± 0.02	5.85
06	Froth Effluent 6	32.9	13.22 ± 0.08	0.88 ± 0.03	16.22 ± 0.24	29.99 ± 0.14	53.79	70.39 ± 0.06	4.31 ± 0.16	1.31 ± 0.00	1.98 ± 0.02	5.79
07	Froth Effluent 7	23.6	14.31 ± 0.11	1.06 ± 0.02	14.96 ± 0.02	30.64 ± 0.28	54.40	71.43 ± 0.16	3.92 ± 0.07	1.31 ± 0.01	2.03 ± 0.01	6.34
08	Froth Effluent 8	20.6	14.80 ± 0.14	0.83 ± 0.04	14.79 ± 0.20	29.94 ± 0.45	55.27	71.51 ± 0.16	3.95 ± 0.19	1.32 ± 0.03	2.11 ± 0.01	6.32
09	Froth Effluent Compos-ite 1-4	26.7	15.82 ± 0.11	0.83 ± 0.05	15.02 ± 0.10	29.37 ± 0.01	55.61	71.66 ± 0.17	3.85 ± 0.15	1.35 ± 0.05	1.83 ± 0.02	6.29
10	Froth Effluent Compos-ite 5-8	32.9	14.53 ± 0.00	0.93 ± 0.02	15.67 ± 0.04	29.52 ± 0.32	54.81	70.85 ± 0.11	3.79 ± 0.02	1.26 ± 0.02	1.85 ± 0.01	6.58

Close inspection of the Pittsburgh froth cell samples in the last report showed that they all had a fairly high ash yield (ranging from13.3 to 17.1%) largely because of an associated clay-mineral fraction that coated the surface of the coal particles. By simply washing away the minus 45 μm size fraction a vast improvement in the quality of the produce was realized as seen in **Figure 57** where the larger particles are very pure and highly reactive vitrinite particles while the smaller white particles are inertinite and very small particles are mostly clay. **Figure 58** illustrates the simple schematics of removing clay, commonly referred to as "slime" and inertinites from the froth. The process could easily be a continuous one with little cost to the beneficiation plant.

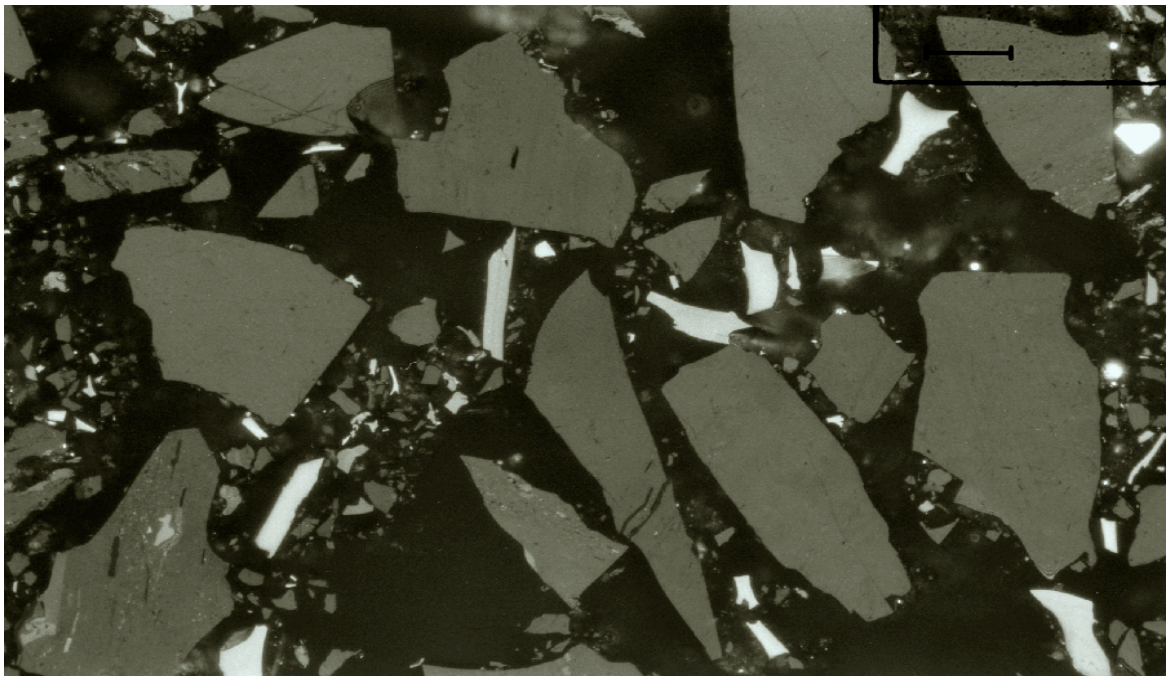

Figure 57: Froth sample #9 where the larger particles are very pure and highly reactive vitrinite particles while the smaller white particles are inertinite and very small particles are mostly clay.

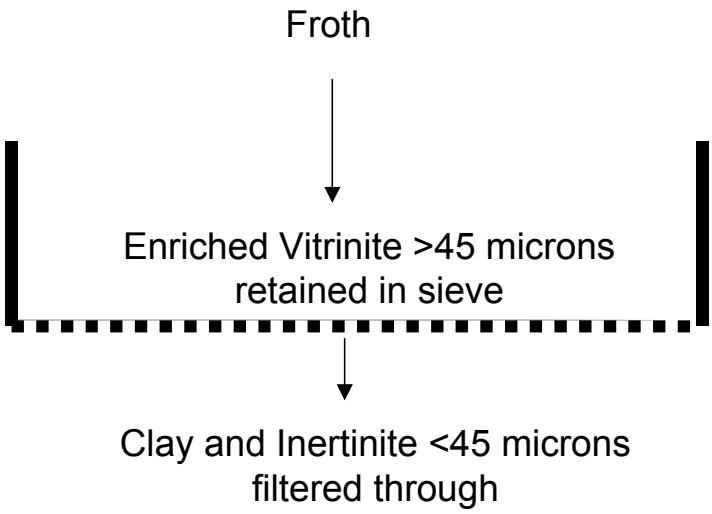

Figure 58. Schematics of removing clay, commonly referred to as "slime" and inertinites from the froth.

Table 26 indicates that >45µm fraction is between 22 to 37% of the froth, with an average of 1/3. Table 27 shows that the sieved fraction of Sample#10 only has a ~3% mineral matter. This indicates that over 80% of the "slime" can be removed through sieving where the <45µm fraction has over 30% mineral matter.

Table 26: Mass balances of sieving the froth streams collected.

Barrel ID#	> 45µm (g)	< 45µm (g)	> 45µm (%)	< 45µm (%)
1	Drying	3306		
2	1601	2774	36.6	63.4
3	1071	2084	33.9	66.1
4	Drying	Drying		
5	1496	3624	29.2	70.8
6	Drying	Drying		
7	1107	2260	32.9	67.1
8	Drying	2195		
9	Drying	3585		
10	1886	6621	22.2	77.8

Table 27: Elemental analysis of the sieved fraction of Sample#10.

% Moist. Sample (Dried)	% Ash (Dry) Coal	HHV (Btu/lb) (Dry)	% V.M. (Dry)	% F. C. (Dry)	Carbon (Dry)	Hydrogen (Dry)	Nitrogen (Dry)	Sulfur (Dry)	Oxygen (Dry)
1.83 ± 0.03	3.12 ± 0.09		35.19 ± 0.29	61.69	82.62 ± 0.20	5.68 ± 0.01	1.50 ± 0.03	1.18 ± 0.06	5.90

The #10 composite froth sample that had been washed free of its -45 micron particle size fraction was studied under the optical microscope. The particle size distribution was narrow and most of the fine size coals particles have been eliminated. Along with them most of the clay minerals that coated coal particles and formed agglomerates in the typically dried samples are gone. The mineral matter that remains is intimately mixed with the organic fraction, but there are still some small shale particles

and partings as well as a minor amount of calcium carbonate that are free of the matrix. Most of the mineral matter consists of clay minerals intimately and uniformly mixed with the organic matrix, a significant amount of pyrite as small blebs (<20 microns), framboids, euhedra and infillings, and a minor amount of small rounded quartz particles observed along bedding.

The organic composition also has been altered by the elimination of -45 micron particles as illustrated in **Figure 59**. A point count analysis reveals that the product from composite #10 has 90.3% vitrinite, 7.7% inertinite and 2.0% liptinite on a volume percentage basis. This compares with unwashed composite #9 that contained 80.5% vitrinite, 18.6% inertinite and 0.9 % liptinite.

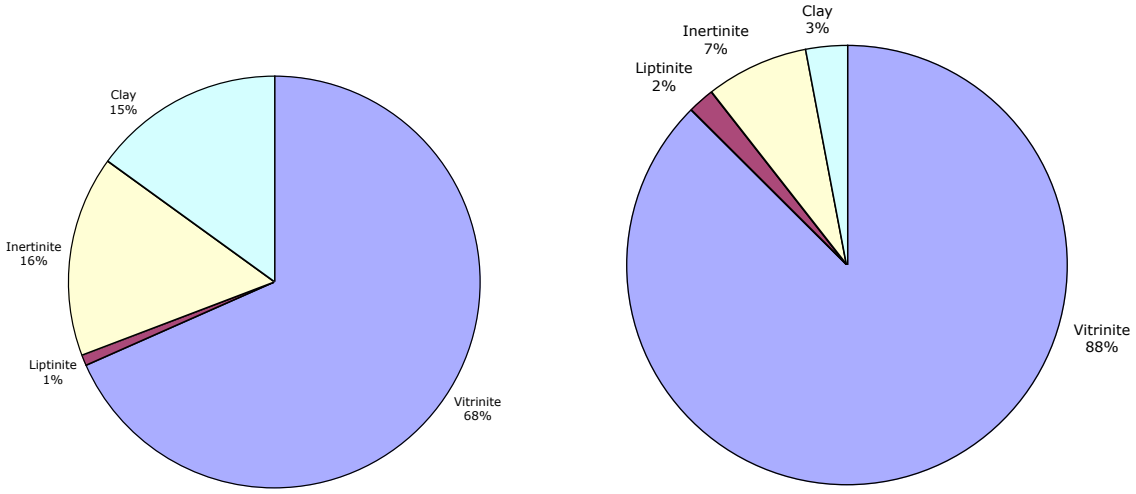

Figure 59. Changes in the organic composition of sample#10 by the elimination of -45 micron particles.

Subtask 5.2: Examine the Resid from Fractionation of the Deeply-Hydrotreated RCO/LCO as a Pitch Material

Supplies and materials were purchased to start to examine the resid from fractionation of the deeply-hydrotreated RCO/LCO as a pitch material following activity in Subtask 5.3.

Subtask 5.3: Co-Coking of Coal and Heavy Petroleum Stream

In the current study, a subsample of the froth flotation cell composite (#10) of the Pittsburgh seam coal was further cleaned and employed in an initial coking run. The delayed coking process and subsequent distillation is shown in **Figure 60**. Run #35 that used 80% of a low-sulfur decant-oil from Seadrift and 20% of a re-cleaned Pittsburgh seam froth sample to generate about 1400 g of coke. The coke was sampled and radial sections were evaluated by optical microscopy to determine the nature and quality of the carbon as well as the distribution of coal- and decant oil- derived textural components.

To make a valuable delayed coke product from coal-petroleum resid blends requires a significant reduction in the coal-derived mineral matter. The Pittsburgh seam coal from Mine #84 in Washington County, PA was selected, not only because it possessed the proper combination of rank and thermoplastic properties, but because the mine possessed advance cleaning facilities that include froth flotation cells. These cells generally deal with the separation of mineral matter from the minus 150 μm size fraction of coal by attaching air bubbles to the carbonaceous surface of coal and floating most

organic particles away from those ladened with minerals. Consequently, the froth cell effluent is a ready-made product for co-coking that has the potential to be cleaned further.

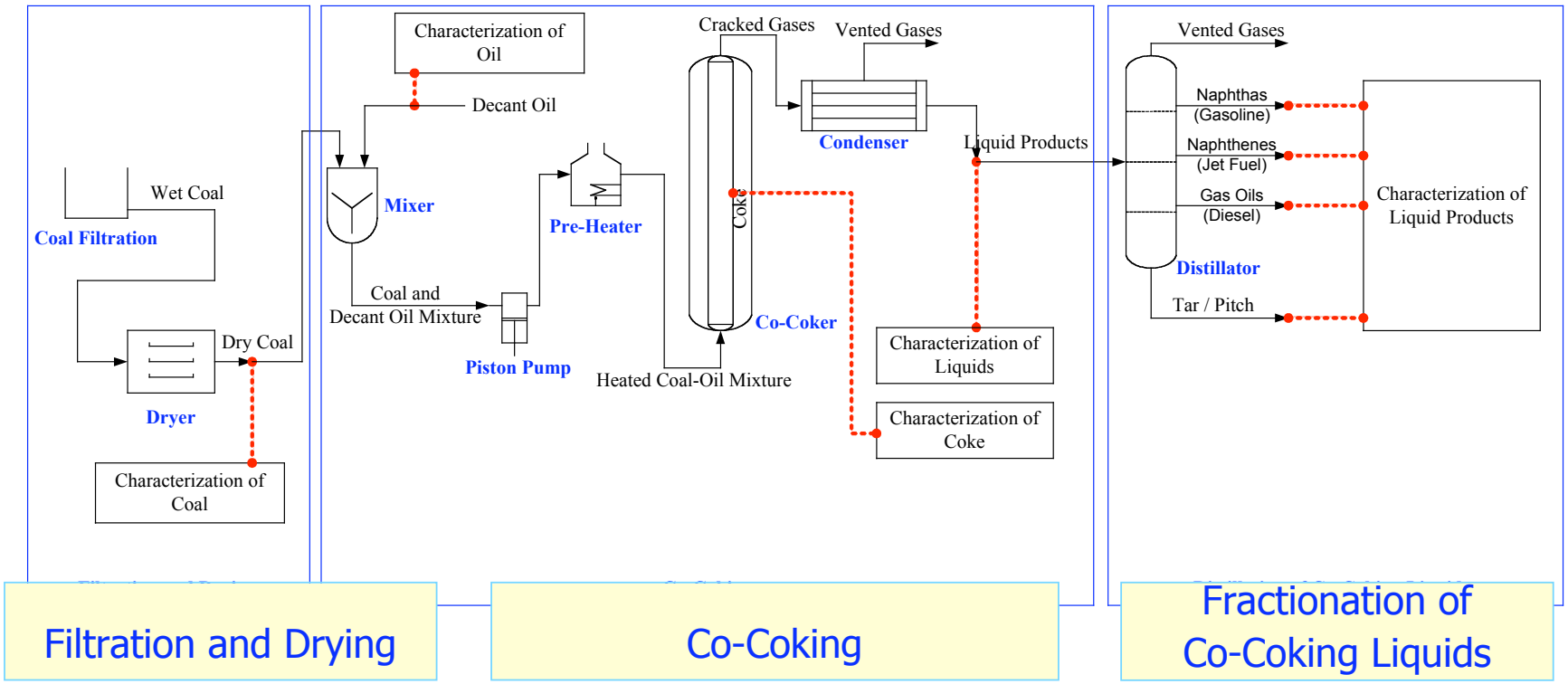

Co-Coker Feed Ratio
Coal:Decant Oil = 1:4

Products
Coke: 32.5%
Liquids: 67.5%

High Vacuum Distillation
To prevent
cracking/polymerization

Figure 60: Schematic of the delayed coking process and subsequent distillation.

Subtask 5.4: Analysis of Co-Coking Coke

Experimental conditions for a coking run that employed 100% decant oil and the run using 80% of the same decant oil with 20% of the +45 μm Pittsburgh froth samples are compared in **Table 28**. Generally, the coker was operated at the same feed rate and heating time, although the thermal profiles of the reactor were different among the runs as were the distributions of products. In particular, much less coke was produced with 100% decant oil compared with the Pittsburgh +45 fraction. After cooling, the cokes were removed from the reaction cylinder (or coke drum) basically as single samples and were subjected to non-destructive Computer Assisted X-ray Tomography (X-ray CAT-Scan) to provide density maps of the coke through cross-sectional areas at five discrete one centimeter intervals along the long axis of the cylindrical specimens, i.e., maps were generated from intervals at 1-2 cm, 6-7 cm, 12-13 cm, 18-19 cm, and 24-25 cm. Following these tests, the selected regions were cut from the coke and radial sections were removed for optical microscopy and for graphitization studies. X-ray CAT-scan and graphitization results will be covered elsewhere or during another reporting period.

Coke discharge samples were observed as mostly competent, slightly tapering cylinders with a smooth shinny black surface near the bottom (or inlet) of the cylinder and becoming slightly more porous and dull toward the top. Fractures were observed at oblique angles to the long axis and were always rough and angular rather than smooth cleavage planes. Fractures appeared to result from shrinkage connecting zones of weakness caused by pore-space density.

Table 28 – Conditions and Yields from the Experimental Delayed Coker

Conditions	**Run #13**	**Run #14**	**Run #35**
Date	10/21/03	10/30/03	7/8/04
Components	Decant Oil	4:1 Decant Oil/ Powellton Coal	4:1 Decant Oil/ +45 μm Pittsburgh Froth
Feed, hrs	6	6	6
Held at 500ºC, hrs	6	6	6
Feed Rate, g/min	16.7	16.7	16.7
Preheater Outlet, ºC	417	419	443
Coke Drum Inlet, ºC	446	474	468
Coke Drum Low/mid., ºC	493	481	469
Coke Drum Top, ºC	458	466	470
Total Feed, g	6028	6054	n.a
Coke Product, g (%)	860 (14.3%)	1917 (31.7%)	1400 (32.5%)
Liquid Product, g, (%)	4800 (79.6%)	3989 (65.9%)	2913 (67.5%)
Gas Product, g, (%)	368 (6.1%)	148 (2.4%)	n.a.

n.a.= not available

Each coke was marked with two grease pencils (one white and one red) side-by-side so that when the white line is positioned to the right of the red, the flow direction is oriented in the upward direction. The one-centimeter slices that were subjected to X-ray CAT scan were marked for cutting using a diamond saw. Owing to the fragile nature of some of the coke regions, special foil-coated duct tape was used to hold particles in position during cutting. Once cut, most of the disk-shaped slices had a distinctive structure that included a competent outer rim of hard porous carbon, with an inner region containing greater pore density and weaker carbon walls. Because the disks measured about 82 to 76 mm in diameter (too large for optical microscopy), an outer section and an inner section together approximately equal to the radius were removed for the preparation of two specimens for optical microscopy.

The optical specimens were oriented as approximately one centimeter thick longitudinal sections so that the direction of flow would be known. Each coke segment was glued into a plastic mold and impregnated with a cold setting epoxy resin by placing them under vacuum several times. Vacuum impregnation effectively forces epoxy to replace the connected air-filled voids in the coke, whereas those voids not connected to the exterior surface remain unfilled. This may be an important distinction later on when porosity and pore shape is evaluated. After the epoxy hardened, the oriented surface of each specimen was ground and polished using a series of grit papers (400 and 600 grit) and alumina polishing slurries (0.3 and 0.05 micron).

All cokes were described in hand specimen as well as inspected using a Zeiss Universal research microscope where a 40X (625X total magnification) Antiflex oil immersion objective using crossed-polarized white-light illumination. Photomicrographs of selected areas of each optical specimen were taken using 200 ASA Elite Chrome color 35 mm slide film and later digitized, but none have been included with this report.

A point count analysis of the volume percentage distribution of carbon textures was performed on selected segments. This analysis was performed at 625X magnification in oil immersion by traversing the sample based upon a 0.2 x 0.2 mm grid perpendicular to the direction of flow and identifying the textural element under a crosshair held in a microscope eyepiece. A total of 1000 counts were accumulated from each surface and the results are given as volume percentages in Tables 29 to 33.

Five different textural elements belonging to carbon derived from decant oil were identified in the core segments, including

Isotropic – a relatively low reflecting, dark gray carbon material that displays little or no optical activity when the specimen is rotated under crossed-polarized light.

Mosaic – a higher reflecting carbon textural element that displays optical anisotropy and is characterized by isochromatic units of less than 10 μm.

Small Domain – is an anisotropic carbon texture, which exhibits isochromatic units of between 10 – 60 μm in diameter.

Domain – is an anisotropic carbon having much larger isochromatic units of greater than 60 μm diameter.

Flow Domain – is an anisotropic texture exhibiting elongated isochromatic areas of greater than 60 μm in length and ≤10 μm wide.

When coal was employed five additional textural components could be identified and are described as follows.

Vitrinite-Derived Mosaic – the characteristic 0.5-2.0 μm diameter isochromatic units typically generated during the carbonization of vitrinite of high volatile bituminous coals. During co-carbonization with decant oil the isochromatic areas of bituminous rank vitrinite can become enhanced to between 2.0 - 6.0 μm. In this investigation a distinction was made between enhanced (approximately >2.0 μm) and non-enhanced (generally <2.0 μm) isochromatic areas derived from vitrinite.

Isotropic Vitrinite – It is possible that some vitrinite may become thermoplastic but not develop a mesophase during carbonization and therefore may remain isotropic.

Inertinite-Derived Texture – angular and irregular shaped particles trapped in the vitrinite or petroleum residua matrix, which may or may not display remnant cell structures and are mostly isotropic.

Mineral Matter – remnant particle of coal-derived mineral matter that usually includes clays, pyrite, quartz and carbonate minerals.

As a result of acquiring samples for optical microscopy a number of cross sectional surfaces were exposed at intervals through the coke discharged from the coke drum. The macroscopic structure of these surfaces change with distance from the inlet and may indeed show differences that result from reaction time, flow rate, particle/liquid interaction, etc. However, the extended soak time (6 hrs at ~500ºC) could mask many of the more profound differences between macro-structure and micro-texture.

Macroscopic Description The cokes made with coal were about 45 cm long, whereas that made from 100% decant oil was about half that size (20 cm). In general a similar structure was observed for all three cokes in that a rim of competent, relatively hard, porous carbon was found from the exterior surface extending inward 12-30 mm toward the center. The width of this zone varied from place to place within a given coke and perhaps was wider for cokes made with coal. Another general observation was that, at least for the first 13 cm length of the cokes, there was some type of central region (often offset from the exact center) containing a single hole or a region of great porosity. The

central region, which was 10 – 45 mm in approximate diameter, can be traced through the solid coke segments back to the inlet of the drum and was composed of relatively weak carbon compared with the outer rim. Presumably, this region represented the main inlet channel for material being added to the drum but which continued to carbonize during the extended hold time at 500ºC. Also, from this central region 3-8 fractures often radiated through the rim carbon, sometimes reaching the outer surface and causing degradation of the coke.

Description of Micro-texture The fact that different regions were observed macroscopically from the exterior to the interior of these coke artifacts, suggests that a materials difference may be the root cause. Petrographic samples were prepared with the natural weakness between outer and inner sections taken into account. After cursory inspection under a reflected-light microscope it was decided to collect information on the distribution of textural elements from two or three regions within each radial section as dictated by the material. Consequently, point-count analyses were performed from the rim and central regions of cokes #13 (100% decant oil, **Table 29**) and #35 (blend with Pittsburgh coal, **Tables 32 and 33**), whereas coke #14 (blend with Powellton coal, **Tables 30 and 31)** was divided into three separate regions.

A number of general observations can be made regarding coke #13. As seen in **Table 29**, the optical textures were typically large with the small domain and domain size isochromatic textures dominating in every location, followed by flow domains and mosaic textures and isotropic carbon. Flow domain and domain carbon represent textures

that are found consistently in high-value needle coke products and are desirable in higher concentration, whereas those of isotropic carbon and mosaic textures are less desirable. Not only was flow domain carbon observed, but a significant fraction of the domain carbon textures were elongated as well. There tended to be more flow domain textures found in the central area of the coke mass, corresponding to a higher concentration of porosity, than found in the outer carbon rim. Furthermore, as carbon deposited on the reactor wall the effective diameter of the reactor would decrease, thus resulting in an increased velocity of the incoming decant oil. As needle coke is produced in delayed cokers at higher flow rates [82], this increase in velocity may influence the appearance of flow domain carbon in the current experimental reactor. Most of the isotropic carbon was observed intimately mixed within the anisotropic textural or structural elements. As a minor trend, there appeared to be more mosaic textures below 7.0 cm, less toward the top of the coke mass, and domain carbon was more common in the outer rim compared with the center, but above 7.0 cm this trend reversed (i.e., more domain textures in the center compared with the rim). In general, the distribution of carbon textures was fairly uniform throughout the coke artifact for these run conditions and this decant oil.

Table 29 – Distribution of Textural Composition of Coke From Run #13 Using 100% Decant Oil, Vol. %

Location from Bottom, cm	Cross Section, mm	Isotropic	Mosaic <10µm	Small Domain 10-60 µm	Domain >60 µm	Flow Domain >60L; <10W
1.0 - 2.0	0.0 – 18.0	0.0	2.7	59.6	35.5	2.2
	18.0 – 47.0	0.7	6.2	67.4	20.5	5.2
6.0 - 7.0	0.0 – 24.0	0.7	2.0	51.9	40.3	5.1
	24.0 – 48.0	1.3	2.3	51.3	34.0	11.1
12.0 – 13.0	0.0 – 18.0	1.0	1.7	63.2	30.9	3.2
	18.0 – 39.0	1.0	1.4	52.8	37.9	6.9
18.0 – 19.8	0.0 – 23.0	1.1	1.1	63.5	29.1	5.2
	23.0 – 43.0	2.8	1.7	52.2	37.2	6.1

Optical textures found in the cokes when coal was added (runs #14 and #35) were completely different from those observed when decant oil was coked alone. For run #14 a considerable variation in the distribution of carbon textures in scanning from outer edge to center of the coke mass was observed. Consequently, quantitative point count analyses were completed at three different intervals from edge to center based upon the natural divisions of each interval of coke (bottom to top). The volume percentages of carbon textures derived from coal and decant oil are provided in **Table 30** and have been summarized in **Table 31** to show the volume percentage of material derived from coal or petroleum compared with the normalized distribution of textures derived from decant oil.

As shown in Table 30, in nearly every case the coke interval on the exterior of the coke mass contained more textures derived from decant oil than coal (except at the 6.0-

7.0 cm interval) and the amount of decant oil-derived carbon in this section increased in concentration with distance from the inlet (bottom). Coal-derived textures became dominant in the intermediate region and were nearly all that was found in the center. Although some domain size textures were observed in most of the intervals, it was not as common as was seen in coke #13; instead small domain and mosaic textures dominated. Consequently, one of the principle influences of co-coking coal with decant oil was the reduction in the size of the isochromatic textures generated from the decant oil. This is demonstrated better in **Table 31** where the textures derived from the decant oil have been normalized.

On the other hand, the size of the isochromatic textures observed from the vitrinite portion of coal was enhanced or enlarged during co-coking in the presence of decant oil. The distribution of enhanced vitrinite-derived textures was greatest in the exterior and middle sections and was generally non-enhanced in the center region. Consequently, in coke run #14 the amount of coal-derived textures increased as the center of the coke mass was approached and the vitrinite-derived texture showed less enhancement at every level from bottom to the 25 cm level of the coke mass. The center region from 1.0 – 13.0 cm was for the most part coal-derived, but above this region the amount of decant oil-derived carbon increased with height **(Table 30**). One plausible explanation for this may be that as partially thermoplastic coal particles were entering the reactor, because of their higher viscosity (than decant oil), they agglomerated with other coal particles forming a mass too large to be moved by the velocity of the incoming blend. This would lead to a separation of coal and decant oil and with the diminished

contact less enhancement of the vitrinite-derived coal textures. Decant-oil would pass through and around the mass of plastic coal and carbonize in the region above.

Another interesting observation involved the fact that inertinite-derived carbon seemed to be concentrated in the center of the coke mass at every level (**Table 30**). Possibly some of this may result from devolatilization and interaction with the decant oil of the reactive coal macerals (vitrinite and liptinite), thus changing the relative concentration of those materials that do not become thermoplastic (i.e., inertinite). A slight increase in observed mineral matter toward the center of the coke mass supports this observation, but unlike mineral matter the concentration of inertinite more than doubles in every case. Furthermore, inertinite particles have been seen as separate entities completely surrounded by decant oil-derived carbon, which suggests that decant-oil could be winnowing inertinite from the plastic coal mass.

Finally, in the presence of coal, decant oil tends to contribute completely to the formation of an anisotropic carbon, i.e., no isotropic carbon derived from decant oil was observed. However, there were many instances where the vitrinite portion of the coal had become thermoplastic, but did not develop any mosaic isochromatic texture. These areas are referred to as being isotropic vitrinite. As seen in **Table 30** the concentration of isotropic vitrinite was found to be greater in the center and toward the bottom of the #14 coke mass.

In contrast, the distribution of carbon textural elements in coke derived from a blend with +45 μm Pittsburgh seam coal showed some similarities but also some significant differences (**Tables 32 and 33**). As found when the Powellton coal was used remnants of the Pittsburgh coal appeared to be concentrated at the bottom and center of the coke artifact and it's presence effectively reduced the size and elongation of the optical textures derived from the decant oil. Further, vitrinite-derived materials seem to have had more contact time or was more homogenized with the decant oil as more enhanced vitrinite-derived texture was observed. Inertinite-derived materials were strangely concentrated in the center region of the coke artifact and in some places were oriented in the direction of flow. As shown in **Tables 29 to 33**, there was a significant decrease in the amount of coal-derived textures in the 12-13 cm interval and almost none above 18 cm, meaning that nearly 100% of the coal remained in the bottom 40% of the coke artifact. However, even though there was a separation of materials the decant-oil-derived optical textures that constitute the upper 60% of the coke on average are smaller and less elongated compared with run #13 (**Table 29**).

Optical microscopy shows that when a thermoplastic coal was combined with decant-oil and pumped through a preheater and then into a heated reaction vessel at 16.7 g/min, a separation of materials occurred. Clearly, in both cases the coals have become thermoplastic and have interacted to some degree with the decant oil to form a resultant coke texture. Presently, the enhanced vitrinite-derived texture and to some degree the decant-oil-derived mosaic represents the resultant carbon texture. However, the existence of non-enhanced vitrinite-derived textures suggests that there was little contact between

the two components during the coking cycle. Because most of the non-enhanced material was found near the bottom and center of the coke artifacts, it seems that the physical separation must occur near the inlet of the reactor. One possible explanation is that upon entering the reactor, the larger thermoplastic coal particles stick together forming an viscous agglomerate, whereas the finer more fully fluid particles travel around or through the agglomeration with a majority of the decant oil. Finer particles of lower density may be the reason for the seemingly inexplicable concentration of inertinite particles in the center of the coke artifact. From our observations the agglomeration process appeared to be more effective with the Pittsburgh seam coal which has lower fluidity and a narrower thermoplastic range compared with the Powellton coal.

Regardless of whether separation occurs as a result of agglomeration during filling of the reactor or because of some settling mechanism or a combination of both, it will be very important to find a way to eliminate the problem. At a larger scale, an agglomeration at the inlet position would become so heavy that new material could not be pumped into the reactor, causing early termination of the operation and expensive clean up or delays. Furthermore, a separation of materials within a process leads to product quality control problems. The blend components need to be homogeneously distributed within the coke to insure product uniformity.

By way of a materials solution, some evidence was presented to suggest that thermoplastic properties and maybe particle size could have an influence on the separation mechanism, but other coal properties need to be examined as well. Also, some

coals lose their thermoplastic properties quite rapidly after grinding and when exposed to air, so perhaps there needs to be better care of the raw materials. However, these solutions may be minor in comparison to changing the operating parameters, i.e., feed rate, coal concentration, more uniform mixing of the blend, mixing or preheat temperatures, etc.

Currently, we are looking at inexpensive methods for obtaining a coal product that has an ash yield below 1.0% without regard for coal production yield. An example of such a procedure would be to take the froth flotation cell effluent, wash away the fines to eliminate the associated clay minerals, and then removing the material that floats on a 1.35 specific gravity solution. The coal product yield might very well be 10 to 20% of the froth, but it will have the proper cleanliness to make a competitive premium carbon product.

Efforts are underway to evaluate what combination of materials handling and engineering solutions might produce a uniform coke product. Recently, a run was made with the fresh Pittsburgh coal seam sample (DECS-34) that was crushed to 90% below 176 μm and feed into the reactor at twice the feed rate (~33 g/min). The coke will be inspected and other experiments designed to achieve a uniform distribution of decant-oil- and coal- derived carbon textures.

Table 30 – Petrographic Analysis of Carbon Textures in Coker Sample #14 by Size and Origin, Vol. %

Long. Interval, cm	Cross Section, mm	Vitrinite-derived		Inert-derived	Isotropic Vitrinite	Min. Matter	Isotropic Petroleum derived	Mosaic, <10μm	Small Domain, 10-60μm	Domain >60μm	Flow Domain, >60μm L, <10μm W
		Enhanced	Non- enhan.								
1.0 – 2.0	0.0 – 15.0	37.0	1.6	6.0	0.0	0.7	0.1	22.1	26.0	6.5	0.0
	15.0 – 28.0	41.1	23.1	12.0	0.5	0.5	0.0	18.2	4.3	0.3	0.0
	28.0 – 57.0	2.7	75.7	18.0	2.1	0.8	0.0	0.2	0.4	0.1	0.0
6.0 – 7.0	0.0 – 14.0	44.0	0.8	7.9	0.0	0.8	0.0	25.8	15.8	4.9	0.0
	14.0 – 22.0	42.1	25.4	13.8	0.7	1.0	0.0	15.7	1.3	0.0	0.0
	22.0 – 42.0	1.3	77.8	14.8	3.7	1.5	0.0	0.9	0.0	0.0	0.0
12.0 – 13.0	0.0 – 13.0	34.0	0.0	5.8	0.1	0.6	0.0	28.8	23.4	6.1	1.2
	13.0 – 26.0	21.7	40.4	12.1	0.1	1.0	0.0	18.0	5.6	0.2	0.9
	26.0 – 55.0	0.6	80.0	16.7	1.3	1.3	0.0	0.1	0.0	0.0	0.0
18.0 – 19.0	0.0 – 13.0	12.2	10.4	5.1	0.2	0.2	0.0	8.6	51.4	9.3	2.6
	13.0 – 29.0	10.8	40.6	9.8	0.0	0.8	0.0	10.5	20.8	4.1	2.6
	29.0 – 54.0	7.0	69.3	16.3	0.5	1.0	0.0	4.6	1.3	0.0	0.0
24.0 – 25.0	0.0 – 7.5	11.1	18.3	6.6	0.2	0.7	0.0	10.4	41.1	10.3	1.3
	7.5 – 15.0	7.0	61.8	11.8	0.3	0.9	0.0	8.0	8.8	1.4	0.0
	15.0 – 31.0	5.9	68.7	12.9	0.2	0.9	0.0	8.1	3.1	0.0	0.2

Table 31 – Proportion of Textures Derived from Coal and Decant Oil Compared with the Normalized Concentration of Decant Oil Textures in Coke from Run #14, Vol. %

Long. Interval, cm	Cross Section, mm	% Coal-derived	% Petroleum-derived	Isotropic Petroleum-derived	Mosaic, <10μm	Small Domain, 10-60μm	Domain >60μm	Flow Domain, >60μm L, <10μm W
1.0 – 2.0	0.0 – 15.0	45.3	54.7	0.2	40.4	47.5	11.9	0.0
	15.0 – 28.0	77.2	22.8	0.0	79.8	18.9	1.3	0.0
	28.0 – 57.0	99.3	0.7	0.0	28.6	57.1	14.3	0.0
6.0 – 7.0	0.0 – 14.0	53.5	46.5	0.0	55.5	34.0	10.5	0.0
	14.0 – 22.0	83.0	17.0	0.0	92.4	7.6	0.0	0.0
	22.0 – 42.0	99.1	0.9	0.0	100.0	0.0	0.0	0.0
12.0 – 13.0	0.0 – 13.0	40.5	59.5	0.0	48.4	39.3	10.3	2.0
	13.0 – 26.0	75.3	24.7	0.0	72.9	22.7	0.8	3.6
	26.0 – 55.0	99.9	0.1	0.0	100.0	0.0	0.0	0.0
18.0 – 19.0	0.0 – 13.0	28.1	71.9	0.0	12.0	71.5	12.9	3.6
	13.0 – 29.0	62.0	38.0	0.0	27.6	54.8	10.8	6.8
	29.0 – 54.0	94.1	5.9	0.0	78.0	22.0	0.0	0.0
24.0 – 25.0	0.0 – 7.5	36.9	63.1	0.0	16.5	65.1	16.3	2.1
	7.5 – 15.0	81.8	18.2	0.0	44.0	48.3	7.7	0.0
	15.0 – 31.0	88.6	11.4	0.0	71.0	27.2	0.0	1.8

Table 32– Petrographic Analysis of Carbon Textures in Coker Sample #35 by Size and Origin, Vol. %

Long. Interval, cm	Cross Section, mm	Vitrinite-derived		Inert-derived	Isotropic Vitrinite	Min. Matter	Isotropic Petroleum derived	Mosaic, <10μm	Small Domain, 10-60μm	Domain >60μm	Flow Domain, >60μm L, <10μm W
		Enhanced	Non- enhan.								
1.0 – 2.0	0.0 – 27.5	37.5	0.4	5.4	0.0	1.1	0.3	46.3	8.8	0.2	0.0
	27.5 – 49.2	20.3	40.5	18.6	0.0	1.6	0.9	16.1	2.1	0.0	0.0
6.0 – 7.0	0.0 – 25.5	44.4	1.5	4.4	0.0	0.5	0.7	34.3	13.4	0.7	0.1
	25.5 – 41.0	7.7	42.5	34.9	1.7	2.3	2.2	7.8	0.8	0.1	0.0
12.0 – 13.0	0.0 – 19.8	17.9	0.5	2.2	0.0	0.5	0.1	31.8	42.5	4.5	0.0
	19.8 – 41.2	20.0	0.4	3.8	0.0	0.7	0.0	43.5	30.2	1.4	0.0
18.0 – 19.0	0.0 – 15.1	3.4	0.0	0.6	0.0	0.1	1.0	18.0	61.4	14.0	1.5
	15.1 – 35.6	0.0	0.0	0.0	0.0	0.0	1.1	5.9	70.5	19.4	3.1
24.0 – 25.0	0.0 – 17.7	0.0	0.0	0.0	0.0	0.0	1.4	4.1	78.8	12.7	3.0
	17.7 – 36.4	0.0	0.0	0.0	0.0	0.0	1.9	5.2	72.2	18.0	2.7

Table 33 – Proportion of Textures Derived from Pittsburgh Seam Coal and Decant Oil Compared with the Normalized Concentration of Decant Oil Textures in Coke from Run #35, Vol. %

Long. Interval, cm	Cross Section, mm	% Coal-derived	% Petroleum-derived	Isotropic Petroleum-derived	Mosaic, <10μm	Small Domain, 10-60μm	Domain >60μm	Flow Domain, >60μm L, <10μm W
1.0 – 2.0	0.0 – 27.5	44.4	55.6	0.5	83.8	15.8	0.4	0.0
	27.5 – 49.2	81.0	19.0	4.5	84.5	11.0	0.0	0.0
6.0 – 7.0	0.0 – 25.5	50.8	49.2	1.4	69.8	27.2	1.4	0.2
	25.5 – 41.0	89.1	10.9	20.2	71.6	7.3	0.9	0.0
12.0 – 13.0	0.0 – 19.8	21.1	78.9	0.1	40.3	53.9	5.7	0.0
	19.8 – 41.2	24.9	75.1	0.0	57.9	40.2	1.9	0.0
18.0 – 19.0	0.0 – 15.1	4.1	95.9	1.0	18.8	64.0	14.6	1.6
	15.1 – 35.6	0.0	100.0	1.1	5.9	70.5	19.4	3.1
24.0 – 25.0	0.0 – 17.7	0.0	100.0	1.4	4.1	78.8	12.7	3.0
	17.7 – 36.4	0.0	100.0	1.9	5.2	72.2	18.0	2.7

Subtask 5.5: Distillation And Analysis Of Co-Coking Binder Pitch

As illustrated in **Figure 5.15** the liquid product from the co-coking run#35 was further distilled to yield a pitch material. **Figure 5.16** shows the different cuts obtained and their respective yields. About 13% was in the pitch boiling point range. The different cuts were analyzed by GC-MS to access their chemical makeup and **Figure 5.17** shows the GC-MS traces. Obviously, there is a shift from lighter to more heavy compounds with boiling point. The coal compounds appears to be present in the Jet fuel and Diesel range, while the pitch compound also appear to have a makeup of compounds from the coal. This indicate that most of the decant oil may add to the fuel oil range. The real benefit from adding coal is therefore an increased jet fuel production and a heavier stream that can replace binder pitches as shown below.

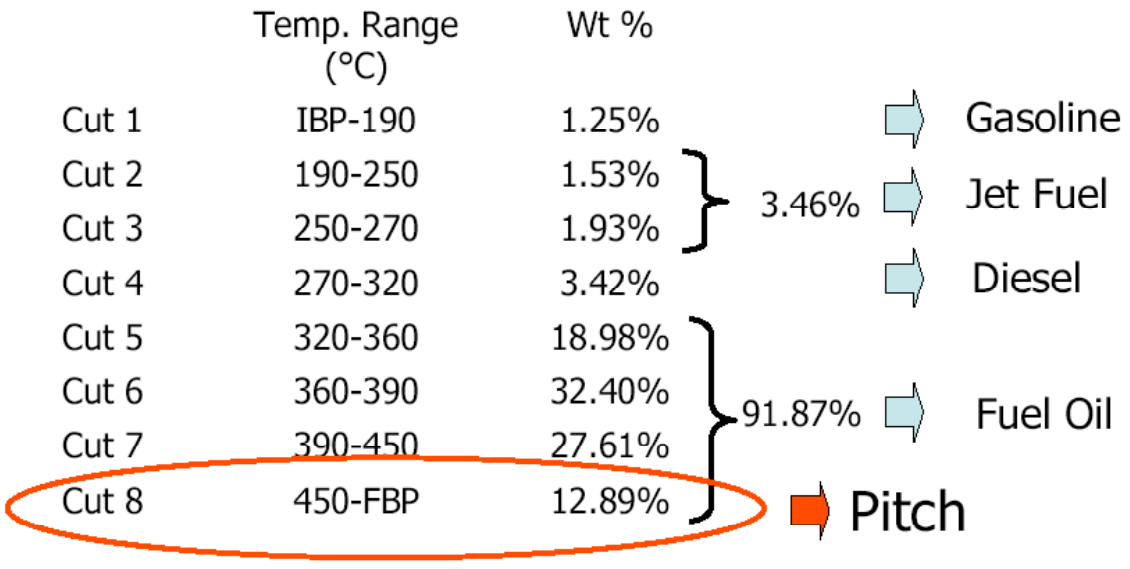

Figure 61. Different distillation cuts obtained from the liquid product from the co-coking run#35 and their respective yields.

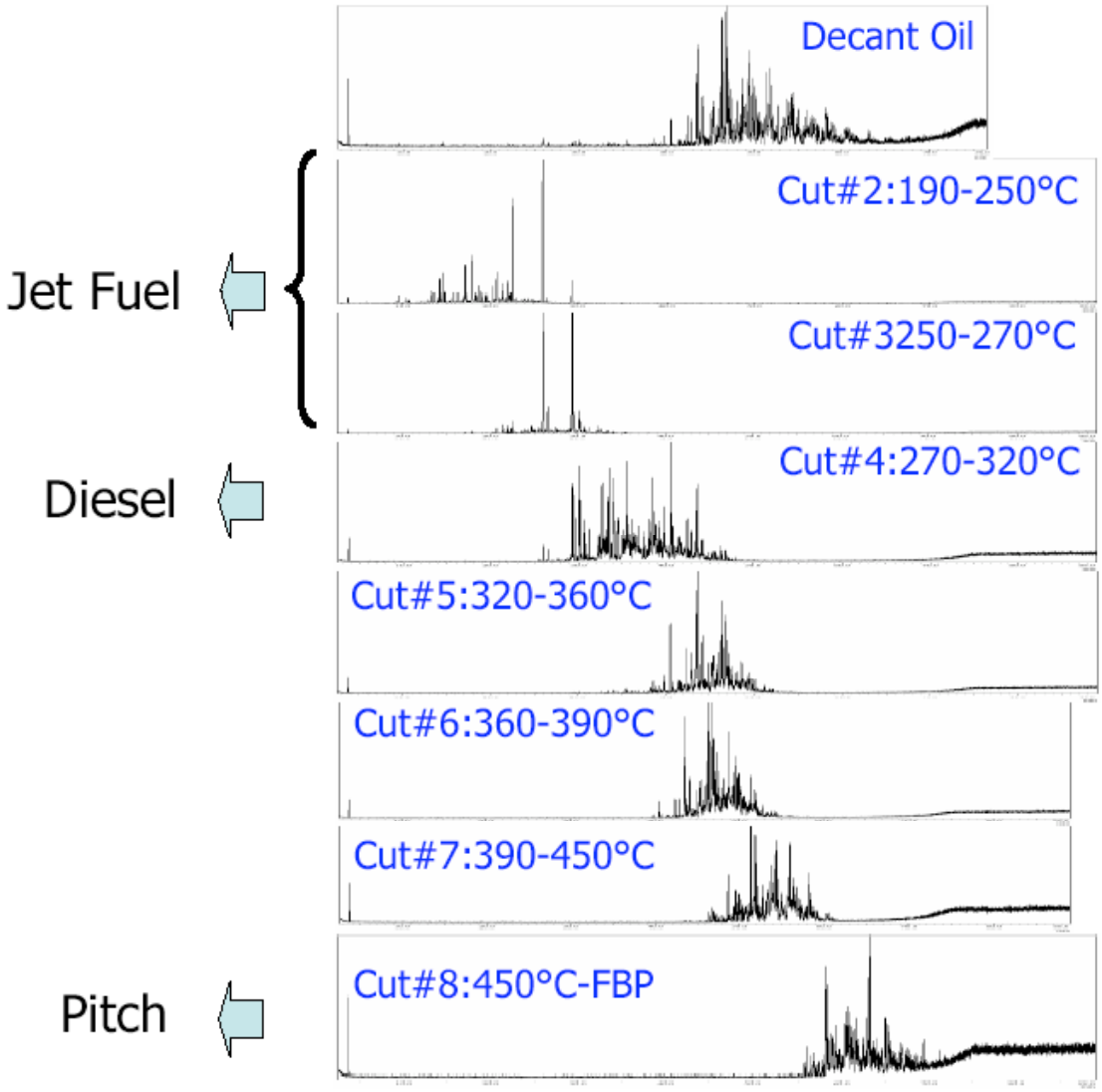

Figure 62. GC-MS traces of the different distillation cuts.

Figure 63 compares typical coal tar pitch compounds with that found for the co-coking pitch. The real benefit of the co-coking pitch is the very low content of 2-4 ring aromatics that typically result in air pollution associated with industrial use of coal tar pitch. Most of the 4-6 rings compound found in the co-coking pitch have also been identified in coal tar pitch extracts. However, the co-coking pitch have larger thiophene

ring system that can promote condensation when used as a binder. Also, larger ring-systems are being investigated using MALDI-MS since the GC-MS has typically a limit of 6 member rings.

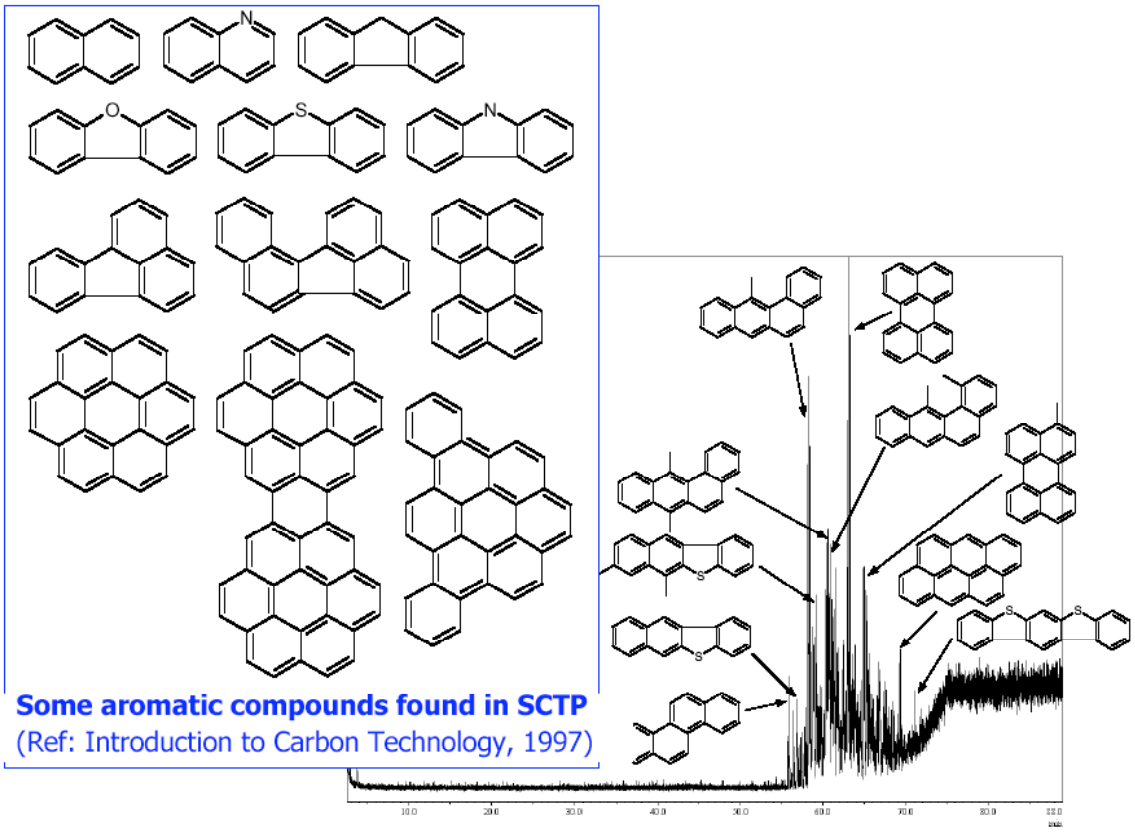

Figure 63. Comparison of typical coal tar pitch compounds with that found for the co-coking pitch.

The co-coking pitch does behave like a coal tar pitch in terms of its viscosity profile as shown in **Figure 64**. However, the softening point is about 60°C as opposed to a desired softening point of 110°C. This can be adjusted with further distillation.

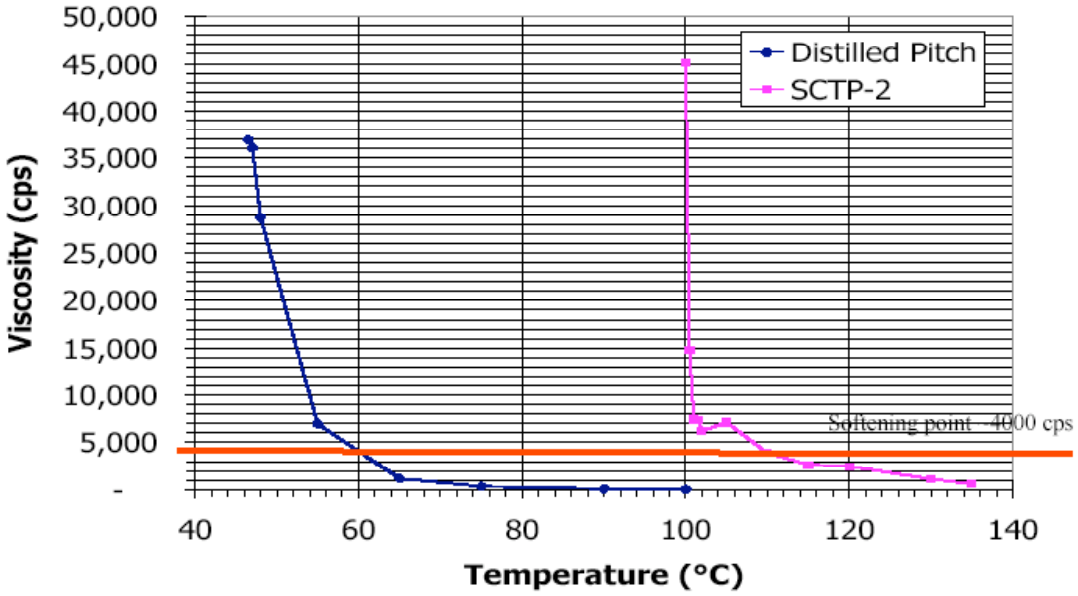

Figure 64. Comparion of the viscosity profile of the co-coking pitch and a standard coal tar pitch.

Subtask 5.6: Manufacture And Testing Of Carbon Artifacts

Laboratory setup and materials for manufacture and testing of carbon artifacts was prepared during the reporting period. **Figure 65** shows the carbon artifact preparation route to simulate industrial processes. Typical laboratory pellets have 22 wt% binder but this level might be reduced to meet the 17-18 wt% used by industry. Further, the baking process has been optimized to a 7 day cycle to avoid excessive pitch loss during baking as shown in **Figure 66**.

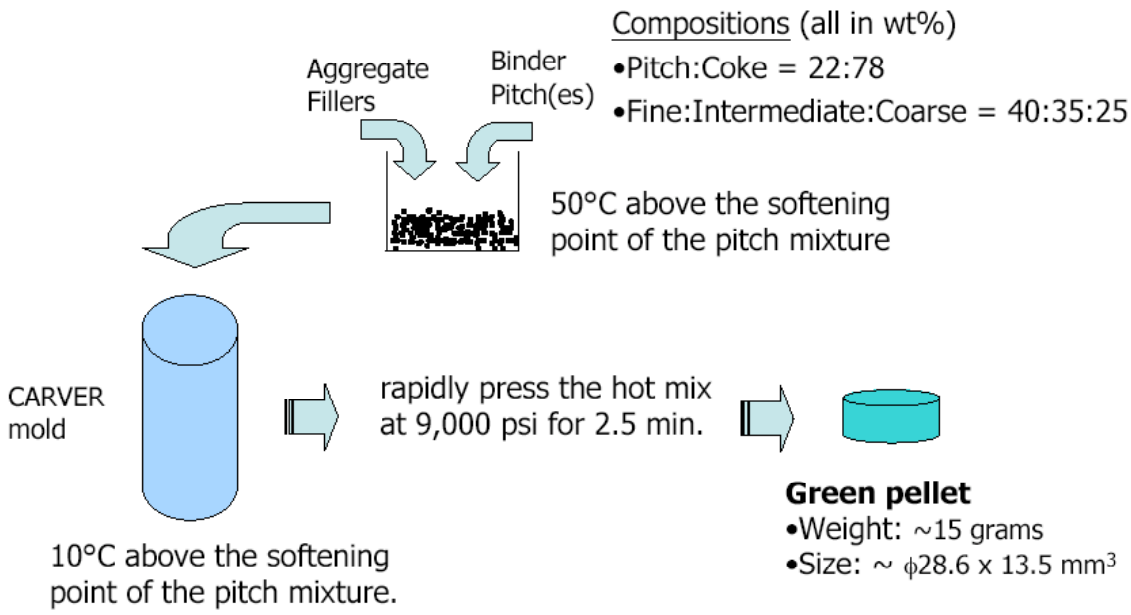

Figure 65. Carbon artifact preparation route

.

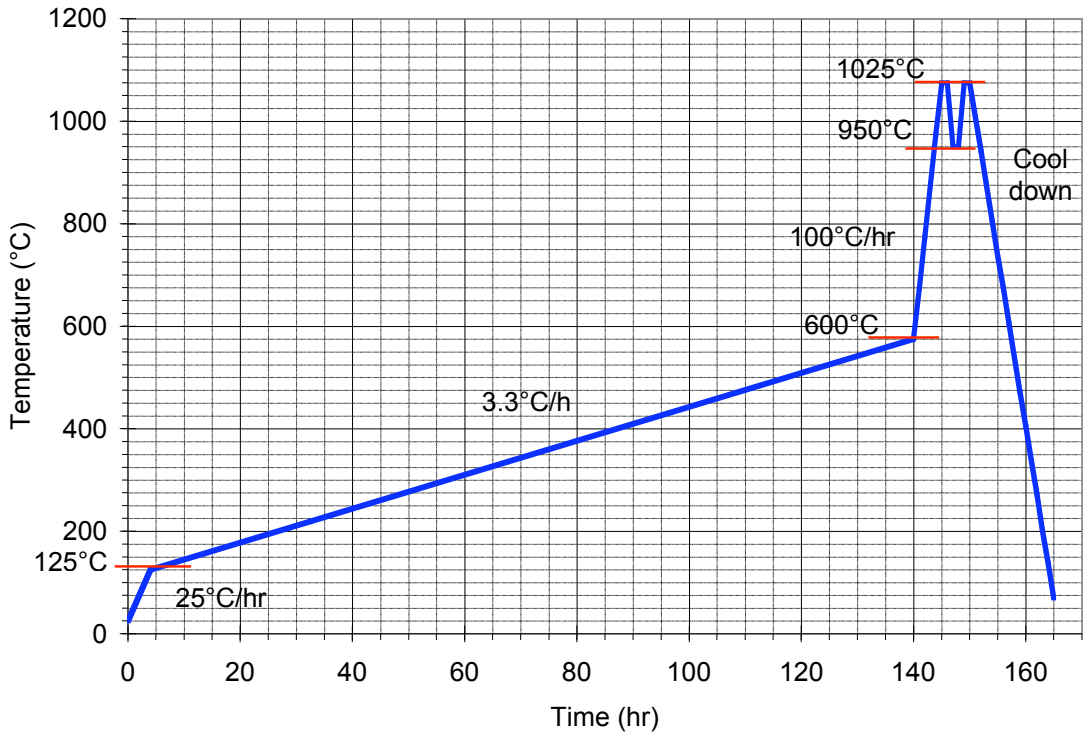

Figure 66. Schematic of the 7 day baking process.

References

1. Schobert, H. H., Advanced Thermally Stable Coal-Based Jet Fuels, Annual Progress Report, AFOSR Grant F49620-99-1-0290, 2001-2002

2. Schobert, H. H., Advanced Thermally Stable Coal-Based Jet Fuels, Annual Progress Report, AFOSR Grant F49620-99-1-0290, 2000-2001

3. Schobert, H. H., Advanced Thermally Stable Coal-Based Jet Fuels, Annual Progress Report, AFOSR Grant F49620-99-1-0290, 1999-2000

4. Coleman, M. M., Fearnley, S. P., Kumar, S. and Sobkowiak, M., Fuel Stabilization, AFRL-PR-WP-TR-2000-2007, Final Report for 07/01/1995 – 12/31/1998, September 1999.

5. Song, C., Lai, W.-C., Schobert, H.H. Hydrogen-Transferring Pyrolysis of Long-Chain Alkanes and Thermal Stability Improvement of Jet Fuels by Hydrogen Donors. Ind. Eng. Chem. Res., 1994, 33 (3), 548-557

6. Lai, W.-C and Song, C., 1996a Prepr. Pap.- Amer. Chem. Soc. Div. Fuel Chem. 41:524

7. Lai, W.-C and Song, C., 1996b Fuel Processing Technology 48:1

8. Selvaraj, L., Sobkowiak, M., Song, C., Stallman, J., Coleman, M. M. A Model System for the Study of Additives Designed to Enhance the Stability of Jet Fuels at Temperatures Above 400°C. Energy & Fuels, 1994, 8 (4), 839-845.

9. Yoon, E.M., Selvaraj, L., Song, C., Stallman, J., Coleman, M. M., High Temperature Stabilizers for Jet Fuels and Similar Hydrocarbon Mixtures. 1. Comparative Studies of Hydrogen Donors. Energy & Fuels, 1996a, 10 (3), 806-811.

10. Yoon, E.M., Selvaraj, L., Eser, S. and Coleman, M. M., High Temperature Stabilizers for Jet Fuels and Similar Hydrocarbon Mixtures. 2. Kinetic studies, Energy & Fuels, 1996a, 10 (3), 812-815.

11. Andrésen, J.M., Strohm, J.J., Boyer, M.L., Song, C, Schobert, H.H. and Butnark, S., Am. Chem. Soc. Div. Petrol. Chem. Prepr., 2001a, 46(1), 208-209.

12. Andrésen, J.M., Strohm, J.J., Sun, L., Song, C. Energy & Fuels, 2001b, 15(3), 714-723.

13. Badger, M. W., Fickinger, A. E.,Martin, S. C.,Mitchell, G. D. and Schobert, H. H.,1998 Proc. 8th Austrlian Coal Science Conference 245.

14. Badger, M. W., Fickinger, A. E., Mitchell, G. D., Adams, A. N. and Schobert, H. H., Proc. 205th International Technical Conference on Coal Utilization and Fuel Systems (in press).

15. Butnark, S., Badger, M.W. and Schobert, H.H., Amer. Chem. Soc., Div. Fuel Chem. Prepr., 1999, 44 (3), 662-665.

16. Butnark, S., Badger, M. W. and Schobert, H. H., 2000 Prepr. Pap.- Amer. Chem. Soc. Div. Petrol. Chem., 45:493.

17. Fickinger, A. E., 2000, M. S. Thesis, The Pennsylvania State University, University Park, PA.

18. Fickinger, A. E., Badger, M. W., Mitchell, G. D. and Schobert, H. H., 1999, Prepr. Pap.- Amer. Chem. Soc. Div. Fuel Chem 44:106.

19. Fickinger, A. E., Badger, M. W., Mitchell, G. D. and Schobert, H. H., 2000, Prepr. Pap.- Amer. Chem. Soc. Div. Fuel Chem 45:299.

20. Song, C., and Schobert, H. H., 2000, Prepr. Pap.- Amer. Chem. Soc. Div. Fuel Chem. 45:819.

21. Butnark, S., Badger, M. W. and Schobert, H. H., Determining the Desired Chemical Composition for Thermally Stable Jet Fuel, Amer. Chem. Soc., Div. Fuel Chem. Prepr., 2001, 46 (2), 492-494.

22. Butnark, S., Badger, M. W. and Schobert, H. H. and Wilson, G. R., Selection of Prototype Thermally Stable Jet Fuels 3. Jet Fuel Boiling Range and its Affect on Pyrolytic Stability, 2002 Prepr. Pap.- Amer. Chem. Soc. Div. Petrol. Chem., 47(3),:201..

23. Schobert, H. H., Badger, M. W. and Santoro, R. J., Progress Toward Coal-Based JP-900, 2002 Prepr. Pap.- Amer. Chem. Soc. Div. Petrol. Chem., 47:192.

24. Wilson, G. R., Project Report on AFOSR-Subcontract for Advanced Thermally Stable Coal-Based Jet Fuels for the Pennsylvania State University, PARC Technical Services Inc., Pittsburgh, PA. August 2002.

25. Hazlett, R.N., Thermal Oxidation Stability of Aviation Turbine Fuels, ASTM, Philadelphia, 1991.

26. Song, C.; Ma, X. Appl. Catal. B:Env., 2003, 41, 207; Song, C. Catal. Today, 2003, 86, 265..

27. Whitehurst, D.D., Isoda, T. Mochida, I. Adv. Catal. 1998, 42, 345.

28. Kwak, C., Lee, J. J., Bae, J. S. and Moon, S. H., Appl. Catal. B 35 (2001) 59.

29. Kabe, T., Aoyama, Y., Wang, D., Ishihara, A., Qian, W., Hosoya, M., Zhang, Q., Appl. Catal. A 209 (2001) 237

30. Oyama, S. T., Wang, X., Lee, Y.-K., Bando, K., Requejo, F. G., J. Catal. 210 (2002) 207

31. Stinner, C., Prins, R., and Weber, Th., J. Catal. 202 (2001) 187

32. Oyama, S. T., J. Catal. 216 (2003) 343.

33. Sie, S. T., Fuel Proc. Tech. 61 (1999) 149.

34. Broderick, D. H. and Gates, B. C., AIChE J. 27 (1981) 663.

35. Sakanishi, K., Nagamatsu, T., Mochida I., Whitehurst, D., J. Mol. Catal. A 155 (2000) 101.

36. Kim, J. H., Ma, X., Song, C., Lee, Y.-K. Oyama, S. T., Energy & Fuel, submitted for publication.

37. Kim, J. H., Ma, X., Song, C., Lee, Y.-K. Oyama, S. T, Am. Chem. Soc., Div. Fuel Chem. 48(1) (2003) 40.

38. Ma, X., Kim, J. H., Song, C., Prepr. Am. Chem. Soc., Div. Fuel Chem. 48(2) (2003) 553.

39. Turaga, U. T., Wang, G., Ma, X., Song, C. and Schobert, H. H., Am. Chem. Soc. Div. Petrol. Chem. 47(1) 2002 89-92.

40. Lee, S.-W.; Ryu, J. W.; Min, W. Catal. Surv. Asia 2003, 7, 271.

41. Sano, Y.; Choi, K.-H.; Korai, Y.; Mochida, I. Appl. Catal. B 2004, 49, 219

42. Sano, Y.; Choi, K.-H.; Korai, Y.; Mochida, I. Energy & Fuels 2004, 18, 644.

43. Kulprathipanja, S., Nemeth, L. T., Holmgren, J. S., Process for Removing Sulfur Compounds from Hydrocarbon Stream, U.S. Patent 5,807,475, 1998.

44. Turaga, U.T., Wang, G., Ma, X., Song, C., Am. Chem. Soc., Div. Fuel Chem., 48 (2) (2003) 550.

45. Turaga, U.T., Wang, G., Ma, X., Song, C., Catal. Today 86 (2003) 265.

46. Beck, J. S., Vartuli, J. C., Roth, W. J., Leonowicz, M. E., Kresge, C. T., Schmitt, K. D., Chu, C. T. W., Olson, D. H., Sheppard, E. W., McCullen, S. B., Higgins, J. B., Schlenker, J. L., J. Am. Chem. Soc., 114(27) (1992) 10834-10843.

47. Kim, J. H., Ma, X., Song, C., Lee, Y.-K., Oyama, S. T., Prepr. Pap. Am. Chem. Soc., Div. Petro. Chem., 2004, 49 (1), 44

48. Ma, X.; Kim, J. H.; Song, C. Prepr. Pap.-Am. Chem. Soc. Div. Fuel Chem. 2003, 48, 135

49. Hernández-Maldonado, A. J.; Yang, R. T. Angew. Chem. Int. Ed. 2004, 43, 1004

50. Yang, R. T.; Hernández-Maldonado, A. J.; Yang, F. H. Science 2003, 301, 79.

51. Zhou, A; Ma, X.; Song, C. Prepr. Pap.-Am. Chem. Soc. Div. Pet. Chem. 2004, 49, 329

52. Montes-Morán, M. A.; Suárenz, D.; Menéndez, J. A.; Fuente, E. Carbon 2004, 42, 1219.

53. Sano, Y.; Choi, K.-H.; Korai, Y.; Mochida, I. Energy & Fuels 2004, 18, 644.

54. Stanislaus, A, and Cooper, B. H. 1994. Aromatic Hydrogenation Catalysis: A Review. Catal. Rev. - Sci. Eng., 36, 75-123.

55. Cooper, B. H. and Donnis, B. B. L. 1996. Aromatic Saturation of Distillates: An Overview. Appl. Catal. A., 137, 203-223.

56. Song, C., S. Eser, H. H. Schobert, and P. G. Hatcher. 1993. Pyrolytic Degradation Studies of a Coal-Derived and a Petroleum-Derived Aviation Jet Fuel. Energy & Fuels, 1993, 7 (2), 234-243.

57. Song, C. and W.-C. Lai. 1998. Chemistry for Thermal Degradation of Bicyclic Hydrocarbon Components of Jet Fuels in Pyrolytic Regime. Am. Chem. Soc. Div. Petrol. Chem. Prepr., 1998, 43 (3), 462-466.

58. Dalla Betta, R.A.; Boudart, M. *Proc. 5th Int. Congr. Catal.* **1972**, 1329

59. Song, C. 2002c. Selective Conversion of Polycyclic Hydrocarbons to Specialty Chemicals over Zeolite Catalysts. Cattech, 2002, 6 (2), 64-77.

60. Schobert H.H. and C. Song. 2002. Chemicals and Materials from Coal in the 21st Century. Fuel, 2002, 81 (1), 15-32.

61. Shen, J.-P., C. Song and L. Sun. 2000. Preparation of High-Performance Catalyst for Shape-Selective Methylation of 2-Methyl naphthalene into 2,6-Dimethylnaphthalene. Paper presented at I&EC Symp on Green Chemistry, American Chemical Society Spring 2002 National Meeting, Orlando, FL, April 7-11, 2002.

62. Pu, S.-B. and Inui, T. 1996. Synthesis of 2,6-dimethylnaphthalene by methylation of methylnaphthalene on various medium and large-pore zeolite catalysts, Appl. Catal. A: General, 1996, 146, 305-316.

63. Fraenkel, D., Cherniavsky, M., Ittah, B. and Levy, M., 1986. Shape-selective alkylation of naphthalene and methylnaphthalene with methanol over H-ZSM-5 zeolite catalysts, J. Catal., 1986, 101, 273-383.

64. Singer, J.G. (editor), Combustion: Fossil Power Systems, Combustion Engineering, Inc., pp.2-28 – 2-31, 1981.

65. Federal Register, Title 40 CFR Part 63, National Emission Standards for Hazardous Air Pollutants for Industrial, Commercial, and Institutional Boilers and Process Heaters; Final Rule, 55218-55286, 2004.

66. ASTM D5184-01, Standard Test Methods for Determination of Aluminum and Silicon in Fuel Oils by Ashing, Fusion, Inductively Coupled Plasma Atomic Emission Spectrometry, and Atomic Absorption Spectrometry. American Society Testing Materials.

67. Miller, B.G., A.W. Scaroni, S.A. Britton, D.A. Clark, J.L. Morrison, S.V. Pisupati, R.L. Poe, P.M. Walsh, R.T. Wincek, and J. Xie, Final Report for Coal Water Fuel Combustion Testing in a Fuel Oil-Designed Industrial Boiler, Prepared for the U.S. Department of Energy, Federal Energy Technology Center, Pittsburgh, Pennsylvania, March 10, 1997, DE-FC22-89PC88697, Appendix E.

68. Chung, I-P., C. Strupp, and J. Karan, New Fuel Oil Atomizer for Improved Combustion Performance and Reduced Emissions, Proceedings of the 6th European Conference on Industrial Furnace and Boilers, 2000.

69. Clarke, Lee B. and Sloss, Lesley L., Trace elements – emissions from coal combustion and gasification, IEACR/49, IEA Coal Research, London, 111 pp., 1992.

70. U.S. EPA, Office of Air Quality planning and Standards, Compilation of Air Pollution Emission Factors" (AP-42), http://www.epa.gov/tnn/chief/ap42/ch01/, 1993.

71. U.S. Environmental Protection Agency, Standard Test Method for Elemental, Oxidized, Particle-bound and Total Mercury in Flue Gas Generated from Coal-Fire Stationary Sources (Ontario-Hydro Method), http://www.epa:80/ttnemc01 /prelim/pre_003.pdf, May 12, 1999.

72. Federal Register, Title 40 CFR Parts 60 and 61, Standards of Performance for New Stationary Sources National Emission Standards for Hazardous Air Pollutants Addition of Method 29 to Appendix A of Part 60 and Amendments to Method 101A of Appendix B of Part 61, 18260-18279, 1996.

73. Falcone Miller, S., R. T. Wincek, B. G. Miller and A. W. Scaroni, Evaluation of a Hybrid Sampling Train for Measuring Trace Elements and Identifying Mercury Species in Combustion Flue Gas, presented at 24th International Technical Conference on Coal Utilization and Fuel Systems, Clearwater, FL, March 8-11, 1999.

74. Falcone Miller, S., R. T. Wincek, B. G. Miller and A. W. Scaroni, Development of a PSU Methodology for Measuring Trace Elements and Identifying Mercury Species in Combustion Flue Gas, presented at EPRI-DOE-EPA Combined Utility Air Pollution Control Symposium: The MEGA Symposium, Atlanta, GA, August 16-20, 1999.

75. U.S. Environmental Protection Agency, Methods 3050, 3051, 6010, 7470 and 7471, Test Methods for Evaluating Solid Waste: Physical/Chemical Methods. SW-846, 3rd Ed., NTIS, September 1988.

76. U.S. EPA, Report on Revisions to 5th Edition AP-12, Section 1.3, Fuel Oil Combustion, Office of Air Quality planning and Standards, Compilation of Air Pollution Emission Factors" (AP-42), http://www.epa.gov/ttn/chief/ap42/ch01 /final/c01s03.pdf, 1996.

77. Delhaes, P. Graphite and Precursors, Gordon and Breach Sci. Pub., Amsterdam, 2001

78. Farzin, Y.H. Resource and Energy Economics 2001, 23, 271-291.

79. Marsh, H. Introduction to Carbon Science Butterworth & Co Ltd., London, 1989.

80. Speight, J. G.; and Özüm, B. Petroleum refining processes Marcel Dekker, New York, 2002.

81. L.R.Rudnick, O. Gul, and H. H. Schobert, 'Co-coking Decant Oil and Coal in a Laboratory-Scale Coking Unit", 128th Annual International Coal Conference, Osaka, Japan, September 13-17, 2004

82. Mochida, I., Fujimoto, K.-i. and Oyama, T. (1991), Chapter 3. Chemistry in the Production and Utilization of Needle Coke, Chemistry and Physics of Carbon, Ed. P.A. Thrower, Vol. 24, Marcel Dekker, Inc., New York, pp. 111-212.

List of Acronyms and Abbreviations

1THQ	1,2,3,4-tetrahydroquinoline
5THQ	5,6,7,8-tetrahydroquinoline
AFOSR	Air Force Office of Scientific Research
API	American Petroleum Institute
BT	benzothiophene
CFR	Cooperative Fuels Research
DBT	dibenzothiophene
DDC	Detroit Diesel Corporation
DDS	direct desulfurization
DHQ	decahydroquinoline
DMBP	dimethyl biphenyl
DMDBT	dimethyldibenzothiophene
DMDCH	dimethyl dicyclohexyl
DMN	dimethyl naphthalene
EN	ethyl naphthalene
EPA	Environmental Protection Agency
FBP	final boiling point
FCC	fluid catalytic cracking
FID	flame ionizaton detector
FTIR	Fourier Transform Infrared
GCMS	gas chromatography-mass spectrometry

HDMDBT	hydrodimethyl dibenzothiophene
HDS	hydrodesulfurization
HDT	hydrotreated
HM	H-mordenite
HY	H Y-type zeolite
HYD	hydrogenation pathway
HZSM	H-synthetic zeolite material
IBP	initial boiling point
IC	internal combustion
IQT	ignition quality test
JP-900	jet fuel prototype stable to 900 F
LCO	light cycle oil
LHSV	liquid hourly space velocity
LTHDA	low temperature hydrotreating and dearomatization
MCHT	methyl cyclohexyl toluene
MCM	mesopourous catalytic material
MN	methyl naphthalene
NTP	normal temperature and pressure
PARC	Pennsylvania Applied Research Corporation
PB	propyl benzene
PCH	propyl cyclohexane
PCHE	propyl cyclohexene
RCO	refined chemical oil

SI	spark ignited
SpGr	specific gravity
SwRI	Southwest Research Institute
TLP	total liquid product
TOS	time on stream
WHSV	weight hourly space velocity